Effect of Carbon Supports on Supercritical Hexane Mediated, Fe-Catalyzed Fischer-Tropsch Synthesis

by

David Patrick Roe

A dissertation submitted to the Graduate Faculty of
Auburn University
in partial fulfillment of the
requirements for the Degree of
Doctor of Philosophy

Auburn, Alabama
December 16, 2017

Keywords: Fischer-Tropsch, Nanoparticles, Supercritical Fluid, Carbon Nanotubes, Aldehyde

Approved by

Christopher B. Roberts, Chair, Dean of Engineering
Mario Eden, Department Chair of Chemical Engineering
Virginia Davis, Alumni Professor of Chemical Engineering
Sushil Adhikari, Alumni Associate Professor of Biosystems Engineering

Abstract

The Fischer-Tropsch synthesis (FTS) process consists of surface-catalyzed reactions that collectively convert syngas into hydrocarbons, oxygenates, CO_2, water, and heat. In this work, five Fe-based, carbon-supported catalysts were synthesized, characterized, and evaluated for FTS reaction performance. Carbon supports consisted of large-diameter multi-walled carbon nanotubes (MWNTs), small-diameter MWNTs, carbon nanofibers, and graphene nanoplatelets and each catalyst was tested under both gas phase and supercritical reaction conditions to more thoroughly interrogate their behavior.

All of the carbon-supported catalysts were highly active relative to a more traditional precipitated catalyst, but wide variations in conversion, CO_2 selectivity, propagation probability, and product functionality between catalysts make it clear that that carbon support structure can significantly impact FTS catalyst performance. Of the catalysts studied, the K-promoted catalyst supported on large-diameter MWNTS had the most unique behavior, producing long-chain aldehydes under both gas phase and supercritical reaction conditions. This production and extraction of significant quantities of aldehydes in Fe-catalyzed, gas phase FTS is unprecedented in the literature, where such behavior is limited to slurry phase or supercritical conditions. In the larger context of the catalyst's behavior, this unique result also serves as significant evidence that an oxygenate-based mechanism is active in product formation in Fe-based FTS.

Acknowledgements

I would like to express my deepest thanks to my advisor, Dr. Christopher Roberts. Dr. Roberts' provided tireless support, endless positivity, and a commitment to my success far in excess of his professional obligation throughout my Ph.D. studies. His willingness to always go above and beyond to help his students has left me beyond grateful.

I am thankful for the help of my committee members: Dr. Mario Eden, Dr. Virginia Davis, and Dr. Sushil Adhikari. Throughout the lifetime of my research project, their input and advice has helped guide and enable my research and has definitely had a positive impact on my project.

I would also like to thank the past members of the Roberts group: Dr. Rui Xu, Dr. Pranav Vengsarkar, Dr. Jennifer Boice, Dr. Sihe Zhang, and Charlotte Stewart. Group members were always there for me both personally and professionally with unwavering support. I couldn't have asked for better friends as coworkers.

I would also like to acknowledge the help I received from Brian Schwieker, Steven Moore, and Dr. Michael Miller. Brian was always willing and able to provide technical assistance, while without Steve and Dr. Miller, I probably would not have half on the characterization knowledge or data that I do. Thank you.

I would like to thank my family as well as my friends. Without the support of my parents, brothers, sister-in-law, and all the little Roes, I can't say I would have able or willing to make it through graduate school. Without my friends at Auburn, I can't it would have been worth it. Thank you all.

Finally, we gratefully acknowledge the funding sources that enabled the research in this document: Auburn NSF IGERT and Biorefining [NSF-IGERT No.1069004], and U.S. Department of Agriculture/NIFA-AFRI IBSS Consortium [Grant No. 2011-68005-30410)].

Table of Contents

List of Tables

List of Figures

Chapter 1: A Review of Fischer-Tropsch Synthesis

1.1 General

1.1.1 Motivation

Currently, much of the world's energy supply is derived from fossil fuels. Due to the finite nature of these fuels and an increased concern for their environmental impact, the use of fossil fuels must be supplemented and eventually replaced by alternative energy sources. While nuclear, hydroelectric, wind, and solar methods are increasingly feasible for renewable electricity generation, the transportation infrastructure in the United States and elsewhere is still very dependent on liquid transportation fuels. It is because of this dependence upon liquid fuels that there exists a demand for a liquid petroleum alternative that can be more sustainably produced while remaining economically competitive.

1.1.2 Introduction

Fischer-Tropsch Synthesis (FTS) is a process to produce hydrocarbons and oxygenates from carbon monoxide and hydrogen. Because CO and H_2 can be generated from resources such as coal, natural gas, and biomass, FTS enables the production of many fuels and chemicals that are typically thought of as petrochemicals without the use of crude oil. Like crude oil however, the FTS product 'syncrude' mixture contains a variety compounds and must be refined via separation and upgrading reactions to obtain higher yields of desired products.[1]

A general overview for the process of converting a carbon resource into fuel is shown in Figure 1.1. Collectively, the process for generating, cleaning, and utilizing syngas to produce liquid fuels is known as XTL where 'TL' is the conversion 'to liquid' and 'X' can be biomass (BTL), coal (CTL), natural gas (GTL), or some other carbon source.

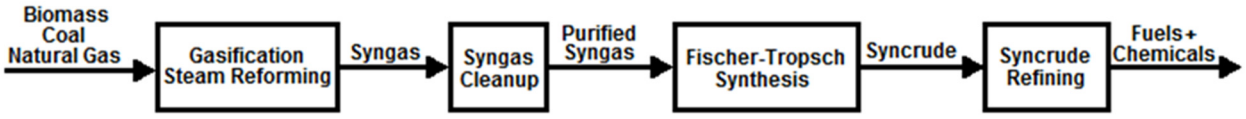

Figure 1.1 Overview of XTL process adapted from Durham.[3]

As with many energy conversion technologies, it is much preferred to conduct the Fischer-Tropsch process at large (hundreds of thousands of tons per year) capacities due to economies of scale.[2] With the significant costs of syngas cleanup and oxygen generation,[1,2] FTS becomes very capitally intensive process whose profitability is highly dependent on the volatile price of petroleum[1] as well as the cost of feedstock. Due to the generally challenging economics, but attractive potential of the process to generate fuels, many researchers are focused on improving various aspects of the XTL process in an effort to bring the whole process closer to the realm of profitability.

1.1.3 Fischer-Tropsch Synthesis History

The Fischer-Tropsch (FT) process has its first roots in the work of Sabatier and Senderens, two French scientists who, in 1902, discovered the capability of iron, cobalt, and nickel to convert CO and H_2 into methane.[3] It wasn't until the 1920's that Drs. Franz Fischer and Hans Tropsch of the Kaiser Wilhelm Institute in Germany began to produce hydrocarbons over an Fe-based catalyst via coal-derived syngas.[4] By the 1930's, industrial scale FTS was up and running in Germany aided by the nation's strong coal/coke supply and desire to overcome its dependence on foreign oil.[2] The global FT capacity expanded rapidly from approximately 2,000 BPD in 1935 to 12,000 BPD in 1943.[3]

While one high temperature Fischer-Tropsch GTL facility briefly operated in Brownsville, Texas from 1951-1957, for the decades following WWII, the history of FTS is largely synonymous with that of South Africa's Sasol.[2] Sasol greatly advanced FTS catalyst and reactor technology and demonstrated the commercial viability of Fischer-Tropsch synthesis. As of the opening of its Mossel Bay facility in 1992, Sasol's portfolio included three facilities producing fuels and a wide array of chemicals from coal and natural gas via Fischer-Tropsch synthesis.

More recently, cheaper natural gas and fluctuating oil prices have caused an increased interest in Fischer-Tropsch synthesis for GTL applications.[5] In addition to the continued operation of Sasol, Shell has constructed GTL plants in both Malaysia and Qatar. And while Shell's Qatar facility is the largest GTL plant yet constructed with 260,000 barrels per day of liquid products capacity,[6] companies such as Rentech,

Calumet, British Airways, and numerous others have invested in and are building smaller scale facilities around the globe as well. The current outlook of Fischer-Tropsch synthesis in the U.S. seems slanted towards GTL utilizing low cost natural gas and the sale, rather than cracking, of heavy wax products.[7]

1.1.4 Fischer-Tropsch Reaction Overview

Fischer-Tropsch synthesis is the heterogeneous, surface-catalyzed polymerization and hydrogenation of carbon monoxide, typically utilizing either a cobalt or iron-based catalyst. Generally conducted in the range of 200-350 ºC and 10-60 bar, FTS produces a product slate that can be skewed towards light olefins, gasoline, diesel, or heavy waxes, all with very low sulfur content.[8,9]

1.1.4.1 Reaction Chemistry

The major reactions of Fischer-Tropsch synthesis are summarized as follows:[10]

$$2n\ H_2 + n\ CO \rightarrow -(CH_2)-_n + n\ H_2O \quad (1.1)$$

$$CO + H_2O \leftrightarrow CO_2 + H_2 \quad (1.2)$$

$$3\ H_2 + CO \rightarrow CH_4 + H_2O \quad (1.3)$$

$$2\ CO \leftrightarrow C + CO_2 \quad (1.4)$$

Eq. 1.1 is the primary reaction of FTS and the one by which the hydrocarbon monomer unit is generated. From this equation, it follows that, ideally, syngas fed to a FT reactor should have a ratio of H_2/CO of approximately 2. Eq. 1.2 is the water-gas shift (WGS) reaction. While Co and Ru catalysts have negligible WGS activity, a typical K-promoted, Fe-based catalyst is very WGS active, making such catalysts more tolerant of different H_2/CO ratios.[1] The final two reactions, shown in Eq. 1.3 and 1.4 respectively, are methanation and the Boudouard reactions, each of which 'wastes' carbon by forming an undesired side product.

As written, each of the reactions shown in Eqs. 1-4 has a significant exotherm. The most exothermic and thermodynamically favorable[11] reaction, methanation, has a ΔH_R^0 = -213 kJ/mol at 250 ºC, while the Boudouard, polymerization, and WGS reactions have ΔH_R^0 of -175.6 kJ/mol, -158.5 kJ/mol (n = 1), and -39.5 kJ/mol at 250 ºC, respectively. At elevated temperatures, thermodynamic control and an endothermic product desorption step lead to more methanation and short-chain products.[2] Thus, to obtain good selectivity towards heavier, more valuable products, maintaining kinetic control by managing the reaction temperature is of utmost importance.[10]

1.1.4.2 Mechanism and Products

While FTS products consist primarily of linear paraffins and linear, terminal olefins, other product types and functionalities can be produced depending on the reaction conditions and catalyst.[8,12] Other products can include alcohols, aldehydes, ketones, aromatics, carboxylic acids, cyclic compounds, dienes, esters, ethers, furans, and phenols.[2] Where applicable, linear isomers with terminal functional groups are far more predominant but branched compounds and products with non-terminal functional groups do form.[2] The mechanisms that account for this variety of product types are a matter of contention, but the basics of the reaction and formation of products can be understood in the context of polymerization without a precise grasp of each elemental step. A simple reaction schematic is shown in Figure 1.2.

Figure 1.2 is only for illustrative purposes, and it must be emphasized that it does not show the true

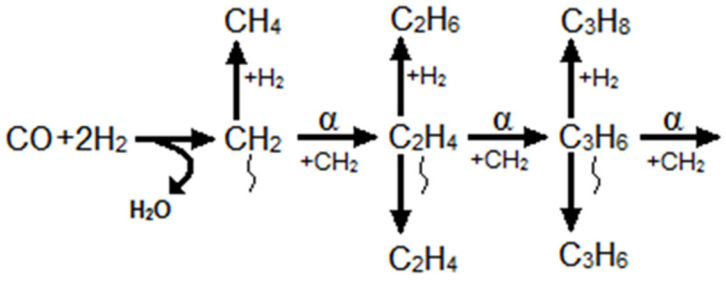

Figure 1.2 Simplified FTS reaction schematic adapted from Dry.[1]

initiation, elongation, and termination steps for the polymer chain, but rather accounts for these key steps in the polymerization in a simplified manner. For any given carbon chain length, the growing hydrocarbon

chain adsorbed to the catalyst surface can further react in two ways. First, the chain can terminate, for example by desorption or hydrogenation, to generate a product molecule. Alternatively, the growing chain can further react and integrate another -CH_2- (or equivalent, depending on mechanism) monomer.[2] The chain growth chance for an adsorbed intermediate is typically indicated as α.[8] An important feature that this simplified reaction schematic has in common with most, if not all, of the more detailed proposed mechanisms is that it shows the generally accepted idea of carbon chain growth as occurring one carbon at a time.[1]

As for the true mechanism of the FTS reaction and its elementary steps, there are numerous proposed reaction pathways with varying degrees of support and popularity. Four such pathways are summarized in Table 1.1 and enumerated in the following sections. Generally, it is assumed that multiple parallel pathways each contribute to the ultimate product distribution in FTS.[2]

Table 1.1 Summary of some popular FTS reaction mechanisms adapted from Steynberg and Dry.[2]

Mechanism	Chain Initiator	Chain Propagation
Alkyl		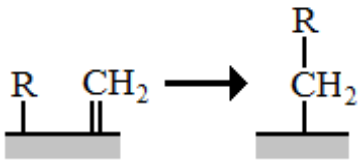
Alkenyl	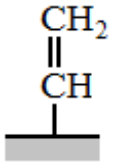	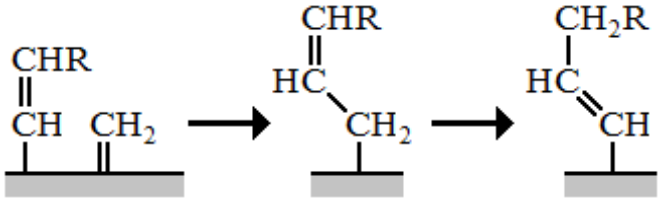
Enol	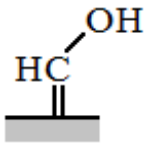	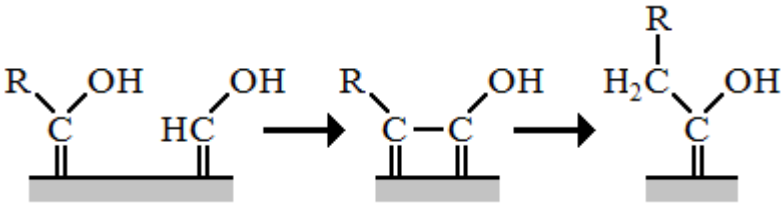
CO Insertion		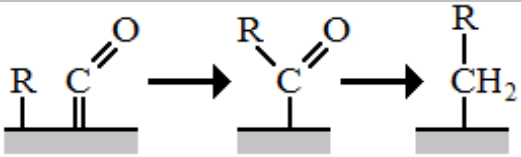

1.1.4.2.1 Alkyl Mechanism

Perhaps most widely accepted mechanism proposed is the so-called alkyl mechanism, which was developed by Brady and Pettit[13] from the carbide mechanism proposed by Craxford and Rideal in 1939.[14] In both the proposed carbide mechanism and the alkyl mechanism, CO chemisorbs dissociatively to the metal surface. Oxygen reacts with hydrogen or CO and desorbs as H_2O or CO_2. Carbon is sequentially hydrogenated to CH, CH_2, and then CH_3, the chain initiator. Propagation occurs as additional CH_2 units insert into the growing CH_2R chain. The growing chain can terminate to a terminal olefin (α-olefin) via ß-H-elimination or as a paraffin via hydrogenation. While olefins can readsorb and continue to react, chain growth and termination to paraffins are regarded as irreversible, although some cracking activity has been observed.[2]

The alkyl mechanism struggles to explain the presence of branched paraffins and oxygenates in the product. Branched products could be generated via readsorbed olefins incorporating into a growing chain at the olefin's ß carbon, but branched products are formed in higher quantities than would be expected from this mechanism. Oxygenates could be formed by the reaction of an adsorbed surface hydroxyl group reacting with or terminating the growing polymer chain, but there is not yet sufficient experimental evidence to support this mechanism.[2]

1.1.4.2.2 Alkenyl Mechanism

Similar to the alkyl mechanism, the alkenyl mechanism proposed by Maitlis[15] posits that CO dissociatively chemisorbs and is hydrogenated. Unlike in the alkyl mechanism, in the alkenyl mechanism, CH and CH_2 form and react to form a surface vinyl group ($CHCH_2$) which acts as the chain initiator. Chain propagation occurs when CH_2 inserts between the vinyl group and metal surface resulting in an allyl group (CH_2CHCHR) which isomerizes back into a vinyl group to continue propagation. Hydrogen addition leads to desorption of an α-olefin.

Branched products could result from the allyl intermediate isomerizing (growing chain shifts from γ-carbon to ß-carbon) prior to the allyl-vinyl isomerization. This mechanism fails, however, to explain the primary production of paraffins or formation of oxygenates.[2]

1.1.4.2.3 Enol Mechanism

Unlike in the alkyl and alkenyl mechanisms, in the enol mechanism proposed by Storch,[16] CO chemisorbs non-dissociatively. CO is hydrogenated to CHOH which acts as both chain initiator and monomer. Propagation occurs when two monomers or a monomer and a growing chain react, eliminate water to form a RCCOH intermediate, and hydrogenate to RCH_2COH. Branched hydrocarbons could form from the intermediate if the COH from the monomer is instead hydrogenated to CH_3, forming $RCOHCH_3$. Termination can occur via desorption, forming aldehydes. Additionally, the surface-bound carbon can be hydrogenated once, allowing an α-olefin to form, which could then hydrogenate further into a paraffin.[2,17]

The enol mechanism can explain formation of most oxygenates, but would lead to paraffinic species being secondary products formed from readsorbed olefins, which is inconsistent with experimental data showing paraffins as primary products.[2]

1.1.4.2.4 CO Insertion Mechanism

Similar to the enol mechanism, in the CO insertion mechanism postulated by Pichler and Schulz[18] CO chemisorbs nondissociatively. CO is hydrogenated to a methyl group which remains on the metal surface and acts as the chain initiator. Propagation occurs as CO inserts into the metal-alkyl bond of the growing chain and sequentially hydrogenates to RCHOH, then RCH_2, eliminating water. As with the alkyl mechanism, *n*-paraffins and α-olefins form via hydrogenation and ß-carbon hydrogen elimination, respectively. Aldehydes can form from the hydrogenation of the intermediate acyl (RCO) species or hydrogen elimination from RCHOH followed by isomerization. Alcohols form via hydrogenation of the same RCHOH intermediate.[2,19]

1.1.4.3 ASF Kinetic Model

The Anderson-Schulz-Flory (ASF) kinetic model is one common way of describing FTS kinetics and predicting product carbon number distribution. At the heart of the ASF model is the observation that the molar amount of products declines exponentially with carbon number.[2] This implies that a single-carbon monomer is responsible for chain growth.[20] The ASF model is slightly idealized and assumes that the chain growth probability, α, is a constant independent of chain length and that both chain initiation and chain addition occur via single carbon monomers. From these two assumptions, it is possible to derive the following equations:[2,21]

$$y_n = \alpha^{n-1}(1-\alpha) \tag{1.5}$$

$$W_n = n\,\alpha^{n-1}(1-\alpha)^2 \tag{1.6}$$

$$\ln\left(\frac{W_n}{n}\right) = n\ln(\alpha) + \ln\left(\frac{(1-\alpha)^2}{\alpha}\right) \tag{1.7}$$

where y_n and W_n are the mole fraction and weight fraction of n-length carbon chain molecules in the product, respectively. Ideally, when $\ln(W_n/n)$ is plotted against n as per Eq. 1.7, a straight line will result, allowing for the determination of α. This is known as an ASF diagram.[2]

The key implications of the ASF kinetic model are that the product distribution of the FTS reaction is constrained and entirely dependent on α. It is impossible, for example, to obtain an 80 wt% selectivity towards diesel-ranged products from FTS under the ASF model. A plot of product weight selectivity as a function of α is shown in Figure 1.3.

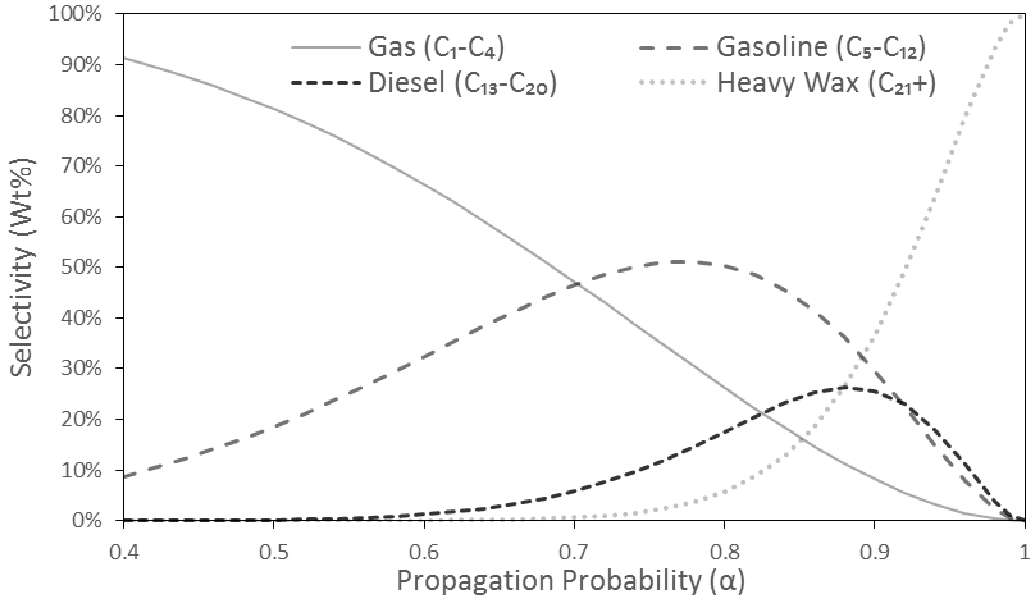

Figure 1.3 Fischer-Tropsch synthesis product selectivity as a function of α.

As seen in Figure 1.3, yields of various product classes undergo maxima as a function of α. Of particular note is the diesel-range yield, which is maximized near $\alpha = 0.88$.[2] This is a typical target for many LTFT facilities as the saturated, linear hydrocarbons in the FTS product are inherently well-suited for use as diesel fuel.[1] Alternatively, it is possible to attempt to maximize α, (approximately $\alpha = 0.95$) then crack excess heavy waxes back into the fuel range, obtaining a diesel yield of around 80%.[20] Another view of the effect of α on product distribution can be seen in Figure 1.4, which shows the product carbon number distribution for a single, fixed value of α. HTFT facilities tend to operate at a lower α value to produce more

light products and because the operation of a fluidized bed would be severely inhibited by heaver, liquid products.[2]

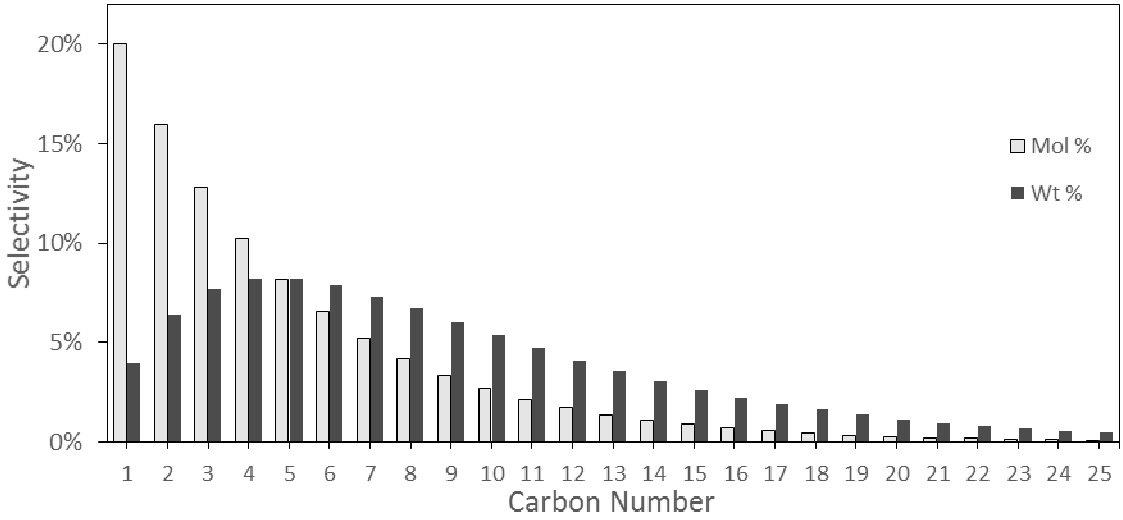

Figure 1.4 FTS product distribution by carbon number for ideal ASF kinetics with $\alpha = 0.8$

1.1.4.4 Reaction Modes and Catalysts

Fischer-Tropsch synthesis is can be operated in the temperature range of approximately 200-350 ºC. This temperature range can be further divided into the two primary FTS reaction modes: high temperature (HTFT), which is typically conducted near 340 ºC with an iron catalyst,[1] and low temperature (LTFT), which is utilized at temperatures between 200-240 ºC.[20] Ni, Fe, Co, and Ru are all active catalysts for LTFT, but the high methanation activity of nickel and extreme cost of ruthenium leave iron and cobalt as the sole viable catalyst options for industrial FTS.[1]

For both iron and cobalt, the catalyst metal oxide is typically synthesized with promoters and/or a support prior to being placed into the reactor and reduced with hydrogen, carbon monoxide, or syngas.[20] Promoters can act in a variety of different capacities including providing physical support, spacing, altering catalyst electronic properties, and assisting reduction and *in situ* re-reduction.[1,22–25] Reduction activates the catalyst, helps to increase metal surface area, and, depending on conditions, can improve selectivity and activity.[1,2,22,23]

The first FTS reaction mode, HTFT, is utilized for production of lighter hydrocarbons, aromatics, and particularly olefins, generally with a target product of light olefins, which can be sold as a chemical feedstock or oligomerized into fuel compounds.[26] Because cobalt has stronger hydrogenation activity relative to iron, at higher temperatures its methane selectivity is excessive.[26] As a result, HTFT is exclusively conducted on iron catalysts, generally a fused magnetite catalyst with added K_2O and structural promoters.[2,26] HTFT was utilized in the Brownsville, Texas FTS plant in the 1950's, and is still used extensively by Sasol in their older 'Synthol' and newer 'Sasol Advanced Synthol' (SAS) reactors which are in the Mossel Bay and Secunda, South Africa.[27] These Synthol and SAS reactors respectively utilize circulating and fixed fluidized beds and keep the reaction propagation probability in the neighborhood of $\alpha = 0.7$ in order to balance productivity, coking, and product selectivity.[2]

In contrast to HTFT, LTFT is utilized primarily in the direct production of heavy waxes and liquid fuels and can be conducted in either the gas phase with a fixed bed reactor or in a liquid medium with a slurry bed reactor.[28] The liquid product yield is maximized by raising the reaction α and hydrocracking excess waxes into the diesel range.[27] LTFT, especially utilizing a cobalt catalyst, is especially industrially relevant with the current glut of cheaper natural gas.[5] Large scale LTFT facilities include Shell's Bintulu, Malaysia plant as well as the Pearl GTL plant.[27] Both the Pearl GTL plant and the Oryx GTL plant, a joint venture between Sasol and Qatar Petroleum, utilize a cobalt-based catalyst, and are located in Ras Laffen, Qatar, where they utilize a low cost, stable supply of natural gas as a feedstock.[27] The Sasol ARGE reactors, an older, fixed bed design at the Sasolburg facility, utilize an iron-based catalyst.[27]

1.2 Low Temperature Fischer-Tropsch Synthesis

As the work covered in this document is solely concerned with the low temperature Fischer-Tropsch reaction, additional background information on the catalyst, reactor, and process are merited.

1.2.1 Catalysts

As mentioned in section 1.1.4.4, the two industrially relevant LTFT catalysts are cobalt-based and iron-based catalysts. Both iron and cobalt can be used to make viable LTFT catalysts, but their properties lead to slightly different applications for each.

The first and perhaps most important difference between iron and cobalt catalysts is cost. Cobalt metal is roughly three orders of magnitude more expensive than scrap iron.[1] While a seemingly insurmountable disadvantage, the initial cost of catalyst can be less significant relative to other capital costs as well as the indirect costs of potential process shutdown, less favorable product selectivity, or less efficient reactant usage that could result from using a cheaper catalyst with less favorable properties.[29]

Primarily as a result of the cost of the metal, cobalt is almost always supported in order to economically maximize the reactive surface area.[2,22,30] Supports also give the catalyst physical strength and attrition resistance.[31] Supported cobalt catalysts typically contain on the order of 20% Co dispersed onto the surface and into the pores of oxidic supports such as alumina, silica, titania, and zinc oxide.[2,32] Zeolite and carbon-based supports can also be viable.[33,34] Catalyst supports can have a significant impact on metal dispersion, which in turn greatly impacts particle size, reducibility, activity, and selectivity.[11,30] With the correct formulation and reaction conditions, supported cobalt is highly active and stable, allowing for very long catalyst lifetime.[1,2]

In contrast to cobalt, iron-based catalysts are most often precipitated, rather than supported.[1] Iron catalysts' strong interactions with traditional supports tend to lower activity and worsen selectivity of supported iron.[35] Without a support, precipitated iron catalysts with high surface area are physically weaker—and more subject to attrition[31]—than supported cobalt catalysts. Structural promoters for iron include silica, which acts as a binder and spacer,[2] as well alumina[36] and zinc, which increase surface area and help to prevent sintering low to moderate (<10%) loading.[37] Precipitated iron catalysts have a higher active site density relative to supported cobalt, so on a mass basis, their activities are closer than would be expected from the higher turn-over frequency of cobalt alone.[29]

Another significant difference between iron and cobalt is their sensitivity to contaminants. For example, while both catalysts are irreversibly deactivated by sulfur, iron is more resistant relative to cobalt.[38] Consequently, to minimize the very significant expense of syngas cleanup, iron catalysts are favored in applications where the feed contains significant levels of sulfur in particular.[2] The prime examples of a feed justifying the use of an iron-based catalyst are biomass and coal, as their low ratio of H_2/CO and, in the case of coal, sulfur content are both offset by iron's WGS activity and improved sulfur tolerance, respectively.[31] Cobalt on the other hand is very well suited for applications with syngas derived from natural gas due to natural gas' higher purity and favorable (higher) ratio of H_2 to CO.[5]

The way cobalt and iron catalysts behave *in situ* are significantly different. Cobalt, as previously mentioned, has stronger hydrogenation activity relative to iron.[1] Related to this, cobalt produces a more paraffinic product and more methane—around 5% selectivity at the lowest—but is more resistant to coking.[27,31,39] With the possible exception of surface atoms or very small (<5nm) particles, cobalt is not oxidized by water,[40] which would inhibit the catalyst at higher conversions. Because of their resistance to water inhibition and lack of WGS activity, cobalt catalysts can function at higher single-pass conversions but require a richer syngas with a ratio of H_2 to CO near 2.[2,40] Relative to iron catalysts, cobalt catalysts produce a negligible amount of CO_2.[31] Combined, its properties mean that *in situ*, a supported cobalt has a relatively clean metal surface, good chemically stability, and high sustained activity.

In contrast to cobalt, iron's relatively lower hydrogenation activity results in an olefin-rich product and less methane.[2] Iron catalysts produce significant amounts of CO_2 due to WGS activity, but can use a leaner syngas, such as that produced from coal or biomass.[31] Unlike cobalt, at high syngas conversion, iron is inhibited by the water produced by FTS.[31]

The final practical difference between iron-based and cobalt-based catalysts is catalyst promotion. Pure cobalt deposited on a support is a good FTS catalyst, but cobalt can also be promoted with a variety of metals such as ruthenium, lanthanum, rhenium, and platinum.[1,41] In some cases, these promoters may enhance heavy product selectivity, but the primary benefit is that they can increase cobalt's ability to reduce

and re-reduce in situ to maintain a clean, catalytically active surface.[1,2] The ability to be re-reduced helps to extend the life of the expensive catalyst and is very useful for industrial reactors.

Whereas the addition of a promoter can significantly improve catalytic performance for cobalt, for an iron catalyst, promotion is an absolutely vital step towards obtaining acceptable levels of performance. Alkali metals lower methane selectivity, increase WGS shift activity, raise olefin selectivity relative to paraffins at higher carbon numbers, and elevate higher hydrocarbon selectivity.[1,4,24,42] Utilizing the correct level of alkali metal is integral to obtaining good catalytic activity as well as selectivity towards heavy hydrocarbons. Potassium in particular has been shown to be a superior promoter relative to sodium and lithium in terms of both activity and selectivity towards heavy products.[36] It is thought alkali metals may affect selectivity by increasing the amount of CO that chemisorbs to the iron surface relative to hydrogen and thus increasing the likelihood of resulting CH_2 'monomers' forming and combining rather than being hydrogenated.[4]

While alkali metals, particularly potassium, are the most important component in a good iron-based catalyst, other promoters also enhance performance. Copper promotion facilitates the activation of the catalyst by reduction of iron oxide to the base metal.[2,24] In practice, this allows for a lower activation temperature and the use of syngas or pure hydrogen, rather than carbon monoxide for this step.[42] Other promoters include structural promoters, which help to add physical and thermal stability to the catalyst particles.[24] Silica is the classic choice for structural promoter that acts as a binder and spacer while reducing sintering,[2] while zinc has also been shown to increase activity without detrimental effects on selectivity.

For both iron and cobalt catalysts, reduction is the final step of catalyst preparation prior to reaction and how a catalyst is reduced can have a significant impact on its behavior. Reduction of metal oxides to the base metal is generally performed *in situ* at elevated temperatures in the range of 200-400 ºC.[2,8,24] Cobalt is reduced with H_2 but Cu-promoted, Fe-based catalysts can be reduced with H_2, CO, or syngas.[8] The specifics of reduction temperature and gas selection are fairly catalyst-dependent, but in general there seems to be a trade-off between increased extent of reduction at higher temperatures and reduced dispersion and sintering, which decreases available reactive surface area.[30,42] Highly dispersed catalysts and high reduction

temperatures can also induce reaction between the metal and oxidic supports to form effectively irreducible inactive mixed oxides such as cobalt silicates or aluminates.[31]

1.2.2 Reactors

As previously mentioned, controlling the reaction temperature in FTS is vital in order to obtain good selectivity. Reactor design is one of the primary methods to manage reaction heat and is thus a very important aspect of FTS.[2,39] In LTFT, there are two dominant reactor types: fixed bed and slurry bed. Fixed bed reactors utilize a shell-and-tube design with a fixed catalyst bed in each of the many parallel tubes. Slurry bed reactors were developed by Sasol in the 1990's and, similar to a CSTR, operate by bubbling syngas through a liquid wax media with suspended fine catalyst particles.[2]

1.2.2.1 Fixed Bed Reactors

Fixed bed reactors are an older and simpler design relative to slurry bed reactors. As can be seen in Figure 1.5, these reactors manage the large heat of reaction in FTS by utilizing numerous parallel, vertical tubes to increase heat transfer area and minimize the distance between catalyst bed and heat exchanger.[2,39] The shell side of the reactor contains water as a cooling medium and produces steam for power generation, while each tube consists of a fixed reactor bed where reactant gases and products flow downward across the metal catalyst.[4] Tail gas is often partially recycled and co-fed, diluting the reactants and increasing the linear velocity of the gas, which in turn serves to increase the rate of heat transfer.[2] Narrow tubes aid heat transfer between catalyst and cooling medium, but are relatively expensive for a given catalyst loading, hard to unload and reload, and result in a large pressure drop across the reaction bed. Wider tubes are easier to load and have a lower pressure differential, but would impede heat transfer.[39] As a compromise between the opposed design drives, the tubes in this reactor configuration are preferentially on the order of 5 cm in diameter for iron-based catalysts. As cobalt is more active, it generates more heat per unit volume and its tubes must be narrower still to manage that heat.[2]

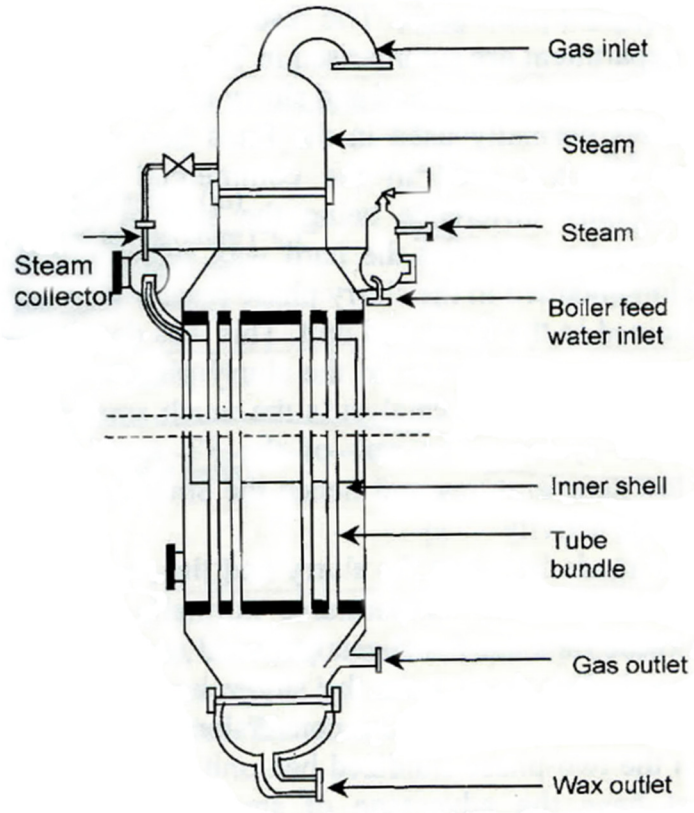

Figure 1.5 Sasol ARGE reactor[2]

Because on-line catalyst replacement is not possible with a fixed bed, catalyst lifetime becomes a very important variable in catalyst selection and formulation as well as reactor operation. For gas phase FTS in a fixed bed reactor, generally poor heat transfer exacerbates the tendency of the catalyst to sinter due to elevated temperatures and localized overheating, while liquid products are slow to diffuse out of the catalyst pores. Thus, poor catalyst selection, reactor design, or reactor conditions can easily lead to a sintered, coked catalyst with little to no activity, forcing a reactor shut down for a costly replacement.[2,39]

Fixed bed reactors are costly to scale up,[39] but there are a few benefits offered by the reactor configuration as well. Because reactor scale-up is simply accomplished by the addition of more tubes, commercial scale performance can be predicted easily with a small pilot plant.[2] For syngas with higher contaminant levels, the top catalyst in the bed can act as a sorbent, protecting the remainder of the bed and helping maintain activity.[1] Finally, because the catalyst is fixed in place and both reactants and products

flow freely downward, separation of products and tail gas is relatively simple.[2] The Sasol ARGE, shown in Figure 1.5, and Shell Middle Distillate Synthesis reactors are examples of this design in current use.

1.2.2.2 Slurry Bed Reactors

In contrast to the simplicity of the multi-tubular fixed bed reactor, the slurry bed reactor developed by Sasol is a more complicated system. The slurry bed reactor is a 3-phase system; syngas is bubbled through a liquefied heavy hydrocarbon media with smaller catalyst particles slurried within.[39] The liquid media acts as a heat sink and conductor, allowing for more thermally uniform operation and a slightly elevated reaction temperature.[39] The catalyst particles are smaller than are used in fixed bed operation,[2] allowing for higher activity with similar or lower loading. Unfortunately, the catalyst activity is somewhat offset by the slow diffusion of syngas through the liquid and into catalyst micropores.[43] Due to its design, on-line catalyst replacement is possible for a slurry bed system, allowing longer runs.[2] Compression costs are lower for slurry operation because the pressure differential across the slurry bed is due only to the hydrostatic head of the media, rather than the tightly packed fixed bed.[29,39]

The improved temperature control and product solubility in the slurry bed reactor system allow for higher selectivity towards heavy products and olefins as well as reduced CH_4 selectivity.[28] Slurry bed operation introduces the challenge of separating the fine catalyst particles, products, and media. While Sasol did eventually devise a method for this separation, this hurdle and the risk of a new reactor type delayed Sasol's implementation of the slurry reactor and has so far left Sasol as the only company to utilize it commercially.

Economically, the slurry bed reactor is a significant improvement over the fixed bed reactor for LTFT. The cost of a slurry bed reactor train is only 25-60% of the cost of a fixed bed system with the same capacity.[1,2,39] Low catalyst loading results in catalyst consumption 'four times lower' than in a fixed bad.[2] More isothermal operation allows for higher temperature operation, higher conversion, and, with online catalyst replacement, much lower down time.[1,2]

1.2.3 Process Condition Effects

While catalyst and reactor selection have a large impact on LTFT, operating conditions also have a significant impact on the reaction performance and selectivity. Operating temperature is probably the biggest factor, but reactant partial pressures, total pressure, reduction, and extent of conversion can affect the process.

At elevated temperatures, LTFT begins to more resemble HTFT in some respects. Conversion, methane selectivity, coking, and more hydrogenated, short chain product selectivities increase, while heavy product selectivity decreases.[8,11,44] Secondary products such as branched products, ketones and aromatics are also formed with increased frequency at higher temperatures.[1] Many of these effects of temperature are largely due to desorption, a primary termination step, being endothermic and more favored as temperature rises.[2] More generally, with an increase and temperature and reaction rates, thermodynamic control begins to dominate.[2]

Cobalt catalysts have a marked increase in heavy wax selectivity with increasing pressure,[29] while iron catalysts are largely unaffected.[45] Increased pressure is also linked to decreased methane selectivity[11] and increased oxygenate selectivity.[8] The impact of the ratio of H_2/CO partial pressures in the feed is fairly intuitive. As this ratio is increased, hydrogen becomes more available to the catalyst and hydrogenation becomes a more dominant aspect of the reaction. Chain lengths shorten, methane selectivity increases, and products become more saturated.[8] With higher H_2 partial pressure, coking is also decreased.

The extent of conversion—closely tied to syngas space velocity—also affects the selectivity in the FTS reaction. Decreasing space velocity results in increased conversion,[12] decreased productivity and hydrocarbon selectivity,[45] increased CO_2 formation,[45] decreased CH_4 formation,[8,12] either increased[12] or unchanged[23] long-chain hydrocarbon selectivity, and decreased olefin selectivity.[8] Many of these results are attributed to the inhibiting effect of water on iron, increasing relevance the water gas shift reaction at elevated conversion, and shift towards primary products at low conversion.[23]

1.3 Advances in Fischer-Tropsch Synthesis Technology

While in its industrial application low-temperature FTS has remained relatively unchanged since the advent of the slurry bed in the 1990's, in academia, there have been numerous advances in FTS technology that can improve upon the process. Two advances in particular are relevant to this work and will be discussed here: the use of a supercritical fluid as a reaction medium and the use of nanoscale catalysts.

1.3.1 Supercritical Fluids

Under gas phase conditions, the Fischer-Tropsch reaction has a high reaction rate and high diffusivity of gaseous reactants and products, but poor heat transfer and a tendency for liquid products to agglomerate in catalyst pores and block reactant access.[39] The high reaction rate and poor heat removal tend to cause catalyst sintering, coking, and elevated methane selectivity.[2] Slurry phase operation was designed to mitigate the problems of gas phase FTS. The slurry bed's heavy hydrocarbon media enhances heat transfer and solubility of heavy products, but has the disadvantages of impeding syngas diffusion to the active sites within the porous metal catalyst.[46] Ideally then, it follows that FTS would perform well in a medium with gas-like diffusivity, but more liquid-like thermal density, conductivity, and product solubility. The desire to find such a reaction medium is what has led researchers into investigations of supercritical fluids.

A supercritical fluid (SCF) consists of any substance above a substance-specific critical point, which consists of a critical temperature and a critical pressure.[21,47] In the supercritical phase, the properties exhibited by the fluid are intermediate between those of a liquid and those of a gas, with the potential for gases and liquids to be, respectively, miscible or soluble in the SCF.[3] Near the critical point, the thermophyscial properties of a SCF are highly tunable with small temperature and pressure changes.[47] As a result of this tenability of thermophyscial properties, while operating near the critical point of a SCF, it is possible to obtain a reaction medium that has the beneficial combination of liquid-like density and thermal properties, gas-like diffusivity and viscosity, and very low surface tension.[48]

1.3.1.1 Supercritical Fluid Effect on Fischer-Tropsch

In terms of their application as a FTS solvent medium, the unique properties of SCFs bring utility in a few significant ways. Due to the tunable properties of SCFs lying between those of a gas and a liquid, a SCF reaction medium can offer a combination of the benefits of each. Because gases and liquids are either miscible or soluble in SCFs, a SCF reaction medium allows for single-phase fixed bed.[21] The liquid-like density and thermal conductivity of SCFs aid heat transfer, reducing local superheating[46] 'hot spots' and increasing thermal uniformity without requiring a complicated media separation step.[11] Liquid-like density and low viscosity allow the SCF to extract heavy products from the catalyst surface as well as from within catalyst pores, greatly enhancing mass transfer.[49] Gas-like diffusivity allows reactant and product gases to diffuse into and away from active sites more effectively than in the slurry bed.[49]

As a result of the process enhancements SCFs can offer, numerous benefits have been documented. Yokota[46], working in Kaoru Fujimoto's group, was the first to use SCFs for Fischer-Tropsch synthesis. Using a cobalt catalyst, it was demonstrated that a supercritical *n*-hexane reaction medium manages heat far better than in a gas phase reaction and comparably to a liquid medium. This enhanced heat management drastically reduced methane selectivity relative to the gas phase reaction. Arrhenius plots indicated elevated apparent activation energy for the supercritical reaction, similar to the gas phase, relative to the liquid phase reaction. As depressed apparent activation energy is indicative of mass transfer limitation,[47] this result indicated that the supercritical hexane medium had enhanced syngas diffusion to surface and micropore active sites. Finally for this work, Yokota and Fujimoto observed a much higher selectivity towards olefins in the SCF phase reaction relative to either gas or liquid phase. The olefin production was attributed to more efficient overall product extraction. In the gas phase, heavy products cannot easily desorb, while in the liquid phase, diffusion is slow. In both cases, the mass transport limitation allows for longer contact time of the primary olefin product with the catalyst, allowing for more hydrogenation or isomerization. As the supercritical fluid has enhanced extraction and diffusion relative to gas phase and liquid phase, respectively, product olefins can be removed from the catalyst prior to further reaction.

Since the Fujimoto group's publication of the initial studies[50] on SCF reaction media use in FTS, numerous other groups have done related research confirming and expanding upon those results. Experiments have been conducted with iron-based[28,51–55], cobalt-based[11,41,43,44,46,54,56–59], and ruthenium-based[41,54] catalysts and a few results are typical throughout the literature. Firstly, as Yokota and Fujimoto found, 1-olefin selectivity—particularly for higher carbon numbers—is increased under supercritical operation.[28,43,44,51,52,54,55,59,60] Because more olefin intermediates are extracted prior to further reaction,[60] the selectivity towards side products such as 2-olefins[51,52] is reduced. CO conversion is often either intermediate[41,46,54] or improved[11,28,43,57,58] relative to gas and liquid phase operation. Activity maintenance is improved by heat management and wax extraction[3,59,61] Methane[11,43,44,50,53,54,57–59] and CO_2[3,11,44,53,54] selectivities are typically depressed relative to the gas phase, and α and heavy product selectivity are similar or improved relative to the gas phase and elevated relative to the liquid phase.[11,41,43,44,46,54,57–59]

1.3.1.2 Process variables

With the introduction of a supercritical fluid reaction media, two new process variables—solvent selection and media ratio—are introduced. Additionally, other process variables' effects on the reaction performance can be altered.

Yokota and Fujimoto[54] proposed the following criteria for supercritical reaction media selection in FTS:

1. The critical temperature and pressure of the fluid should be slightly below the temperature and pressure of the reaction
2. The fluid should be stable under reaction conditions and should not poison the catalyst
3. The fluid should have a strong affinity for paraffins in order to better extract products from the catalyst and reactor.

According to the criteria set out by Yokota and Fujimoto, saturated hydrocarbons, particularly pentane and hexane, seem to be the most likely candidates for media selection as they are have suitable critical

properties, are inert in FTS, and are very suitable solvents for FTS products.[61] Unsurprisingly then, the most commonly used solvents in supercritical FTS are pentane,[11,41,44,57,58] and hexane,[3,11,28,41,44,53–56,62] but numerous other solvents including hydrocarbons[28,44,51,52,54,56] like propane, heptane, decane, and benzene or oxygenates like methanol,[54] have also been utilized at supercritical or near-critical conditions.

Liu et al[56] compared Fischer-Tropsch reaction performance with a cobalt catalyst under a variety of solvents. For *n*-paraffin solvents ranging from hexane to hexadecane, they saw negligible effect of solvent carbon chain length on α value, CH_4 selectivity, or light olefin selectivity, but did observe a slight decrease in CO conversion and significantly more heavy 1-olefins under operation with longer-chain solvents. Reactions conducted with branched solvents were comparable to their *n*-paraffin counterparts in most respects, but had a lower selectivity towards 1-olefins. In similar work, Linghu et al.[44] compared solvents with carbon chain lengths between five (pentane) and ten (decane) and saw little impact of the solvent on CO conversion, CH_4 selectivity, or α. Compared to supercritical pentane, supercritical hexane, and near-critical heptane, decane was well outside of the supercritical region and had a correspondingly lower selectivity towards olefins as well as a higher selectivity towards C_4-C_8 hydrocarbons. Irankhah and Haghtalab[63] saw results similar to those of Linghu, with pentane, hexane, heptane, and mixed solvents having little impact on CO conversion, CH_4 selectivity, or CO_2 selectivity. Perhaps most importantly for industrial application, mixed solvents do not seem to have a negative impact on FTS performance, allowing for a solvent feed via a partial solvent/product recycle.[60,63]

Along with solvent selection, the introduction of a supercritical reaction media adds the ratio of media to syngas as a process variable. The relative amounts of solvent and reactants in the reactor affect the residence time, reactant concentrations, contact time, as well as the mixture properties. Elbashir and Roberts[64] varied the ratio of hexane to syngas over a cobalt catalyst. They saw that transitioning from gas phase to supercritical FTS (hexane:syngas = 3) increased α, decreased CH_4 production, and had little effect on CO conversion. When going to higher ratios of hexane:syngas (6:1, 9:1), there was significant decline in conversion, a minor decrease in CH_4 selectivity, and minimal impact on α. Similarly, Linghu et al[44,60] used nitrogen as a balancing gas to compare hexane:syngas ratios from 0.5 to 3.5 at constant total pressure.

They saw very little difference in conversion, CH_4 selectivity, or product distribution, but increased 1-olefin selectivity at higher hexane:syngas ratios. Further, when comparing the olefin selectivity between a hexane:syngas ratio of 2.5 and 3.5, the higher hexane partial pressure led to a very much enhanced olefin selectivity. This higher selectivity was attributed to enhanced extraction due to the critical pressure of the fluid being surpassed—perhaps more concretely demonstrating the advantage of a SCF solvent over a more traditional liquid solvent.

In addition to the new process variables introduced with the inclusion of a SCF reaction medium, the presence of the SCF media can also alter the effect of more traditional process variables such as temperature, pressure, gas flow rate, or syngas H_2/CO ratio. In general, the effect of changing process conditions under a supercritical solvent is similar to that seen in the gas phase, but less severe.[51,65] In some cases however, perturbing reaction conditions induces a change in solvent properties which can in turn cause larger or different changes in reaction behavior than would be expected due to the perturbation alone. Elbashir and Roberts[64] determined the critical point for the bulk reaction mixture obtained from FTS over a cobalt-based catalyst at ~75% CO conversion (238.2 ºC, 37.2 bar), then examined the effect of temperature and pressure variations around that critical point. In gas phase operation, increasing temperature results in a monotonic decrease in α and increase in CO conversion. Under the influence of a supercritical solvent, reaction behavior is more complicated. Varying temperature from 230 ºC to 260 ºC, they saw a maximum in both CO conversion and α at 250 ºC among conditions studied. Similarly, varying pressure from 35 to 80 bar, they saw a maximum in CO conversion at 65 bar among the pressures examined and very little influence of pressure on α, save that α decreased at the highest pressure studied. Bochniak and Subramaniam,[55] in their work with an iron-based catalyst in supercritical hexane, also saw increased pressure greatly improving CO conversion as well as elevating 1-olefin selectivity. The observed changes in the reaction behavior under a SCF media near its critical point are not attributed to the change in reaction kinetics but rather to changing solvent properties and resulting absorption/desorption equilibria.

In similar work, Durham et al[65] saw a SCF reaction media mitigate the effect of process conditions on an iron-based catalyst. They saw minimal impact of syngas H_2/CO ratio on activity or liquid product

selectivity. Upon increasing temperature near the critical point, they saw increasing apparent activation energy—consistent with decreased diffusion resistance—as the solvent becomes gas-like and less dense. When pressure was increased, selectivity towards aldehydes increased significantly. As aldehydes are believed to be a reaction intermediate not seen under gas phase operation, their presence was attributed to the extraction caused by increased solvent strength of the more dense SCF. Finally, none of the variables investigated greatly impacted α for their system.

1.3.2 Nanoscale Catalysts

The second advance in Fischer-Tropsch technology that is relevant to this work is that of nanoscale catalysts. While somewhat arbitrary, 'nanoscale' will be used here to describe catalysts that are smaller than 100 nm in at least one dimension. Such catalysts are increasingly of interest academically, and remain desirable in some commercial catalysis as well.

Small catalyst particles have higher surface area per mass and, as FTS is a heterogeneous reaction that takes place on the metal surface, increasing the 'surface density' of the catalyst should increase apparent catalyst activity.[66] In a simple catalyst whose structure plays no role in reaction, increasing activity should be seen as catalyst particles approach the size of individual atoms and the catalyst effectively becomes entirely surface. While this is not quite the case in FTS, smaller particles do have higher activity to a point. Iglesia et al.[67] saw that in the range of 10-100 nm, cobalt particles' activity almost directly corresponded to the level of dispersion, which is inversely proportional to particle size. In addition to the activity and throughput increases that come with the increased surface area, some nanoscale catalysts have also been shown to give benefits such as increased olefin selectivity.[68,69] The benefit of increased surface area, backed by findings such as Iglesia's, gives an incentive to synthesize and research nanoscale catalysts for FTS.

1.3.2.1 Nanoscale Catalyst Supports

While cobalt catalysts are almost universally dispersed onto a support in order to maximize surface area per mass of the more expensive metal, traditional iron catalysts, because of their lower cost and

unfavorable interactions with oxidic supports, are typically unsupported. In contrast, for both iron and cobalt catalysts on the nanometer scale, literature sources tend to use a support—such as the multiwalled carbon nanotubes (MWNTs) shown in Figure 1.6—in order to reduce attrition as well as to provide structural stability.[34,35,40,68–72] As with a typical cobalt catalyst, this also aids in maximizing the use of the available catalytic surface.

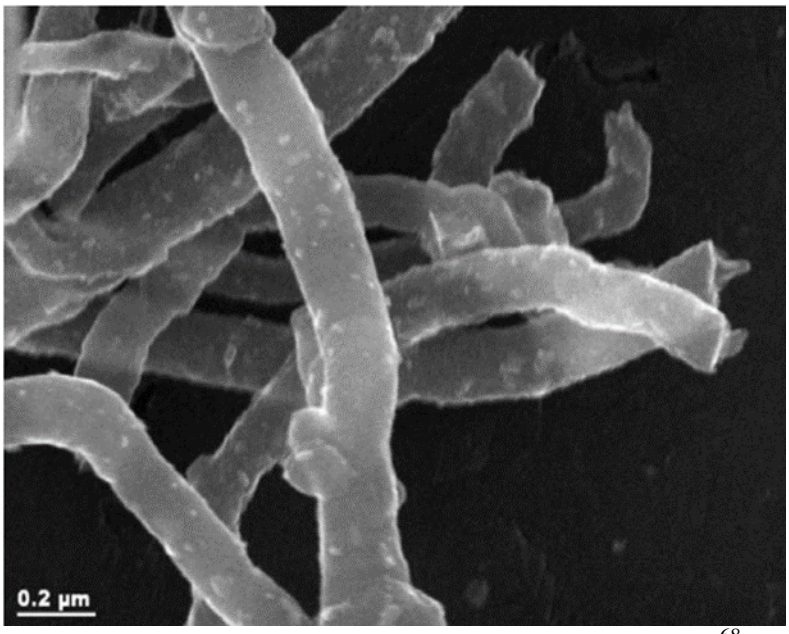

Figure 1.6 Iron nanoparticles (white) supported on MWNTs.[68]

The first option for Fischer-Tropsch catalyst supports are traditional, oxidic supports such as alumina, titania, and silica.[68,73] These supports have high surface area,[1] are porous,[10] and can have strong interactions with the catalyst metal.[31] Unfortunately, while stronger catalyst-support interactions can increase dispersion and impede sintering by stabilizing small crystallites,[73] they can also lead to the formation of inert oxides such as cobalt silicate[34] or iron aluminate,[74] lower activity, and cause poor selectivity towards heavier products.[35] Thus, oxidic supports can yield a well-dispersed catalyst, but risk poor selectivity, irreducibility and extreme activity decline as inert compounds form.[1]

To combat the issues arising from overly strong catalyst-support interactions seen with oxidic supports, one alternative is carbon-based supports like carbon nanofibers (CNFs) or carbon nanotubes (CNTs). Carbon nanofibers and nanotubes are stable and inert under FTS conditions[34,75] and eliminate the possibility of excessive particle-support interactions, even for nanoscale catalysts. In addition to allowing

for better reducibility and activity, this allows for deconvoluting particle-support effects from particle size effects for nanoscale catalysts. Both Bezemer et al.[34] and den Breejen et al.[75] used 'fishbone' type CNFs with diameters around 30 nm for this express purpose. In both studies, the CNFs provided an adequate catalyst support, but neither author focused on their benefits aside from negating the drawbacks of oxidic supports.

Carbon nanotubes are a second viable carbon-based support. Because of their tubular structure and outstanding properties, CNTs present an interesting candidate for a catalyst support material. While individual properties are dependent on tube type, CNTs typically have excellent heat and electrical conductivities, resistance to a variety of chemicals, good mechanical properties, high specific surface area, and a unique molecular structure that presents interesting possibilities for catalyst supports.[48,71,76] Studies have also shown that in FTS, carbon-based supports provide higher selectivity to olefins, a valuable chemical class in most cases, and that among carbon supports, CNTs were more selective still.[68,69]

Bahome et al.[68] demonstrated an active, stable iron-based catalyst supported on multi-walled carbon nanotubes (MWNTs). Testing showed that the MWNT support was inert, stable up to 550 ºC, and that the catalyst was stable with time on stream with low methane selectivity. In contrast, van Steen and Prinsloo,[72] with a slightly different iron-on-carbon catalyst, saw low activity and significant deactivation with time on stream. Van Steen and Prinsloo suggested that iron inside the structure of their herringbone CNT support might have been inaccessible to hydrogen for reduction. Bahome et al. attributed the deactivation to the herringbone, rather than tubular CNT support structure. Herringbone CNTs allow for stronger catalyst-support interaction and better dispersion at the cost of more difficult reduction.

1.3.2.2 Catalyst Synthesis Techniques

Synthesizing and incorporating nanometer scale catalysts into the Fischer-Tropsch process is no simple task. As a result, researchers utilize a wide variety of methods to controllably synthesize their catalysts. Each method has benefits and drawbacks, but the catalyst preparation methodology is important

because it can affect particle size, shape, size distribution, and catalyst-support interactions, all of which affect the activity of the final product.[9]

In addition to those methods covered below, there are numerous colloidal methods, methods utilizing pH and electrostatics to deposit catalysts, and more,[9] but these synthesis methods covered were chosen due to either their popularity, efficacy, or, in the case of the microemulsion method, novel potential.

1.3.2.2.1 Incipient Wetness Impregnation

One method, perhaps the simplest,[9] of dispersing a metal catalyst onto a support surface is incipient wetness impregnation or IWI. In the incipient wetness method, the pore volume of the support is first determined. Typically, this is done by addition of fluid such as DIUF water until a certain visual change such as "looking sticky" is observed.[34] Next, a catalyst precursor such as a metal acetate or nitrate salt is added to a quantity of solvent equivalent to that needed to 'wet' the desired quantity of dry support. A calculated amount of the precursor-solvent solution is then added dropwise to dry support material and dried. After drying, the catalyst precursor and support are calcined at elevated temperature in order to convert the acetate or salt catalyst precursor into the metal oxide.[9]

Some significant variables that can affect the final product include solvent choice, which can be ethanol, water, or even hexane, the catalyst precursor—salt or acetate—as well as catalyst loading onto the support, rate of liquid addition, and the temperature and duration of drying and calcination.[9,69] The amount of catalyst loading, for example, has been shown to be inversely related to dispersion and particle size.[34] The use of ethanol in lieu of water as a solvent also seems to decrease particle size, as ethanol's lower surface tension increases wetting of the support surface, increasing dispersion.[34] Additionally, because of the method in which it dries, use of an acetate precursor tends to give increased dispersion[77] which again has been shown to also yield smaller catalyst particles.[34]

IWI is one of the more straightforward methods to produce a catalyst with small particles but it is not without its drawbacks. Because the rate of particle deposition is somewhat roughly controlled, some

researchers have seen a broad size distribution for the catalyst particles.[9] This is not always the case however, as Bezemer et al. saw distributions with standard deviations below 20% of the particle size.[34]

1.3.2.2.2 Deposition Precipitation

Another major technique being used to synthesize nanoscale catalysts is deposition precipitation or DP. Similar to IWI, a catalyst precursor salt is dissolved, typically in water, and added to a catalyst support. In contrast to IWI, for deposition precipitation, the support is slurried. Next, a precipitating agent such as K_2CO_3, ammonia, or urea is added to the stirring slurry. In this technique, the precipitating agent serves to shift the solution's pH, causing the metal salt to controllably precipitate.[71]

Van Steen and Prinsloo[72] investigated the effect of using K_2CO_3 and urea DP methods alongside IWI and saw that the methods yielded significantly different catalysts. In their study, both DP methods yielded highly dispersed catalyst metals, but the catalyst prepared using K_2CO_3 had much larger crystallites. Of the three catalysts, the IWI catalyst actually outperformed both DP catalysts, but deactivated down to comparable levels with time on stream, as shown in Figure 1.7. Selectivity was comparable between the three differently prepared catalysts and it is hypothesized that differing particle size distributions between the catalysts led to differing activities.

In contrast to the results of van Steen and Prinsloo, Bezemer et al.[34] saw that DP produced particles larger than IWI, but the DP catalyst synthesized with ammonia had selectivity towards higher hydrocarbons (C_{5+}) superior to that of the IWI catalyst. Further, Bahome et al.[68] saw that the while selectivity was comparable between different catalysts, catalysts prepared via a modified DP with a urea precipitating agent showed conversion similar to that of a catalyst prepared via IWI, but as the DP catalyst had a lower loading of active metal, the DP catalyst was more active on the basis of its mass of metal.

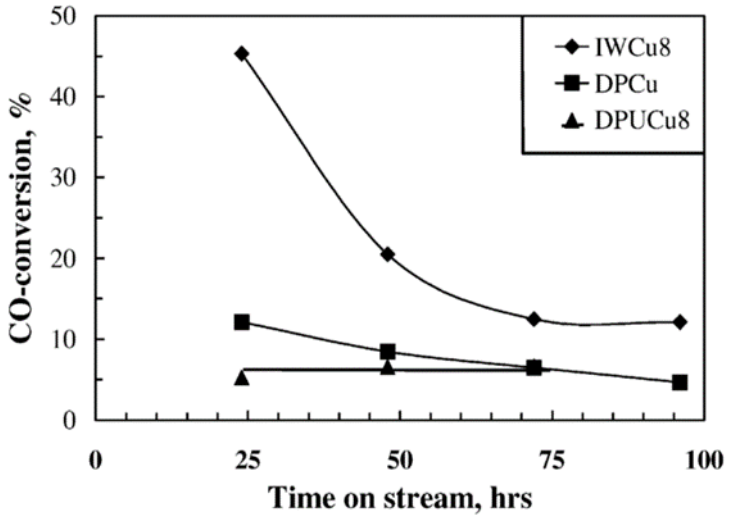

Figure 1.7 Conversion data for IWI and DP catalysts with time on stream.[72]

From the three studies comparing synthesis methods, it seems that the modified DP with urea produces a catalyst that can be comparable in activity to that produced by IWI, but that with potentially superior selectivity towards more valuable (heavier) products.

1.3.2.2.3 Solvothermal

A third method, wholly different from the controlled deposition present in both IWI and DP methods, is the solvothermal method. In this method, metal nanoparticles are synthesized and deposited onto a catalyst support in separate steps. For this catalyst preparation method, a metal oleate precursor was used by both Park et al.[74] and Guczi et al.[69] In those studies, a metal oleate precursor was generated from a metal salt and either sodium oleate or oleic acid. The metal (iron or cobalt) oleate was then placed in octadecene and decomposed via controlled heating. Park took the synthesized nanoparticles and dispersed them in hexane, while Guczi dispersed the particles in ethanol. In both cases, the dispersed nanoparticles were added to a support followed by drying.

Using the solvothermal catalyst synthesis method, Park[74] showed that the produced metal nanoparticles are relatively spherical and uniform, as seen in Figure 1.8, with size being directly related to the temperature at which oleate decomposition took place. For temperatures between 130 ºC and 250 ºC,

synthesized iron oxide particles ranged from 2 nm at 130ºC to 12.4 nm at 250 ºC. After XRD analysis, it was concluded that once the particles were deposited onto the support, there was no significant particle agglomeration. While for smaller particles there were some challenges in reduction, the larger particles produced at elevated temperatures were active with good selectivity. When compared to a control catalyst made via IWI, the solvothermally produced catalysts were superior, but the catalyst produced from IWI may have also been impeded by particle size effects.

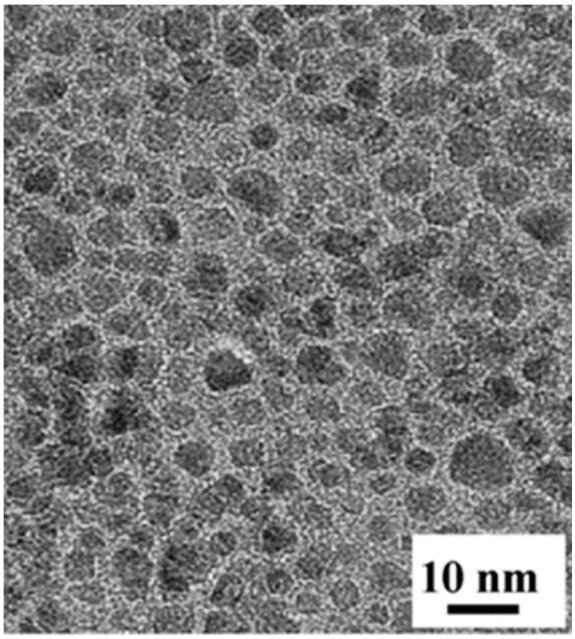

Figure 1.8 Relatively uniform, spherical iron oxide nanoparticles as synthesized from iron oleate at 200 ºC.[74]

In contrast to Park's process, the temperature at which Guczi et al.[69] decomposed the oleate precursor is not given. Additionally, the synthesized iron oxide particles are less uniform and, as seen in Figure 1.9a, tetrahedral. The particles agglomerated to a significant extent when placed onto the support. Similarly, cobalt nanoparticles produced in by the same method were large—on the order of 250 nm—and non-spherical. Both the iron and cobalt nanocatalysts produced in this study had very low chain growth

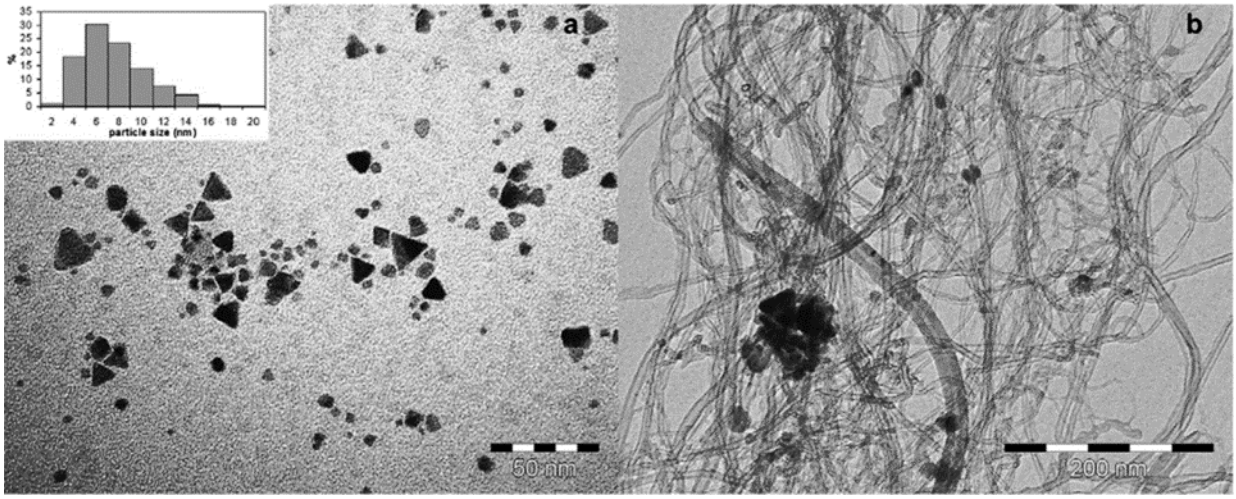

Figure 1.9 (a) Tetrahedral iron oxide particles produced via thermal decomposition of iron oleate and (inset) histogram of particle size. (b) Iron oxide particles agglomerated after deposition onto multiwalled carbon nanotubes.[69]

probabilities, which resulted in poor selectivity towards fuel range (C_{5+}) products. Incomplete reduction is offered as a possible explanation of the poor activity observed for these catalysts. A second set of catalysts in this study were prepared via IWI with an acetate precursor. These catalysts outperformed those prepared via the solvothermal method in reducibility, activity, and selectivity.

It appears from the data presented by Park et al.[74] that the solvothermal method of catalyst preparation has the potential, when tightly controlled, to create uniform spherical nanoparticles that are active and possibly superior to catalysts produced via IWI. Unfortunately, the catalysts were unpromoted, so it is hard to draw conclusions on realistic performance. The data published by Guczi[69] on the other hand, shows that catalysts produced from oleate decomposition could also be very poor FTS catalysts.

1.3.2.2.4 Microemulsion

While thus far less utilized for FTS catalyst synthesis, microemulsions are another possible method for nanoparticle synthesis. Similar to certain polymer synthesis techniques, catalyst synthesis by microemulsion involves the use of a mix of hydrophobic, hydrophilic, and surfactant molecules together to create small micelles in which catalyst particles can form.[9] Using this method allows for creation of a 'nanoreactor' in the stable, isotropic solution wherein it is possible to control size, geometry, and morphology of precipitating particles.[78,79] In this technique, two microemulsions can be mixed to induce precipitation, or a precipitating/reducing agent can be added to a microemulsion. In either case, variables such as relative amounts of surfactant, water, and organic phases, reducing compound, temperature, and electrolyte presence can theoretically be manipulated to yield a highly tailored catalyst synthesis method.[9,79]

Because of the how extensively the method can be tailored, is possible to synthesize precisely sized particles with very narrow particle size distributions via microemulsions. Some synthesized catalysts have been shown to have good selectivities in terms of producing more heavy hydrocarbons and less methane.[9] Unfortunately, though direct scale up seems to be straightforward, the volumetric yield is still a limiting factor.[79] Additional drawbacks include the requirement of relatively harsh chemicals such as hydrazine and the possibility of poor catalyst dispersion on the support. While microemulsions are theoretically a nearly

perfect synthesis method, as a result of its complicated nature and limited reliability, the method is still largely limited to being a curiosity in FTS.

1.3.2.3 Particle Size Effect

Some of the most interesting findings in Fischer-Tropsch research relate to particle size effects. On both iron and cobalt catalysts, activity and conversion increase as particle size decreases from bulk scale down to the nanometer scale.[34,74] As Fischer-Tropsch Synthesis is a surface-catalyzed reaction and reducing particle size increases specific surface area, this is to be expected. Interestingly, the trend abruptly reverses for catalysts around 6-8 nm. Below that particle size, activity and selectivity to heavier products plummet.[34,74,75] This phenomenon is well-documented in the case of cobalt catalysts, but less so for iron-based catalysts.

Figure 1.10 and Figure 1.11 display various aspects of the particle size effect for nanoscale cobalt catalysts supported on carbon nanofibers. In Figure 1.10a,[34] turnover frequency—a normalized surface activity—is displayed as a function of particle size. For particles larger than about 6 nm, this normalized activity is constant; for given surface area, the activity is constant regardless of particle size. Below that threshold, the catalyst activity per surface area drops precipitously. This drop off can also be seen in Figure 1.10b,[34] which shows activity on a mass basis, rather than a on a surface area basis. As shown in this figure, as catalyst size decreases, the surface per mass increases. This trend dominates and causes decreasing

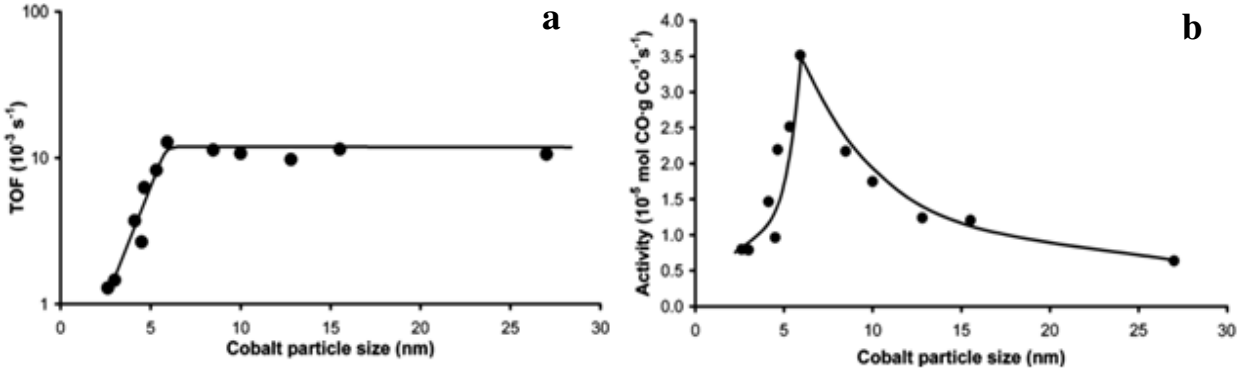

Figure 1.10 (a) Turnover frequency of Co-CNF catalyst as a function of Co particle size. **(b)** Activity of Co-CNF catalyst as a function of Co particle size. (220ºC,1 bar, $H_2/CO = 2$)[34]

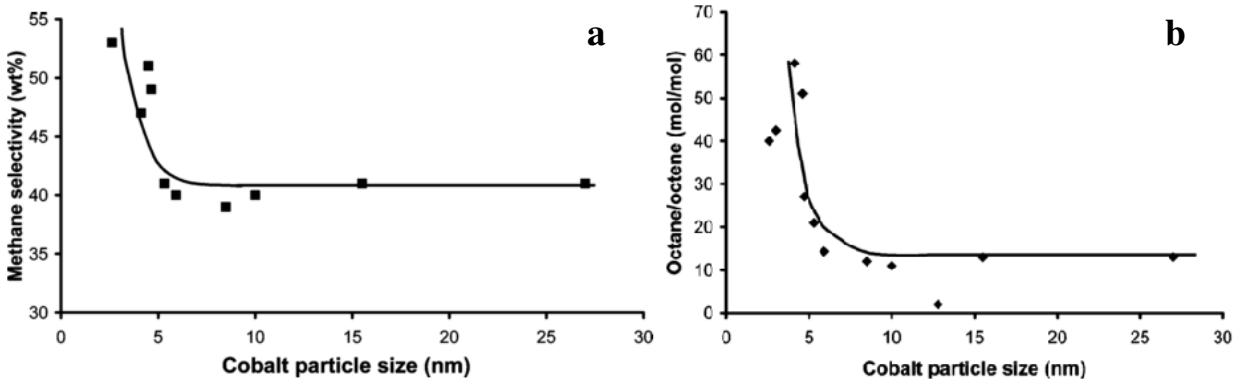

Figure 1.11 (a) Residence time (τ, seconds) of reversibly bound CO and CH_x reaction intermediates as a function of Co particle size **(b)** Residence time (τ, seconds) of reversibly bound CO and OH_x reaction intermediates as a function of Co particle size (210ºC, 1.85 bar, $H_2/CO = 10$).[75]

particle size to greatly increase activity until a sudden fall in activity below around 6 nm. Figure 1.11[75] is from follow-up work by the same group and shows a similar trend and offers some insight into the cause of the plummet in activity. The figure shows methane selectivity and the ratio of octane to octene, each plotted as a function of cobalt particle size. Both of these variables are related to the catalysts' ability to hydrogenate reactants, specifically CO and octene. Bezemer postulated that the continued hydrogenation and hydrogen dissociation at small particle sized may indicate that the active sites for chain growth are becoming inactive, leaving more carbon species to be fully hydrogenated.[34]

Interestingly, a very similar trend of active large particles and inactive small particles was also observed at a more industrially relevant pressure, 35 bar. The particle size at which the sudden activity decrease occurred was 8 nm rather than 6 nm, and the 6 nm particles which were near-optimal at 1 bar showed poor activity at the elevated pressure.[34]

After ruling out other alternatives such as cobalt carbide formation, Bezemer et al. concluded that the particle size effects seen in Co-CNF nanocatalysts were a result of "nonclassical particle size effects in combination with the invasive character of CO."[34] In short, it was hypothesized that the FTS reaction requires multiple different types of active sites and that below a certain particle size, the active domains are unstable or contain the wrong sorts of sites for the individual reaction steps. This greatly elevates the activation energy required for the reaction as a whole and as a result, the optimal particle size for cobalt catalyzed FTS is around or slightly above 6-8 nm.[34]

Den Breejen et al.[75] sought to explain the particle size effect seen by Bezemer. While the catalyst was prepared identically to that of the previous paper, the FTS reaction itself was conducted very differently. The heart of this study is SSITKA—steady-state isotopic transient kinetic analysis. SSITKA involves observation of the reacting catalyst surface *in situ*. During steady-state operation, a reactant in the feed stream is replaced with a different isotope (^{13}CO vs ^{12}CO or D_2 vs H_2) and the isotopically labeled reactants and products are then monitored via GC-MS. This data allows for additional insight into residence time and surface coverage of reactants and reaction intermediates. Here again, the inert nature of the carbon nanofiber support is integral to the utility of the process, allowing for the observation catalyst performance free of interference from the support.

From the SSITKA experiments and subsequent analysis, it was concluded that a few different mechanisms may be at work to cause the particle size effect observed in both studies. First, as can be seen in Figure 1.12, the reversibly bonded CH_x and OH_x surface residence times dramatically increase for particles below 6-7 nm. This may point to increased bonding strength between these intermediates and the cobalt surface, decreased CO dissociation, or slowed hydrogenation of these precursors to methane and water respectively.[75] Similarly, for small particles, the surface coverage of CO, CH_x, and OH_x decrease

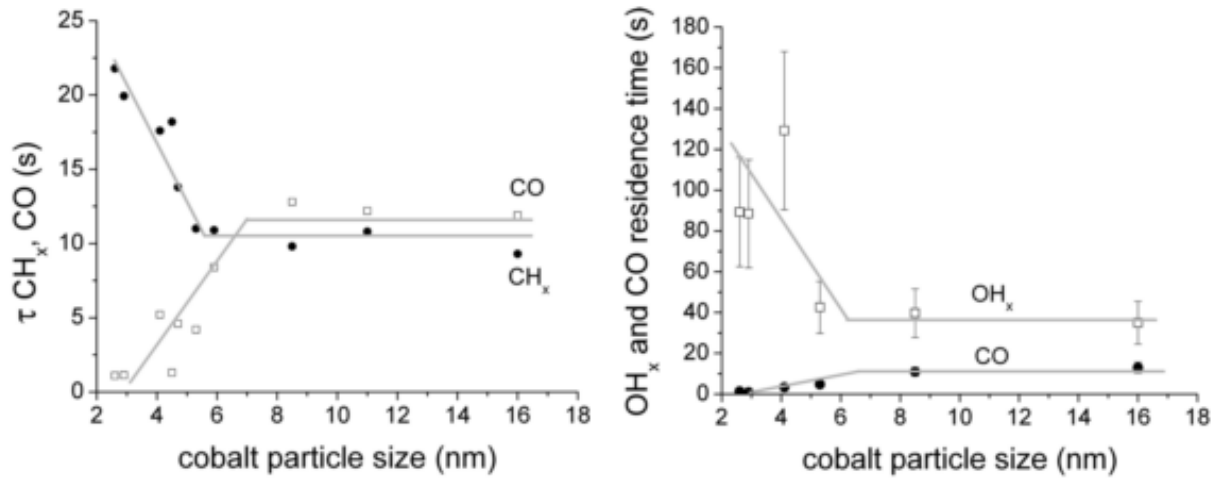

Figure 1.12 (a) Residence time (τ, seconds) of reversibly bound CO and CH_x reaction intermediates as a function of Co particle size. **(b)** Residence time (τ, seconds) of reversibly bound CO and OH_x reaction intermediates as a function of Co particle size (210ºC, 1.85 bar, $H_2/CO = 10$).[75]

while that of H_2 increases. This and an increase in irreversibly bound CO on small particles together led to the conclusion that irreversibly bound CO blocked some of the cobalt surface.[75]

A cuboctahedral geometric model, shown in Figure 1.13, was constructed in an effort to explain observed surface coverage and residence time effects based on the geometry of the catalyst particles. Briefly, coordination number, the number of adjacent atoms for a given catalyst atom, can be related to the geometry of the particle and its diameter. Using calculated irreversible CO coverage and particle size data along with the geometric model, the irreversible CO coverage can then be related to the fraction of surface sites with a given coordination number, as shown in Figure 1.13.[75] From the plot in the figure, the correlation between low coordination numbers—which are more abundant in small particles—and irreversible CO coverage is clear. Den Breejen et al. concluded that adsorbed CO could bind irreversibly to low coordination number sites because of the sites' more localized valence electrons and that this phenomenon was a contributing factor towards poor catalyst performance for particles less than 6-7 nm.[75] A final observation was that while coverage of most compounds dropped for small particle sizes, the H_2 coverage rose for these catalysts, possibly supplying a reason for elevated methanation at these particle sizes.

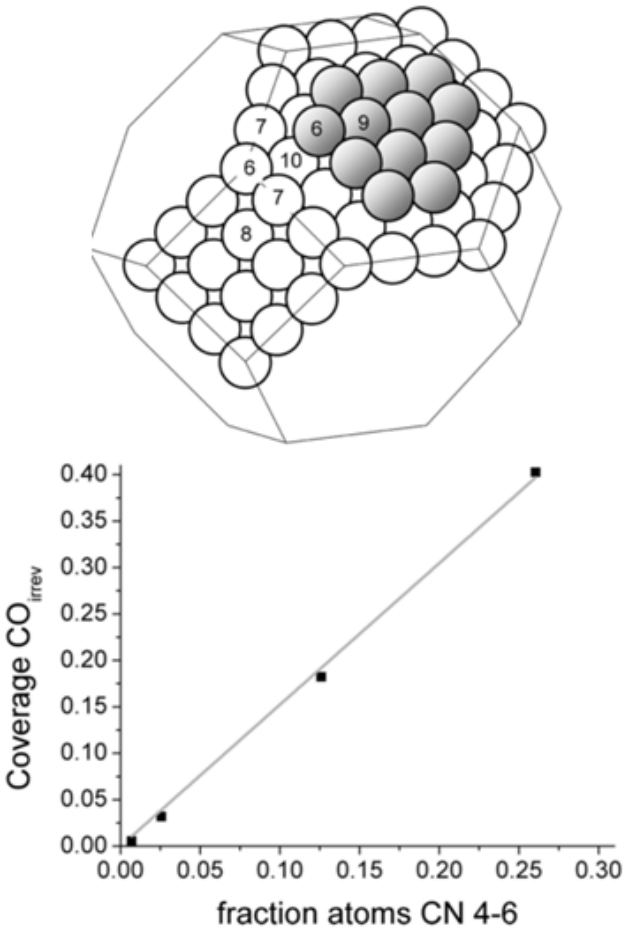

Figure 1.13 Cuboctahedral geometric model and corresponding plot of irreversible CO coverage as a function of the number of low coordination number sites.[75]

The particle size effects seen for small cobalt particles can likely be attributed to the fact that, as the surface area to volume ratio is increasing for small particles, the geometry and chemical affinity of that

surface may change as well, leading to selective or irreversible adsorption of one reactant or intermediate, ultimately compromising the catalyst activity.[34,75]

Chapter 2: Influence of a Carbon Nanotube Support and Supercritical Fluid Reaction Medium on Fe-catalyzed Fischer-Tropsch Synthesis

Foreword

The content of this chapter is largely that of a paper by the same name, published in Applied Catalysis A: General.[80] Follow-up work, featured in Chapter 3, calls some of the conclusions regarding carbon support effect into question, but the text here is kept close to as-published, save where new TGA data allowed for more accurate reporting related to metal content.

2.1 Introduction

Fischer-Tropsch synthesis (FTS) is a well-established catalytic process that produces liquid fuels and chemicals via the polymerization and hydrogenation of CO. FTS is a surface-catalyzed process typically conducted over an iron-based or cobalt-based catalyst. The most common products are straight-chain paraffins and α-olefins, but FTS product functionalities can also include alcohols, aldehydes, branched hydrocarbons, and aromatics.[8,12]Among the more desirable FTS products are the light olefin fraction, which can be used as a feedstock for many other processes, the heavy wax fraction, and the diesel fraction, which has low sulfur, low aromatics content, and a high cetane number.[8,26,28]

Gas phase and slurry phase FTS reaction modes can suffer from significant heat and mass transfer limitations as a result of their multiphase, heterogeneous nature. As an alternative to these traditional reaction modes, research has been conducted on mitigating transport limitations via the use of a supercritical fluid (SCF) reaction medium. SCF properties are intermediate between those of a gas and a liquid and, near the critical point, are highly tunable with small temperature and pressure changes.[47] As a result of this tunability, it is possible to simultaneously obtain liquid-like density and thermal properties, gas-like diffusivity and viscosity, and very low surface tension.[48] A well-selected SCF should be unreactive, slightly above its critical pressure and temperature at reaction conditions, and capable of solvating reaction products.[54] Alkanes fit these criteria as they are inert under FTS conditions,[11,19] can solvate FTS

hydrocarbon products, and some, particularly hexane, (T_c = 234ºC, P_c = 2.97 MPa) have critical points near the reaction conditions of low temperature FTS. When SCFs are utilized as an FTS reaction medium (SC-FTS), their impact is largely due their ability to remove heat and soluble products from the reaction bed, to enable single-phase operation, and to balance product desorption and diffusion relative to gas phase or slurry phase operation.[46]

Since the pioneering study by Yokota and Fujimoto,[50] researchers have reported a variety of benefits from SC-FTS. Because a SCF reaction medium allows for the extraction of olefin intermediates from the catalyst bed prior to further reaction,[60] α-olefin selectivity, particularly at higher carbon numbers, is increased under supercritical operation,[28,43,44,46,51,52,54,55,59,60] while selectivity towards side products such as 2-olefins[51,52] is reduced. Similarly, Durham et al.[53] observed significant extraction of aldehydes and methyl ketones with a K-promoted, precipitated iron catalyst under SC-FTS. Improved mass transfer under SC-FTS can also lead to improved CO conversion relative to gas and slurry phase operation.[11,28,43,57,58] Improved activity maintenance is often observed due to the capability of the SCF to remove heat and heavy hydrocarbons from the reaction bed, which mitigates catalyst deactivation via sintering and coking, respectively.[3,59,61] Improved heat management under SC-FTS suppresses methanation, while more effective removal of water inhibits the water-gas shift reaction. As a result, lower selectivity toward methane and CO_2 are commonly observed under SC-FTS.[3,11,43,44,46,50,53,54,57–59] Finally, the heavy product selectivity observed under SC-FTS is often similar or improved relative to gas phase FTS operation and elevated relative to slurry phase FTS operation.[11,41,43,44,46,54,57–59]

For a surface-catalyzed reaction like FTS, the high specific surface area of nanoscale (<100 nm diameter particles) catalysts presents an opportunity to obtain enhanced activity relative to traditional, precipitated catalysts, but in order to reduce attrition and provide mechanical strength, nanoscale catalysts typically require incorporation onto a support material.[66] Typical oxidic supports (e.g. SiO_2) can prevent sintering and provide mechanical strength, but can also have strong interactions with catalyst particles and prevent reduction, especially for smaller, more dispersed particles.[22,34] More recent investigations have demonstrated that carbon supports, especially carbon nanotubes, can largely avoid excessively strong

catalyst-support interactions while offering superior FTS performance relative to precipitated iron or cobalt catalysts.[34,68,70,72,73,81–83]

Given that with traditional, precipitated catalysts a SCF medium can offer significant operational advantages and enable probing of the FTS reaction products and mechanism, a study was undertaken to investigate whether similar benefits could also be observed over a nanoscale, carbon-supported catalyst. This chapter focuses specifically on the impact of a supercritical hexane reaction medium on FTS reaction performance over iron-based nanoparticle catalysts supported on carbon nanotubes, including a comparison with a traditional precipitated catalyst.

2.2 Materials and Methods

2.2.1 Catalyst Preparation

In this study, two carbon-supported, iron-based nanoscale catalysts were synthesized, characterized, and tested for their FTS catalytic performance. The nanoparticle catalysts were supported on multi-walled carbon nanotubes (MWNTs) and were prepared both with and without potassium promotion in order to enable deconvolution of support and promoter effects. The K-free catalyst is denoted as CFeCu, while the K-promoted catalyst is denoted as CFeCuK. To serve as a basis of comparison for catalytic performance for the carbon-supported catalysts, a traditional, co-precipitated catalyst, denoted FeZnCu, was also synthesized, characterized, and tested.

The MWNT support for the nanoscale catalysts was purchased from Sigma Aldrich (Catalogue No. 659258-10G) and had listed properties of D = 110-170 nm, L = 5-9 μm, and 90+% purity on a carbon basis. In order to remove amorphous carbon, increase surface area, and provide functional group anchoring sites for the catalyst particles, a procedure adapted from Abbaslou et al.[73] was used to pretreat the MWNT support. A portion of the as-received MWNTs was refluxed in 200 mL/g of 35 wt% HNO_3 (from 70% HNO_3, EMD Inc., ACS grade) at 107 ºC for 16 hours. After filtering and rinsing with DIUF water, the support was dried at 80 ºC for 8 hours.

The acid-pretreated MWNT support was ground with a mortar and pestle, then promoted with iron, copper, and potassium with a method slightly modified from the deposition precipitation with urea (DPU) method of van Steen and Prinsloo.[72] Calculated amounts of $Fe(NO_3)_3 \cdot 9H_2O$ (Alfa Aesar, 98%), $Cu(NO_3)_2 \cdot 3H_2O$ (Acros Organics, 99%), KNO_3 (Alfa Aesar, 99%) and urea (Amresco, ultra pure grade) were dissolved in DIUF water, then immediately added dropwise to the acid-washed support. The promoted support was maintained at ambient conditions for 2 hours, and then dried under 0.75 bar of vacuum at 90 ºC for 30 minutes. The catalyst precursor was then placed in a 120 ºC oven for 16 hours. After grinding with mortar and pestle, the promoted catalyst precursor was calcined under N_2 flow with temperature ramping 5 ºC/min to 350 ºC then held for 4 hours. For the potassium-free CFeCu catalyst, the targeted composition was 9.1 wt% iron, with 1 Fe:0.03 Cu on a molar basis. For the K-promoted CFeCuK catalyst, the targeted composition was 9.1 wt% iron and 1 Fe:0.03 Cu:0.02 K on a molar basis.

For comparison of the nanoscale catalysts with a more traditional catalyst, a precipitated FeZnCu catalyst was also synthesized. First, a solution of 1M Fe^{3+} and 0.1M Zn^{2+} was made from $Fe(NO_3)_3 \cdot 9\ H_2O$, $Zn(NO_3)_2 \cdot 6\ H_2O$, (Alfa Aesar, 99% metals basis) and DIUF water. In this case, Zn is present to serve as a structural promoter.[24] A second solution, saturated with $(NH_4)_2CO_3$ (Alfa Aesar, ACS grade), was also created. A large 3-necked flask was placed into an 80 ºC water bath, filled with approximately 150 mL of DIUF water, and agitated with a small, stainless steel impeller. The Fe^{3+}/Zn^{2+} solution was added to the 3-necked flask at a rate of 3 mL/min while the pH was maintained at 7.0 via manual addition of the $(NH_4)_2CO_3$ solution. After filling the flask to a desired volume, the addition of solution was halted and the contents of the flask were allowed to age for an hour while heat and stirring were maintained. The aged, co-precipitated catalyst precursor solution was vacuum filtered then rinsed with the filtrate. Using 80 ºC DIUF water, the precursor was re-slurried and vacuum filtered three more times before finally being rinsed with ethanol. The resulting filter cake was dried overnight at 80 ºC, ground, and then calcined in air at 400 ºC for 4 hours.

The dried FeZn catalyst precursor powder was promoted with $Cu(NO_3)_2 \cdot 3\ H_2O$ dissolved in DIUF water and dried overnight at 80 ºC. The FeZnCu precursor was again ground with a mortar and pestle, then calcined in air at 400 ºC for 4 hours. The final molar composition was 1 Fe:0.1 Zn:0.03 Cu.

2.2.2 Catalyst Characterization

A Micromeritics Tristar II surface area analyzer was used to determine the BET surface area and pore volume of the calcined, precipitated FeZnCu catalyst, the as-received MWNTs, the acid-washed MWNTs, the calcined CFeCu catalyst, and the calcined CFeCuK catalyst. Prior to analysis, the samples were degassed under flowing helium, with temperature ramping from ambient to 350 ºC at 5 ºC/min then held for 4 hours.

A TA Instruments Q5000 sorption analyzer was used for Thermogravimetric Analysis (TGA) in air to evaluate the thermal stability of the MWNT support as well as the CFeCu catalyst. Temperature was ramped at 10 ºC/min to 120 ºC, held for 20 minutes, then ramped 10 ºC/min to 800 ºC.

Raman spectroscopy analysis was used to determine the effect of acid washing on the MWNT surface. Analysis was conducted on samples of the as-received MWNTs as well as the acid washed MWNTs using a Renishaw inVia 80W with a 514 nm laser at 5% power and WiRE software. For each sample, 3 scans were taken with each consisting of 10 accumulations with a 10 second exposure per accumulation.

Using a Nicolet Avatar 360, FT-IR spectroscopy was performed to characterize the surface functionalization of the carbon support before and after acid washing.

Temperature programed reduction with hydrogen (H_2-TPR) was conducted for each catalyst to determine reduction behavior. A Micromeritics Chemisorb 2750 system with an attached ChemiSoft TPx was used. An approximately 0.1 g sample was degassed for 1 hour at 200 ºC under 30 SCCM of He and reduced under 50 SCCM of 10% H_2 in Argon as temperature was ramped from ambient to 700 ºC at 5 ºC/min. Outlet gas from the sample was detected via TCD and H_2 consumption was logged automatically. The degree of reduction was calculated from the theoretical H_2 consumption for the case where all Fe in the catalysts is in the form of Fe_2O_3 and is fully reduced to Fe^{2+}.

Transmission electron microscopy (TEM) was used to verify the support and particle sizes for the carbon-supported nanoscale catalysts, while scanning electron microscopy (SEM) was used for the precipitated catalyst. Samples for TEM were prepared by drop-casting catalyst suspended in ethanol onto

carbon-coated copper grids and viewed using a Zeiss EM 10. SEM imaging was performed with a JEOL JSM-7000F operating at 20 kV with samples attached to stages via double-sided carbon tape.

A Bruker D8 diffractometer using Cu K-α radiation operated at 40 kV and 40 mA was used to obtain XRD patterns for each catalyst prior to placement in the reactor as well as the post-reaction carbon supported catalysts. The diffraction patterns were collected using a step size of 0.01° and 0.2 s/step count time from $10° \leq 2\theta \leq 80°$. The obtained peaks were compared to those of known compounds using the International Center for Diffraction Data (ICDD) database to determine the species present.

2.2.3 Reactor System

The reactor system used for this work is represented in Figure 2.1. In this system, hydrogen (Airgas, UHP grade), nitrogen (Airgas, UHP grade), and premixed syngas (Airgas certified standard spec, 1.50% N_2, 35.39% CO, balance H_2) flow from pressurized cylinders with flowrates controlled via mass flow

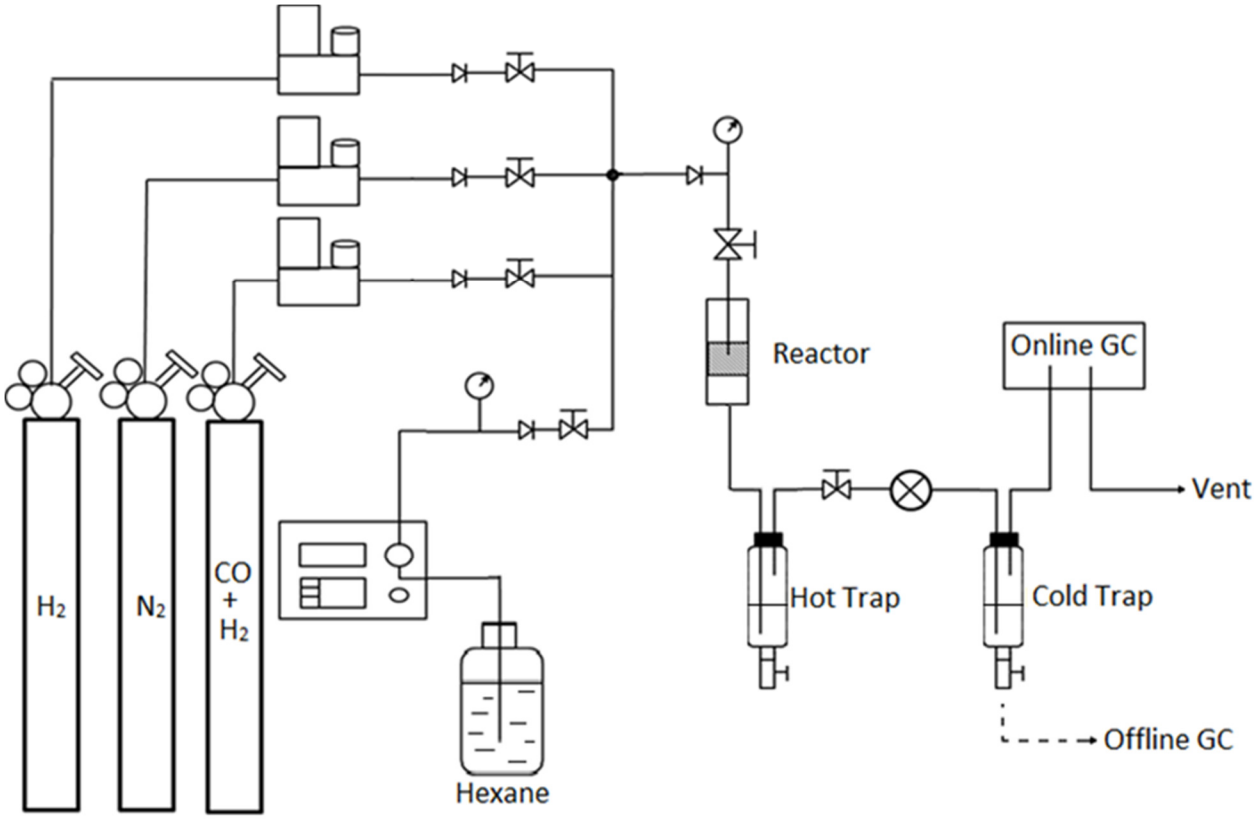

Figure 2.1 Schematic diagram of the reactor system

controllers (Brooks 5850E). A trap containing a lead-based sorbent (BASF E-315) is located between the syngas feed and the remainder of the system to remove iron carbonyls. Nitrogen in the syngas is used as an internal standard. Under supercritical operation, hexanes (EMD Millipore, 98.5% ACS, Cat. No HX0299), a mixture of C_6 isomers, are pumped by an HPLC pump (Beckman 110B) and mixed with the gaseous reactant prior to the reactor. Under gas phase operation, hexane bypasses the reactor and is instead delivered directly to the cold trap.

The tubing, reactor, and hot trap are heated via heating wires (Omegalux FGH-051) controlled by Omega CSC32 mini benchtop controllers and insulated with fiberglass tape. The reactor preheat zone, catalyst bed, and post-reactor tubing each have a controller set point of 240 ºC and are monitored via thermocouple, while the hot trap is similarly monitored and set to 220 ºC. The cold trap is water-cooled and kept at 5 ºC.

The reactor is a tubular 10" downflow fixed bed reactor (HIP) with the upper half having a diameter of 5/8", while the bottom half has a diameter of 9/16". This creates a shelf in the middle of the reactor where a stainless steel frit sits and supports the catalyst bed. The catalyst bed consists of 0.5 g of catalyst immobilized between layers of glass wool. A 6-point thermocouple runs from the bottom of the reactor through the catalyst bed and allows for temperature sampling above, within, and below the bed. System pressure was maintained via a back pressure regulator (BPR, Equilibar EB1-ULF) between the hot trap and the cold trap.

Effluent gas from the cold trap passes through a 6-way valve that directs the stream either to vent or to a 50 µL sample loop and subsequently to a GC-TCD. Online gas analysis was performed with a Varian Chromopack CP-3800 equipped with a packed column (Hayesep DB 100-120 mesh, 30ft x 1/8"). Liquid samples were drawn from the cold trap at approximately 12 hour intervals and analyzed offline with a Bruker 430-GC with a FID detector and a DB-5 column. Samples for GC-FID were each injected in duplicate and verified against another sample taken within 12 hours of time on stream, for a total of 4 chromatograms in close agreement for all reported liquid product data.

Gas concentrations and flow rates were obtained using response factors derived from gas standards in conjunction with the N_2 internal standard. GC-FID response factors were calculated relative to dodecane using the effective carbon number methodology outlined by Scanlon and Willis.[84]

2.2.4 Reaction Procedure

For each reaction run, the reactor system was preheated to 350 ºC for reduction under flowing nitrogen. N_2 flow was stopped and 25 SCCM of H_2 was allowed to flow over the bed for 24 hours. H_2 flow was then halted, and N_2 flow was used to then pressurize the system to 17.2 bar (250 psi) while the reactor cooled from 350 ºC to the 240 ºC reaction temperature.

After pressurization, gas phase FTS operation was conducted with a flowrate of 25 SCCM of a premixed syngas (H_2/CO = 1.78). Hexanes were pumped directly into the cold trap at a rate of 0.4 mL/min in order to facilitate product condensation as well as to allow for more direct comparison (equivalent dilution) with samples from the later supercritical phase operation.

Each FTS reaction experiment was initiated under gas phase reaction conditions. If CO conversion was stable after a minimum of 50 hours of time on stream, then the reaction was transitioned to supercritical operation. This transition to supercritical operating conditions was achieved by redirecting the hexanes from the cold trap to the feed stream and adjusting the BPR to 68.9 bar (1000 psi). The reaction pressure for supercritical operation was chosen to keep the syngas partial pressure constant while maintaining a 3:1 ratio of hexane to syngas molar flow. After 140-200 total hours of time on stream, supercritical operation was stopped by halting syngas flow. After halting the reaction, the reactor was rinsed with supercritical hexane, purged with nitrogen, cooled, and finally depressurized.

2.3 Results and Discussion

2.3.1 Catalyst Characterization

BET surface area, pore volume, and pore radii for the catalysts and support as determined by nitrogen physisorption are summarized in Table 2.1. While surface area and pore volume are low for the MWNT support and nanoscale catalysts relative to the precipitated FeZnCu, they are very comparable to those observed by Bahome et al.[68] and Abbaslou et al.[73] using very similar catalyst synthesis techniques. Acid washing slightly increased surface area, pore volume, and pore radius.

Table 2.1 Characterization results for carbon support material and catalysts

	Precipitated FeZnCu	As-received MWNTs	Acid washed MWNTs	CFeCu	CFeCuK
BET surface area (m^2/g)	120	13	17	23	36
Pore volume (cm^3/g)	0.26	0.024	0.043	0.054	0.065
Average pore radius (nm)	3.5	4.1	5.1	4.5	3.6
Temp. of Max Decomp. Rate (ºC)	--	788	765	612	609
Residual Ash (%)	--	0.66	0.90	11.22	12.30
TPR degree of reduction	81%	--	--	69%	91%
XRD crystallite size (pre/post rxn, nm)	--	--	--	4.2/9.9	2.2/13

For the as-received MWNTs, acid-washed MWNTs, CFeCu catalyst, and CFeCuK catalyst, the adsorption isotherms, shown in Figure 2.2, are type II similar to those observed by Gheorghiu et al.,[85] with the almost-linear middle region of the isotherm extending to very low relative pressure. A type II isotherm is characteristic of an adsorbent with few to no pores smaller than macropores.[86] The FeZnCu catalyst

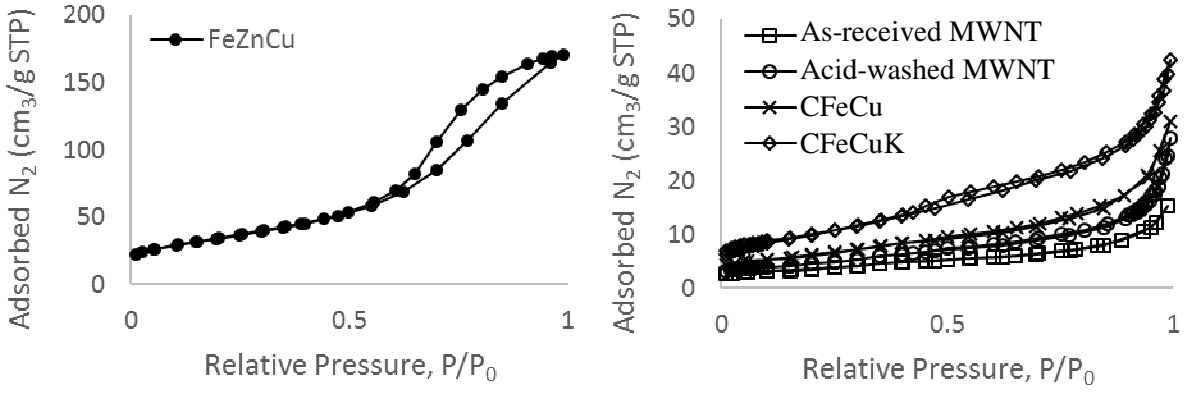

Figure 2.2 Nitrogen physisorption isotherms for the catalysts, raw MWNTs, and acid-washed MWNTs

exhibited a Type IV adsorption isotherm which is similar to a type II isotherm, but with a significant hysteresis loop that is characteristic of non-negligible pore volume.[86]

Thermal stability of the as-recieved MWNT support, acid washed MWNTs, CFeCu catalyst, and CFeCuK catalyst were measured via TGA in air and the data are shown in Table 2.1. In air, the as-received MWNTs began decomposition around 600 ºC and the decomposition rate reached a maximum at 788 ºC. After acid treatment, promotion, and calcination, the catalyst was less thermally resistant but still stable at reaction temperatures with decomposition of CFeCuK, the least stable sample, beginning around 400 ºC and peaking at 610 ºC. This observed drop in stability is in line with that seen by Motchelaho et al.,[87] who also saw depressed stability of MWNTs as a result of both HNO_3 treatment and residual catalyst. After TGA analysis of the MWNT support, the residual weight was less than 1% of the initial sample mass, which indicates near-negligible non-combustible impurity content. In addition, the derivative weight curves (not shown) for each sample contain singular peaks, which is characteristic of nanotubes with no carbonaceous impurities.[88] Assuming all metals are present in their respective oxides (Fe_2O_3, CuO, K_2O) and that ash content of the promoted catalyst samples is indicative of metal loadings, both the CFeCu (7.5 wt% Fe) and CFeCuK (8.3 wt% Fe) catalysts are close to, but slightly below the targeted iron loading levels.

Raman spectroscopy, specifically the ratio of the intensities of the D band (~1350 cm^{-1}) and G band (~1600 cm^{-1}) peaks, was used to characterize the relative quantity of surface defects present in the MWNTs before and after acid washing. Before washing, the D/G ratio was 0.13±0.01, while after it was 0.135±0.003. This negligible change indicates there was little to no functionalization of the MWNT sidewalls as a result of the acid washing. This observation mirrors the results of Bahome et al.[68] who also saw little functionalization with a milder HNO_3 treatment.

FTIR spectroscopy was also used for surface characterization of both the raw and acid-washed support material. The primary observation in this analysis is that the characteristic peak of the C-H stretch was present in the acid-washed tubes, but not in the as-received tubes. This indicates that the nitric acid treatment had at least some effect, but as functionalization is most likely to occur at the ends of the tubes,

this is not necessarily inconsistent with the results from Raman spectroscopy, whose response depends primarily on the characteristics of the sidewalls of the tubes.

Reduction behavior for each catalyst was investigated via H_2-TPR and is shown in Figure 2.3. For iron oxide, reduction typically takes place in two steps: Fe_2O_3 to Fe_3O_4, represented by the peaks between approximately 100 ºC and 250 ºC, and then Fe_3O_4 to metallic Fe, represented by the larger peak, which extends to almost 700 ºC for the FeZnCu catalyst.[73] Raw TCD response vs temperature data was scaled based on the moles of Fe present in the sample, and a calculated degree of reduction is shown in Table 2.1. The breadth of the FeZnCu peak is most likely due to its higher metal content and relatively dilute H_2 used in the reduction process.

SEM and TEM images are provided in Figure 2.4, Figure 2.5, and Figure 2.6. TEM imaging confirmed the dimensions of the MWNT support and showed that catalyst particles are present, relatively dispersed on the surface of the MWNTs, and on the approximate scale of 20-30 nm. SEM imaging showed the micron-scale catalyst particles in the precipitated FeZnCu catalyst.

XRD patterns for the carbon-supported catalysts both before and after reaction are shown in Figure 2.7. For each sample, the peak near a 2Θ angle of 26.5º is indicative of the graphitized outer shell of the MWNTs [00-041-1487]. Peaks near 33º and 35º for the fresh catalysts are characteristic of Fe_2O_3 [00-033-0664], while those near 42.7º for the used catalysts are consistent with the presence of carburized iron [00-037-0999]. The XRD pattern for the FeZnCu catalyst (not shown) had only small peaks characteristic of an amorphous sample.

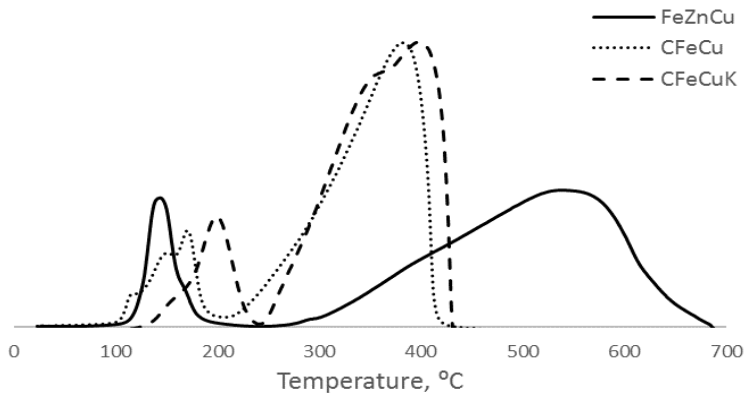

Figure 2.3 TPR curves for the FeZnCu, CFeCu, and CFeCuK catalysts, scaled by moles of Fe per sample analyzed

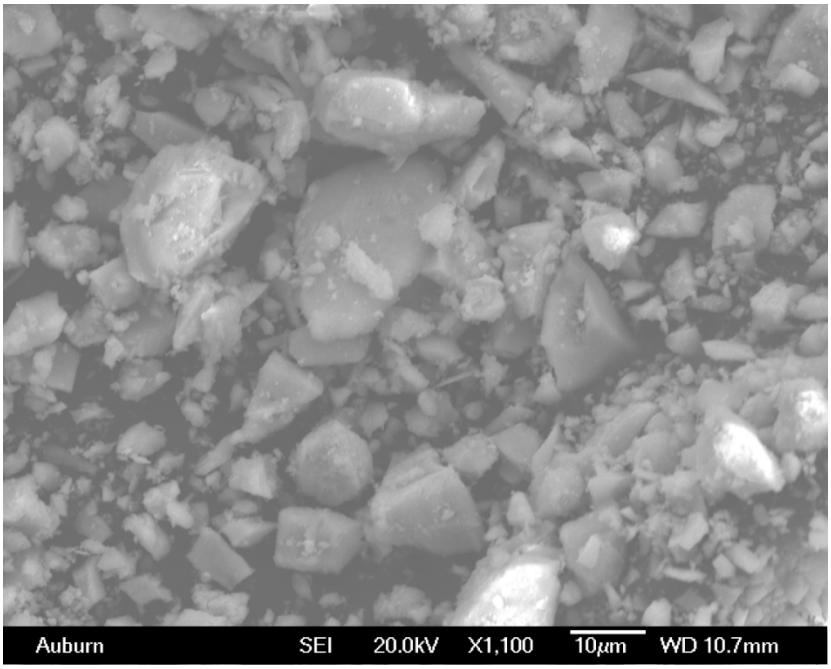

Figure 2.4 SEM image of precipitated FeZnCu catalyst

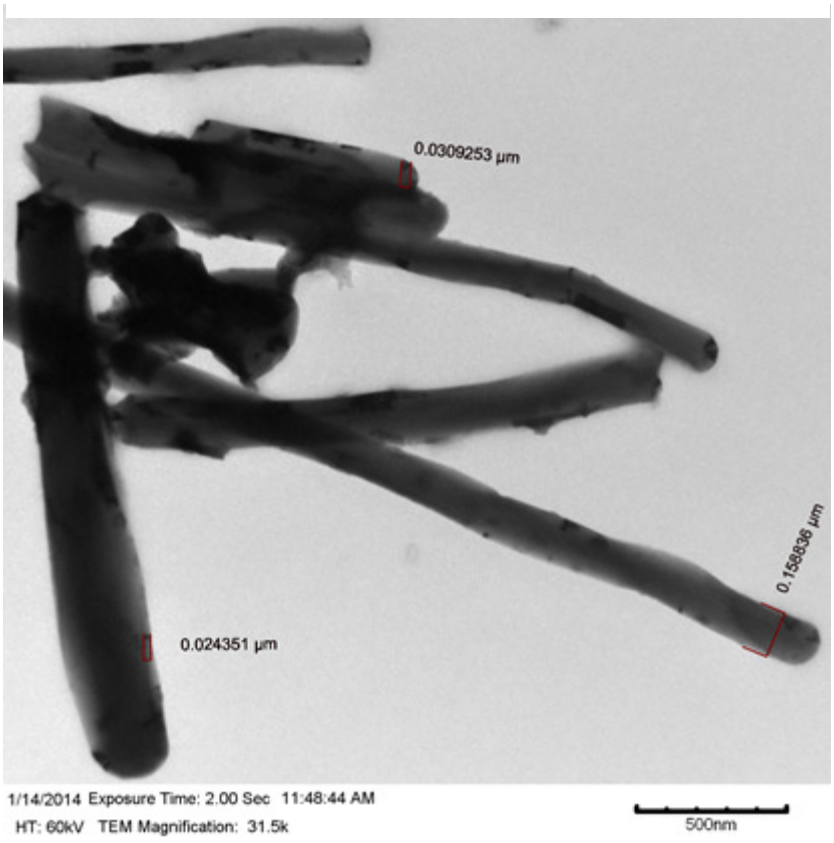

Figure 2.5 TEM image of the CFeCu catalyst. Note: the measurements displayed in the image are a product of the image processing software and the number of displayed digits does not indicate precision.

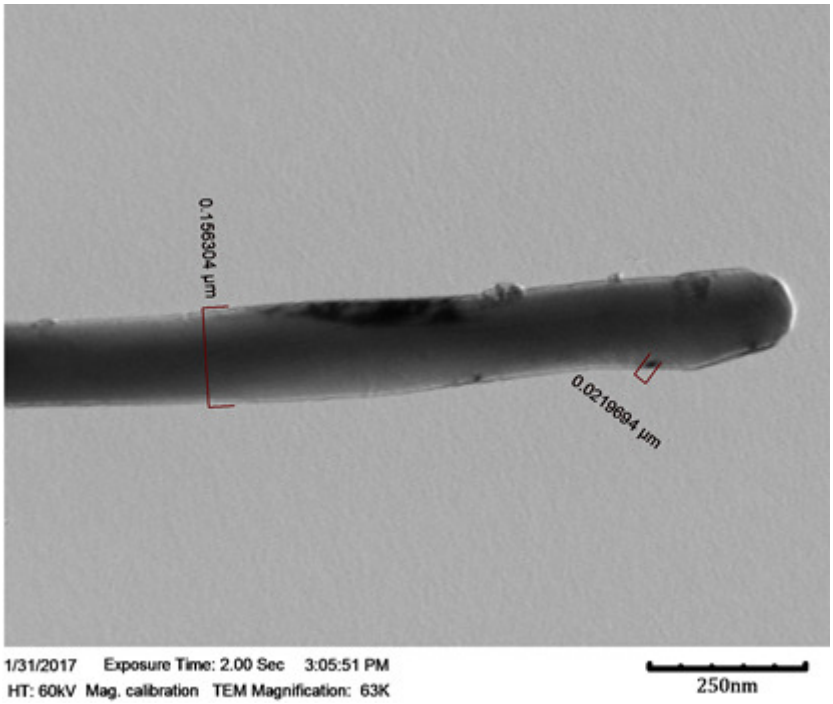

Figure 2.6 TEM image of the CFeCuK catalyst. Note: the measurements displayed in the image are a product of the image processing software and the number of displayed digits does not indicate precision.

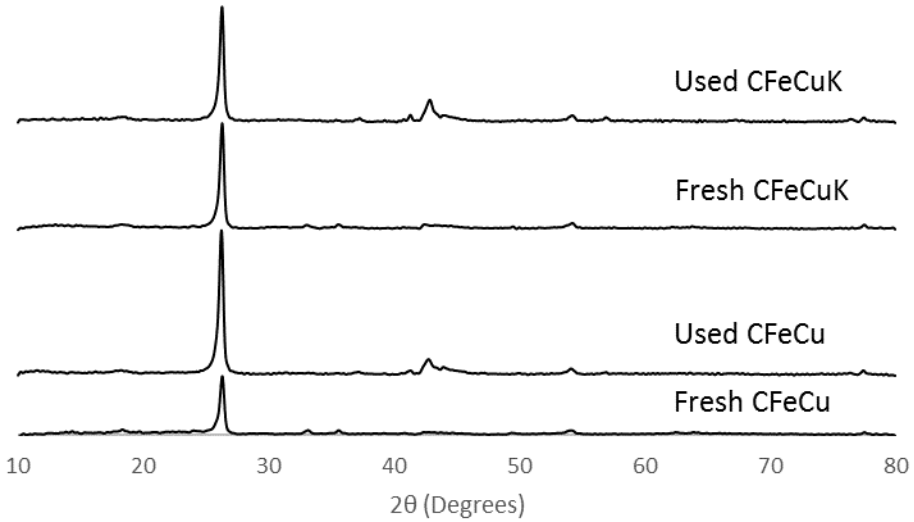

Figure 2.7 XRD patterns for carbon supported catalysts before and after reaction

2.3.2 Reaction Performance

The FTS performance of the precipitated FeZnCu catalyst, the MWNT-supported CFeCu catalyst, and the MWNT-supported CFeCuK catalyst was tested under gas phase conditions (GP-FTS) as well as under supercritical phase conditions with a hexane reaction medium (SC-FTS). The results of these FTS experiments are summarized in Table 2.2. More detailed data showing performance with time on stream is shown in Figure 2.8, where data from gas phase is represented by square markers and data from supercritical operation is represented by diamond markers.

Table 2.2 Fischer-Tropsch synthesis performance* for precipitated and MWNT-supported catalysts under gas phase (GP) and supercritical phase (SC) reaction conditions

	FeZnCu		CFeCu		CFeCuK	
	GP	SC	GP	SC	GP	SC
CO Conversion (%)	45	64	24	28	16	19
H_2 Conversion (%)	36	51	25	28	10	14
CH_4 Sel. (%)	5.1	5.4	5.3	6.5	1.5	1.1
CO_2 Sel. (%)	15	17	5.0	5.8	15	13
H_2:CO Usage Ratio	1.3	1.2	1.7	1.6	1.1	1.2
Activity[1]	3.2	4.6	7.1	8.1	4.3	5.2
C_{7+} α	0.64[2]	0.79	0.71	0.72	0.69[2]	0.79

*Data shown represents average values for stable reaction behavior at the specified conditions

[1] Activity = 10^{-2} mol_{CO} g_{Fe}^{-1} s^{-1}

[2]Apparent 2-alpha distribution with break around C_{15}, given data is average for C_7 to C_{20}

For each of the three catalysts, the CO conversion was relatively stable with only a slight decline during GP-FTS. Under supercritical operation, CO conversion for each catalyst increased before again stabilizing. Increased, stable conversion under SC-FTS is consistent with the literature, where such behavior attributed to the enhanced product extraction and balanced reactant/product mass transport under SC-FTS.[11,57,61]

The CO conversion observed for the CFeCu and CFeCuK catalysts is much lower—approximately one half and one third, respectively—than that of the precipitated FeZnCu catalyst. It should be noted that for the MWNT-supported catalysts, the metal content is less than a tenth (~8%) of that of the precipitated catalyst. As a result, the activity of the MWNT-supported catalysts is actually significantly higher on the basis of metallic mass, likely due to the small, dispersed nature of the supported nanoparticles. Another

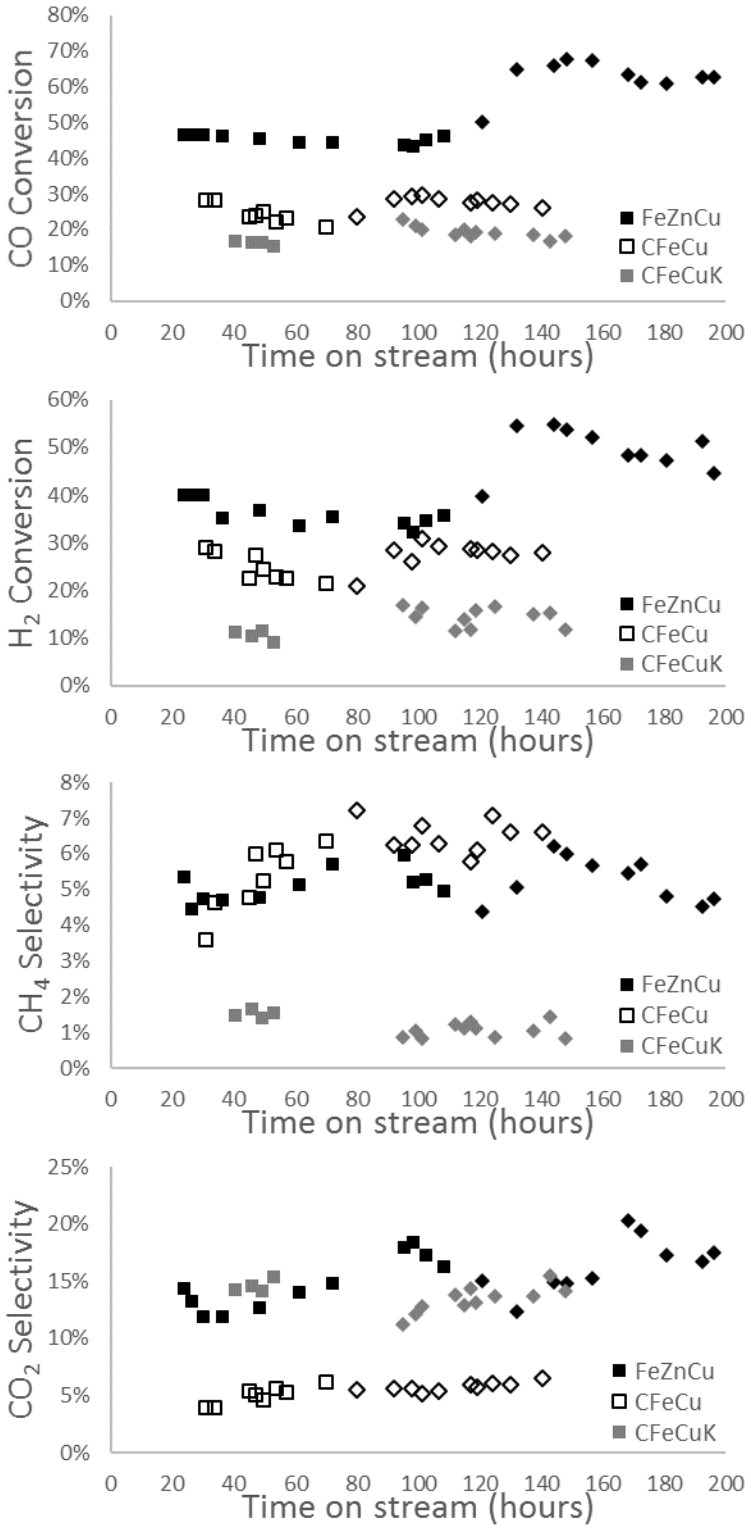

Figure 2.8 CO conversion, H_2 conversion, CH_4 selectivity, and CO_2 selectivity under gas phase (square symbols) and supercritical (diamond symbols) conditions

contributor to elevated activity could include the higher partial pressure of H_2 and lower H_2O partial pressure at lower conversion.[89,90]

The CO_2 and CH_4 selectivities (note: not at isoconversion) for each catalyst as a function of time on stream are shown in Figure 2.8. For precipitated FeZnCu catalyst, the CH_4 and CO_2 selectivities fluctuated, but were approximately 5% and 15% on average, respectively, throughout the course of the reaction. Direct comparison of CH_4 and CO_2 selectivity with other studies in the literature can be misleading due to differences in conversion, catalyst formulation, and reaction conditions, but some literature sources are similar enough in each regard for a rough comparison. Bukur et al.[23] reported CH_4 and CO_2 selectivities of approximately 17% and 45%, respectively, (250 ºC, H_2/CO = 1, CO conv. ~70%) while Li et al.[24] reported a CH_4 selectivity of 6.5% and CO_2 selectivity of 10.2% (220 ºC, H_2/CO = 2, CO conv. ~15%). Durham et al.[65] obtained 8% CH_4 selectivity and 4% CO_2 selectivity in SC-FTS (240 ºC, H_2/CO = 1.56, CO conv. 45%). In the context of these experiments, the FeZnCu catalyst performed within the range that might be expected for a catalyst of its type.

For the CFeCu catalyst, CH_4 selectivity was comparable to that of the FeZnCu catalyst, but CO_2 selectivity was significantly depressed, averaging less than 6% in both GP-FTS and SC-FTS.

In iron-catalyzed FTS, alkali metal promoters, particularly potassium, are known to promote CO chemisorption, inhibit H_2 chemisorption, and suppress secondary reactions. This results in lower methane selectivity, increased WGS shift activity, elevated olefin selectivity relative to paraffins at higher carbon numbers, elevated higher hydrocarbon selectivity, and slightly depressed activity.[1,4,24,42] Figure 2.8 shows that, as might then be expected from the addition of a potassium promoter, the CFeCuK catalyst had significantly depressed CH_4 selectivity (~1%) relative to the other catalysts as well as CO_2 selectivity comparable to the FeZnCu catalyst and elevated relative to the CFeCu catalyst.

In contrast to some sources in the literature,[11,53,54] the transition from GP-FTS to SC-FTS had little effect on the selectivity toward CH_4 for the catalysts and conditions investigated in this study. Reduced CH_4 selectivity in SC-FTS relative to GP-FTS is generally attributed to improved heat management.[44] Since the

flowrate of syngas, conversion, and resulting heat generation in this study were relatively low, there was low CH_4 selectivity in GP-FTS and consequently little room for improvement under supercritical operation.

As shown in Figure 2.9a, the GP-FTS products for the precipitated FeZnCu catalyst consist primarily of alkanes and olefins with alcohols present to a much lesser extent. Products taper off relatively quickly at higher carbon numbers and the data can be represented by a 2-α ASF plot (Figure 2.10), with α_1 = 0.73 from C_7 to C_{16}, and α_2 = 0.48 from C_{16} to C_{22}. Products are increasingly hydrogenated at higher carbon numbers. Both increased hydrogenation and the resulting reduction in α at higher carbon numbers

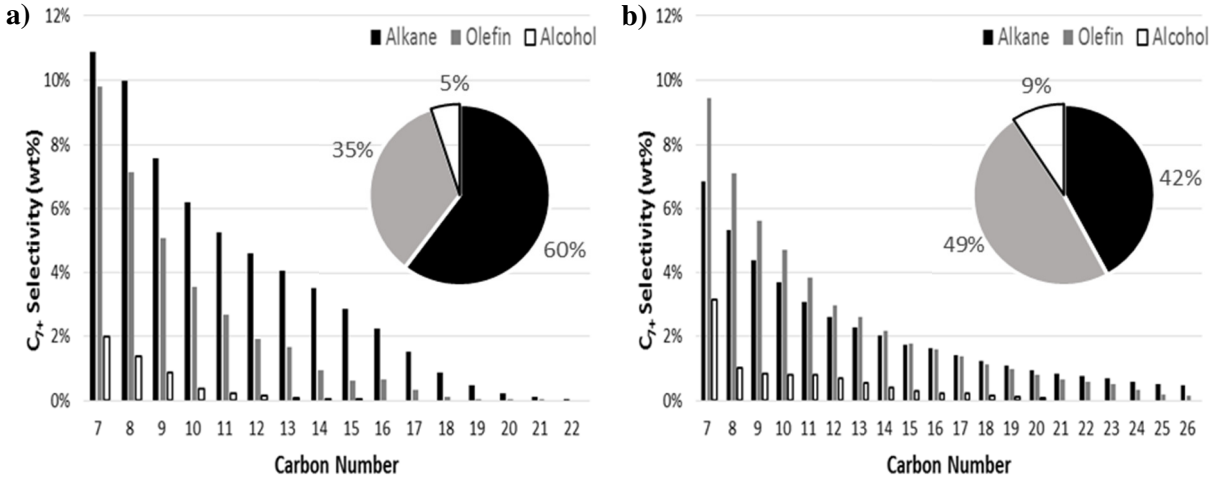

Figure 2.9 Selectivity among C_{7+} products for the FeZnCu catalyst under **a)** gas phase operation (240 ºC, 250 psi) and **b)** supercritical operation (240 ºC, 1000 psi, hexanes/syngas ratio = 3)

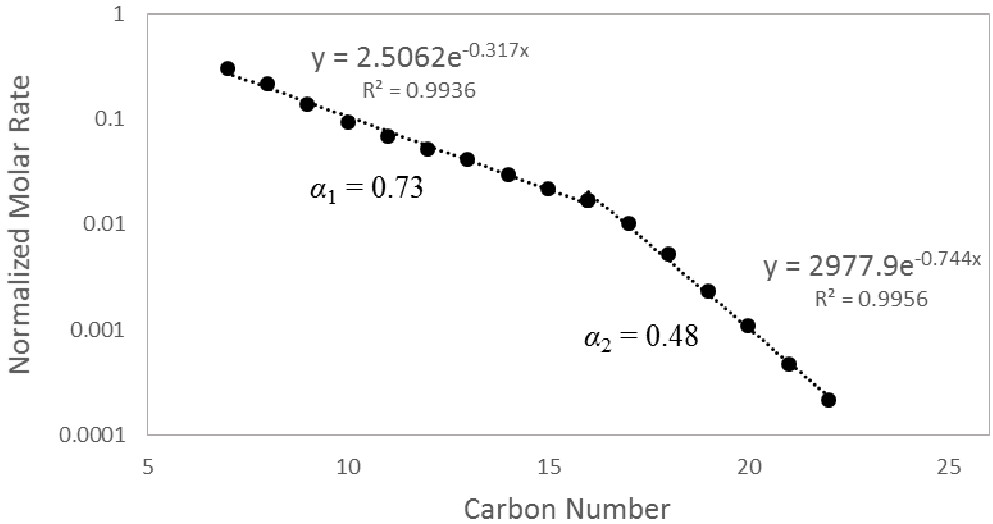

Figure 2.10 ASF plot for the FeZnCu catalyst under GP-FTS (240 ºC, 250 psi, 0.5g catalyst, 25 SCCM syngas)

are can be attributed to inhibited desorption and diffusion for less-volatile reaction intermediates and products.[46]

Figure 2.9b shows the liquid products for the same FeZnCu catalyst in SC-FTS. The selectivities toward olefins, alcohols, and heavy products are significantly elevated relative to GP-FTS. The SC-FTS liquid product distribution can be represented by an ASF plot with α = 0.79 (Figure 2.11). As reported in the literature, elevated α and elevated selectivity towards less-hydrogenated products in SC-FTS are a result of the capability of the SCF to extract and stabilize products and reaction intermediates, particularly at higher carbon numbers.[43,46] Under SC-FTS operation, α, CO conversion, and selectivity in the range of C_{10}-C_{15} were all extremely similar to those observed by Durham et al.[65] for a similar K-free catalyst.

The liquid product distributions for the CFeCu catalyst under GP-FTS and SC-FTS are shown in Figure 2.12a and Figure 2.12b, respectively. Relative to the FeZnCu catalyst, the CFeCu catalyst seems more prone to hydrogenation as liquid products are lighter and mostly paraffinic. As with the FeZnCu catalyst, SC-FTS products for the CFeCu catalyst are slightly heavier and less hydrogenated relative to GP-FTS. While olefins are more typically the dominant non-paraffinic product for iron-catalyzed FTS, alcohols are more predominant in the non-paraffinic products for the CFeCu catalyst. ASF plots for these product samples are shown in Figure 2.13 and Figure 2.14. α was 0.71 for GP-FTS and 0.72 for SC-FTS. The single-

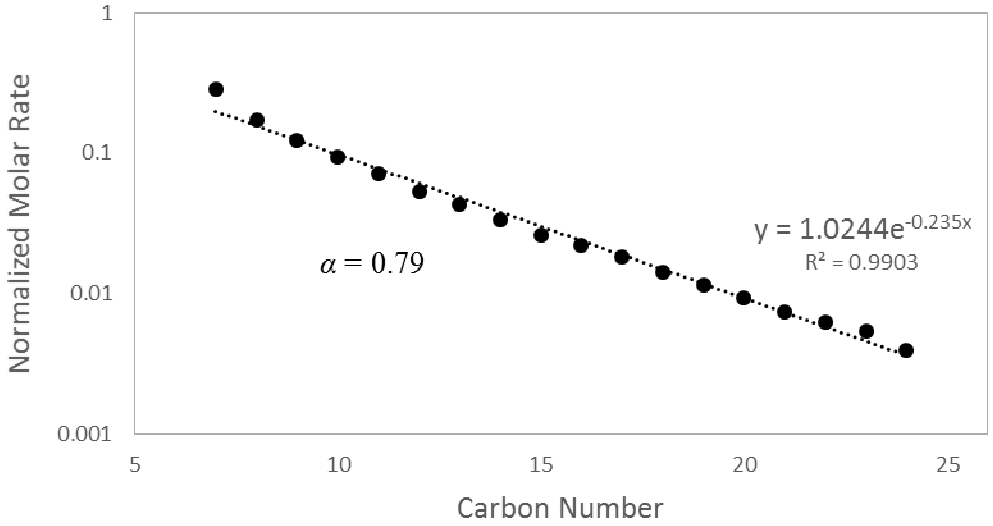

Figure 2.11 ASF plot for the FeZnCu catalyst under SC-FTS (240 ºC, 1000 psi, 0.5g catalyst, 25 SCCM syngas)

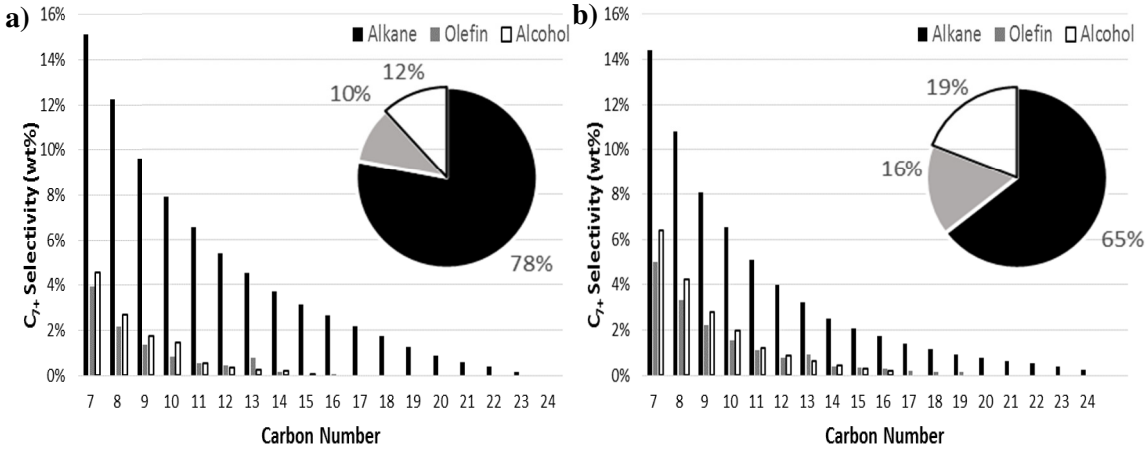

Figure 2.12 Selectivity among C_{7+} products for the CFeCu catalyst under **a)** gas phase operation (240 ºC, 250 psi) and **b)** supercritical operation (240 ºC, 1000 psi, hexanes/syngas ratio = 3)

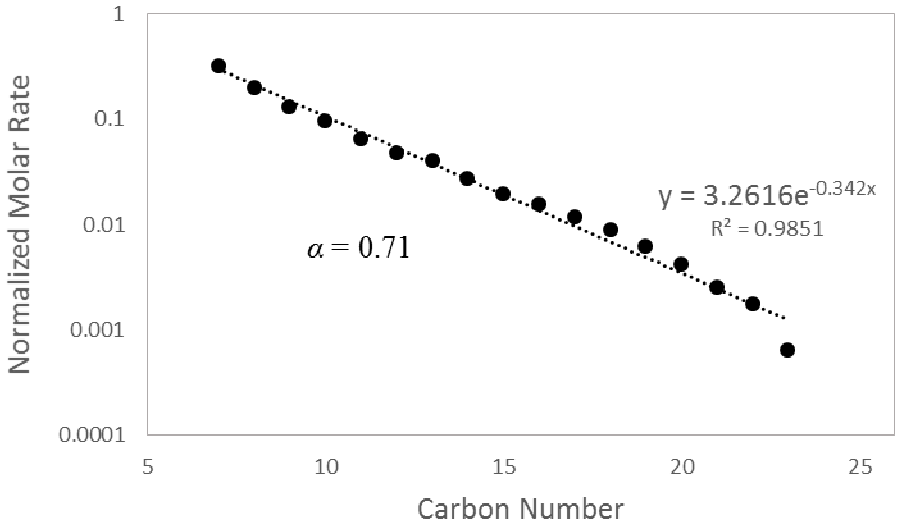

Figure 2.13 ASF plot for the CFeCu catalyst under GP-FTS (240 ºC, 250 psi, 0.5g catalyst, 25 SCCM syngas)

α distribution exhibited by the CFeCu catalyst, even under GP-FTS, is attributed to a lack of the heavy olefins whose hydrogenation led to a 2-α distribution for the FeZnCu catalyst. That the GP-FTS data here can be represented by a single-α ASF plot also effectively rules out the accumulation of liquid in the hot trap as a cause for a 2-α distribution seen elsewhere in this work.

It can be seen in Figure 2.15 that, as expected from the literature, under GP-FTS the potassium promoted CFeCuK catalyst has a much greater selectivity towards less-hydrogenated products relative to the K-free CFeCu catalyst. Olefins dominate the liquid products in GP-FTS, but there is also significant

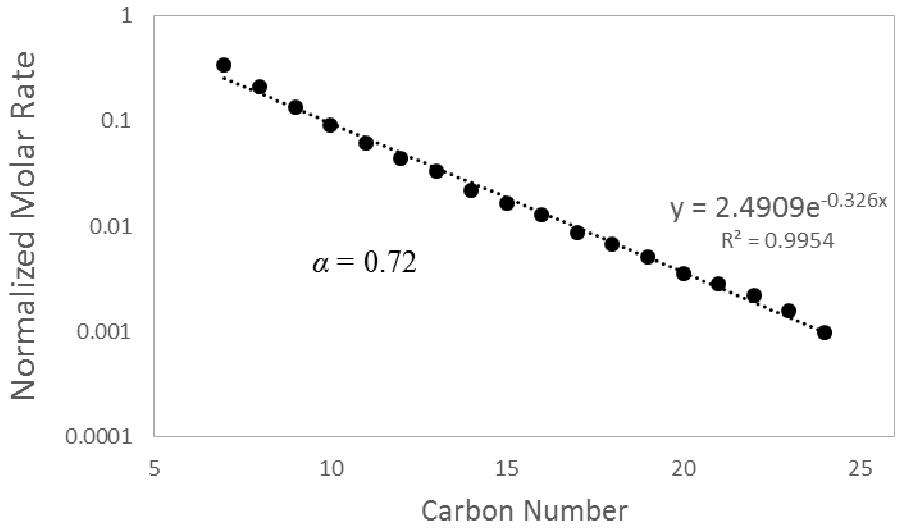

Figure 2.14 ASF plot for the CFeCu catalyst under SC-FTS (240 ºC, 1000 psi, 0.5g catalyst, 25 SCCM syngas)

selectivity towards both alcohols and methyl ketones. Most noteworthy however, is the production and extraction of relatively large quantities of aldehydes which, to the author's knowledge, has only been reported for FTS with a supercritical or liquid reaction medium over K-promoted iron catalysts[53,65,91] or with a CoMn catalyst prepared by oxalate precipitation[92]. As with the FeZnCu catalyst, liquid product data for the CFeCuK catalyst under GP-FTS can be represented by a 2-α ASF plot (Figure 2.16) with $\alpha_1 = 0.76$ up to C_{16} and $\alpha_2 = 0.52$ from C_{16} to C_{20}.

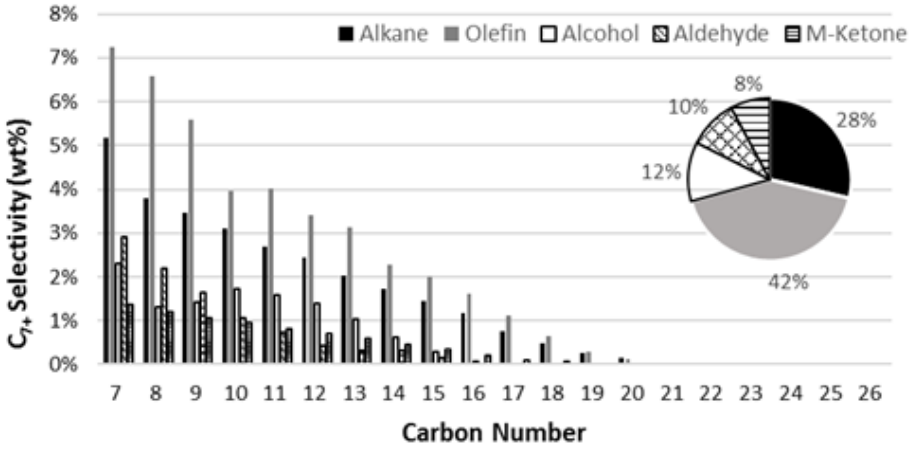

Figure 2.15 Selectivity among C_{7+} products for the CFeCuK catalyst under gas phase operation (240 ºC, 250 psi)

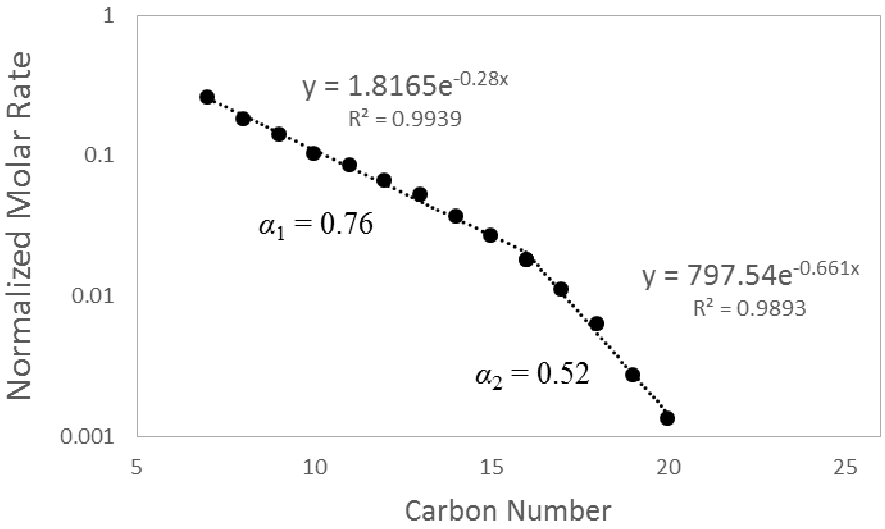

Figure 2.16 ASF plot for the CFeCuK catalyst under GP-FTS (240 ºC, 250 psi, 0.5g catalyst, 25 SCCM syngas)

As shown in Figure 2.17, under SC-FTS the CFeCuK catalyst produced near-equal quantities of paraffins, olefins, and aldehydes with smaller quantities of methyl ketones and alcohols. The ASF α (Figure 2.18) was elevated relative to GP-FTS, increasing to 0.80. Aldehyde selectivity increased very significantly and was accompanied by a decrease in olefin and alcohol selectivities.

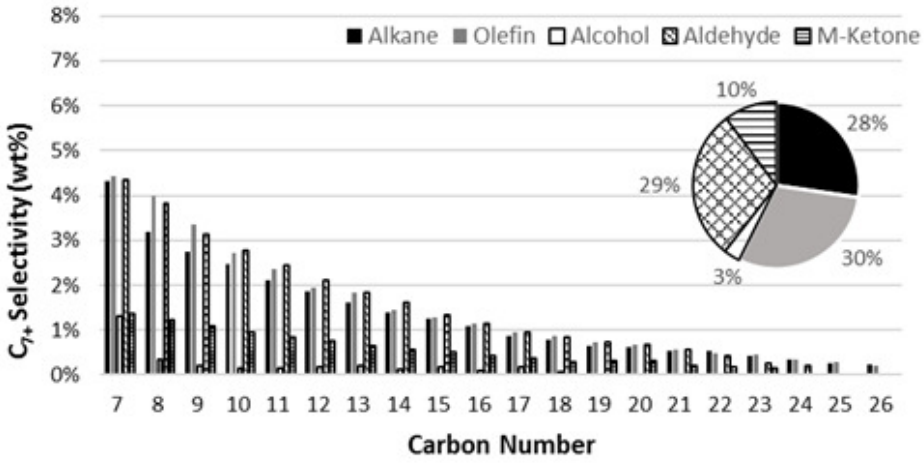

Figure 2.17 Selectivity among C_{7+} products for the CFeCuK catalyst under supercritical operation (240 ºC, 1000 psi)

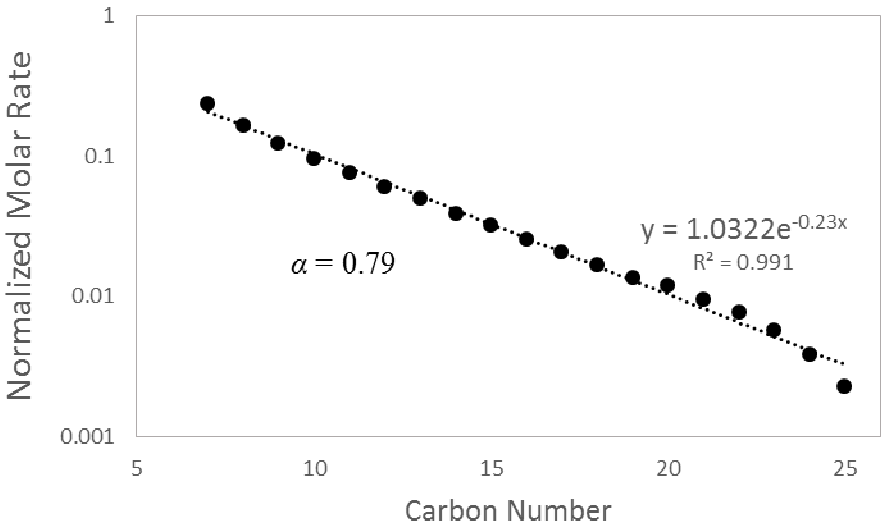

Figure 2.18 ASF plot for the CFeCuK catalyst under SC-FTS (240 ºC, 1000 psi, 0.5g catalyst, 25 SCCM syngas)

2.3.3 Discussion

The marked selectivity of the CFeCuK catalyst towards aldehydes catalyst invites comparison with the work of Durham et al.,[53,65] where significant aldehyde production was observed in SC-FTS and which offers a few conclusions relevant to this work. First, as supported by the data in this study and others,[91] it is concluded that potassium promotion is essential to observe non-negligible production of aldehydes utilizing an Fe-based catalyst.

In the work of Durham, the observation of heavy aldehydes in the SC-FTS product stream is attributed to the ability of the SCF reaction medium to enhance mass transfer and thereby extract reaction products and intermediates from reaction sites prior to secondary hydrogenation to products such as alcohols, olefins, and paraffins.[53] For the CFeCuK catalyst in this study, the significant increase in aldehyde selectivity in SC-FTS relative to GP-FTS was accompanied by plummeting olefin and alcohol selectivities. This observation is consistent with the hypothesis that aldehydes are among the primary FTS products and can sequentially hydrogenate to other products prior to removal from the reactor.

This observed trade-off between the production of aldehydes and more-hydrogenated products parallels the well-documented effect in SC-FTS over more traditional iron-based FTS catalysts—namely that increased olefin selectivity relative to GP-FTS is accompanied by depressed paraffin selectivity. From

these two analogous trends, it appears that the role of the SCF reaction medium in SC-FTS is to aid in the extraction of reaction intermediates, be they aldehydes or olefins, and that what products are ultimately extracted is dependent on the individual catalyst.

In contrast to the results seen by Durham et al. and Dictor and Bell,[65,91] where aldehydes were extracted from the reactor only supercritical or liquid-mediated FTS, in this study, significant levels of aldehydes were detected under both GP-FTS and SC-FTS with the CFeCuK catalyst. This indicates that while supercritical fluids clearly aid in the extraction of aldehydes, for some catalysts, aldehydes can be observed in the reactor effluent even in the absence of a liquid or SCF reaction medium. Additionally, because the CFeCuK catalyst composition, save for the carbon support, is very similar to that of Durham (1 Fe:0.02 K), these results suggest that the presence of the carbon support was a key factor in enabling the observation aldehydes in the GP-FTS product.

According to Butts et al.,[93] a strong Lewis acid can promote CO insertion by increasing the rate of alkyl group migration from the metal surface to the carbon of adsorbed CO as well as by stabilizing the resulting acyl group. Dictor and Bell[91] suggest that in K-promoted, Fe-based catalysts aldehyde production is enabled when the potassium (K^+) ion acts as a Lewis acid, accepting electrons from the oxygen of adsorbed CO and facilitating the carbonylation (CO insertion) step in chain propagation. One possible explanation for the influence of a carbon support on product selectivity seen in the Fe-catalyzed FTS of this work is that the known capacity for carbon nanotubes to readily accept and conduct electrons[94] resulted in an effect similar to that of potassium on the catalyst metal and thereby facilitated increased oxygenate selectivity and the production of aldehydes.

Several studies in the literature[3,11,28,43,44,46,50,53,54,57–59] have illustrated that a SCF reaction medium can have a significant influence on both heat and mass transport in FTS. Under the conditions investigated in this study, the supercritical hexane reaction medium appears to primarily be influencing mass transport. This effect is most clearly seen in the marked increase in the extraction of olefins and oxygenates under SC-FTS operation for the FeZnCu and CFeCuK catalysts. Because, in this case, SC-FTS operation had very little impact on CH_4 selectivity, it is unlikely that the observed product extraction is due to improved heat

management, which can reduce methanation.[46,50] As a result of increased extraction of reaction intermediates and unhydrogenated products in SC-FTS, conversion and α increased as active sites were made available more rapidly and intermediates were able to readsorb and continue propagation.

The final effect of the mass transfer enhancement brought on by the use of a SCF is the elimination of the 2-α distribution seen in GP-FTS for FeZnCu and CFeCuK. For both of these catalysts in GP-FTS, the product distribution drifts away from a linear ASF plot around C_{15} as reaction intermediates and products become increasingly heavy and diffuse more slowly. For both of these catalysts, the transition to SC-FTS eliminated this deviation, likely due to the enhanced solvation and stabilization of unhydrogenated intermediates.

2.4 Conclusions

In this chapter, we present data from the preparation and characterization of Fe-based nanoparticle catalysts supported on a multi-walled carbon nanotube support both with and without a potassium promoter. These carbon-supported catalysts were tested under both gas phase and supercritical phase Fischer-Tropsch synthesis conditions alongside a K-free precipitated catalyst. Relative to the precipitated catalyst, the carbon-supported catalysts had high activity, low CH_4 selectivity, and elevated selectivity toward oxygenates. The transition from gas to supercritical phase FTS resulted in increased conversion, an increased chain growth factor α, and increased selectivity toward unhydrogenated products. Significant quantities of aldehydes were produced over the K-promoted catalyst, while aldehydes were not detected in the products of the other catalysts. These results indicate that potassium is essential for the production and recovery of aldehydes in Fe-catalyzed FTS. For the K-promoted catalyst, the production of aldehydes was observed under gas phase operation and further elevated under supercritical operation. This data indicates for the first time that while a supercritical fluid reaction medium can enhance the production of aldehydes, for some catalysts, significant aldehyde production can be observed in Fe-catalyzed FTS in the absence of a supercritical or liquid medium.

Chapter 3: A Comparison of Carbon Catalyst Supports for Fe-Catalyzed Fischer-Tropsch Synthesis

3.1 Introduction

The Fischer-Tropsch synthesis (FTS) process represents one of the few ways to generate long-chain hydrocarbon products with a potentially renewable, non-petroleum feedstock. As such, when there is a demand for hydrocarbon fuels or chemicals but concerns about dependence on foreign crude supplies, environmental impact, or even impurity content, FTS is one technology that serves as a potential answer. FTS consists of the surface-catalyzed polymerization and hydrogenation of CO with a product spectrum including hydrocarbons of variable carbon chain length and functionality. Selectivity is highly dependent on management of the large reaction exotherm as well as a wide variety of variables such as the catalyst metal and promoters, conversion level, and reaction temperature.[1,2]

Historically, the large heat of reaction has been addressed by methods including the use of numerous small diameter tubular fixed-bed reactors,[2] a hydrocarbon wax-mediated slurry reactor,[95] or novel catalyst designs.[96] Another approach that has been studied since the late 1980's is to utilize a supercritical fluid (SCF) reaction medium.[50] Because of their unique combination of properties, which are tunable near the critical point and intermediate between those of a gas and a liquid, SCFs offer a flexible tool to influence heat and mass transfer in FTS. With the use of a SCF reaction medium, researchers have realized FTS performance improvements such as improved extraction of heavy and unhydrogenated products, increased conversion and activity maintenance, and reduced selectivity towards CH_4 and CO_2.[11,28,43,53,58,59,65]

In Chapter 2, we demonstrated that a carbon catalyst support can significantly impact FTS activity and performance and that a SCF reaction medium can further improve and help to probe reaction behavior. Briefly, in that work, Fe-based nanoparticles were synthesized on large-diameter multi-walled carbon nanotubes (MWNTs) then tested in both gas phase FTS and SCF-mediated FTS. The C-supported nanoscale catalysts proved to be more active that their precipitated counterpart, and relatively selective toward oxygenates. Most interestingly, long carbon chain aldehydes were observed in the liquid product stream for the C-supported, K-promoted catalyst (CFeCuK) under both gas phase and supercritical operation. This

behavior had not previously been observed in Fe-catalyzed FTS without a SCF or liquid reaction medium and merited further investigation.

Accordingly, the work presented in in this chapter was undertaken to see what, if any, benefits could be realized by utilizing carbon catalyst support materials that are similar to the previously-studied large diameter MWNTs. The results of synthesizing, characterizing, and testing three such carbon supports in FTS are presented in this chapter. The supports investigated consist of carbon nanofibers (CNFs), MWNTs with a smaller ~8 nm diameter (sMWNTs), and graphene nanoplatelets (GNPs). CNFs were chosen to see whether the performance of the large MWNT-supported catalyst could be replicated on an inexpensive carbon support that lacked the sp^2 hybridized surface that is characteristic of carbon nanotubes, but that has similar dimensions. Similarly, the sMWNT support provided a contrast in support diameter and the GNPs allowed investigation of a carbon support surface that was chemically similar, but planar rather than curved. Each catalyst was tested under both gas phase and supercritical phase conditions in order to investigate the impact of differing mass and heat transfer regimes on FTS activity and selectivity.

3.2 Materials and Methods

3.2.1 Catalyst Preparation

In this study, three carbon-supported, iron-based FTS catalysts were prepared with copper and potassium promoters. To facilitate comparison, the catalyst preparation methodology followed our previous method[80] as closely as possible. Each catalyst had a targeted composition of 9.1 wt% iron loading and 1 Fe:0.03 Cu:0.02 K on a molar basis. The first catalyst, denoted CNF-FeCuK, was supported on carbon nanofibers. The remaining two catalysts, supported on small-diameter multi-walled carbon nanotubes and graphene nanoplatelets, are denoted sMWNT-FeCuK and GNP-FeCuK, respectively.

The CNF, sMWNT, and GNP support materials were all purchased from Sigma Aldrich. The CNF support (Cat. No. 719803) consists of nested cones of graphitized carbon. Its listed properties are D = 100 nm, L = 20-200 μm, and >98% purity on a carbon basis (≤14000 ppm iron). The sMWNT support (Cat.

No. 724769) has listed properties of D = 6-9 nm, L = 5 µm, and >95% purity on a carbon basis. The GNP support, xGnP® grade C-750, (Cat. No. 900407) has a listed flake diameter of less than 2 µm.

As per our previous methodology adapted from Abbaslou et al.,[73] each as-received carbon support material was refluxed in 200 mL/g of 35 wt% HNO_3 (from 70% HNO_3, EMD Inc., ACS grade) at 107 ºC for 16 hours. This treatment was intended to remove any amorphous carbon or residual impurities while potentially functionalizing the carbon surfaces with oxygenates, which could serve as anchoring sites for the catalyst metal particles. The CNF and sMWNT supports were filtered from the acid solution and the resulting carbon filter cakes were rinsed with DIUF, dried overnight at 80 ºC, then ground with a mortar and pestle.

The GNP support could not be removed from the acid washing solution via the same vacuum filtration methodology as the other carbon support materials, so it was instead separated via centrifugation. Specifically, the acid/GNP mixture was allowed to settle for a day before removal of approximately 80% of the supernatant then rinsed with ~100 mL DIUF water. This process of settling, decanting, and rinsing was repeated two more times as the supernatant faded in color, but remained a muddy red-brown. As separation became more difficult, a Heraeus Megafuge 16 was utilized to centrifuge the rinsed sample at 5000 RPM for 3 minutes. Brownish supernatant was removed, and the soft carbon pellet again rinsed with DIUF. The ~150 mL of washed GNP sample was diluted with 60 mL of ethanol to ease drying, then centrifuged a final time for 1 hour at 5000 RPM. Though some carbon was stably suspended in the completely opaque ethanol solution, most of the GNP carbon formed a pellet which was extracted and dried for 8 hours at 120 ºC. TGA (data below) indicated the presence of some less-stable material in the acid-washed GNP, so it was then calcined for 4 hours at 400 ºC in air.

Calculated amounts of $Fe(NO_3)_3 \cdot 9H_2O$ (Alfa Aesar, 98%), $Cu(NO_3)_2 \cdot 3H_2O$ (Acros Organics, 99%), KNO_3 (Alfa Aesar, 99%) and urea (Amresco, ultra pure grade) were dissolved in DIUF water, then immediately added dropwise to the acid-treated supports. The promoted supports were kept at ambient conditions for 2 hours, and then dried under 0.75 bar of vacuum at 90 ºC for 30 minutes. The catalyst precursors were then dried for an additional 16 hours at 120 ºC. After grinding with mortar and pestle, the

promoted catalyst precursors were calcined under N_2 flow with temperature ramping 5 ºC/min from ambient to 350 ºC then held for 4 hours.

3.2.2 Catalyst Characterization

Due to concern about the combustion potential of oxidized graphene,[97,98] a TA Instruments Q5000 sorption analyzer was used for Thermogravimetric Analysis (TGA) to evaluate the thermal stability of the as-received and acid-washed supports as well as the promoted catalysts in air. Temperature was ramped at 10 ºC/min to 120 ºC, held for 20 minutes, then ramped 10 ºC/min to 800 ºC.

A Micromeritics Tristar II surface area analyzer was used to determine the BET surface area and pore volume of the as-received catalyst supports as well as the promoted, calcined catalysts. Prior to analysis, the samples were degassed under flowing helium, with temperature ramping from ambient to 350 ºC at 5 ºC/min then held for 4 hours.

Raman spectroscopy analysis was conducted on samples of the as-received and acid washed carbon support materials using a Renishaw inVia 80W with a 514 nm laser at 5% power and WiRE software. For each sample, 3 scans were taken with each consisting of 10 accumulations with a 10 second exposure per accumulation.

Transmission electron microscopy (TEM) was used to verify the support and particle sizes for each of the carbon-supported nanoscale catalysts. Samples for TEM were prepared by drop-casting catalyst suspended in ethanol onto carbon-coated copper grids and viewed using a Zeiss EM 10.

3.2.3 Reactor System

The reactor system used for this work is the same as that used in the previous work and is represented in Figure 2.1 and described in section 2.2.3.

3.2.4 Reaction Procedure

The reaction procedure utilized in this work is slightly modified from our previous methodology, primarily to avoid issues with the nitrogen internal standard and gas phase deactivation. After loading the catalyst and pressure testing for each reaction run, the reactor was heated to 350 ºC under flowing nitrogen to prepare for reduction. The catalyst was then reduced under 25 SCCM of H_2 at 350 ºC for 24 h. After reduction, the reactor was cooled to 240 ºC, purged with He, and pressurized with He to 1000 psi for supercritical operation.

Under supercritical operation, the syngas had a flowrate of 25 SCCM, while hexanes were pumped to the reactor at a rate of 0.4 mL/min (3:1 hexane:syngas molar ratio). After 100-125 hours of operation, the reaction was transitioned to gas phase conditions by lowering the pressure to 250 psi and redirecting the hexane flow to the cold trap. After approximately 200 hours of total time on stream, syngas flow was halted and the reaction stopped. The reactor was rinsed with supercritical hexane, purged with nitrogen, cooled, and finally depressurized.

3.3 Results and Discussion

3.3.1 Catalyst Characterization

TGA data for the carbon support materials and carbon-supported catalysts is shown in Table 3.1. The TGA curves of the GNP support taken after acid treatment and before calcination are shown in Figure 3.1. The slight (5.7%) but non-negligible mass loss that occurred for this support below 350 ºC indicates that while this oxidized support might ultimately be stable at the reaction temperature and not explosive, a controlled burn-off was merited prior to promotion. Calcination of the acid-washed GNP support—a deviation from the catalyst preparation methodology of the other two catalysts as well as from that used in Chapter 2—was thus merited to ensure that the catalyst loading levels would be comparable after calcination and the carbon mass loss that it would otherwise entail.

With the assumption that residual ash from TGA is synonymous with total metal content and that all metals are in their base oxide (Fe_2O_3, CuO, K_2O), metallic iron content of the CNF, sMWNT, GNP, and

large MWNT supported catalysts were 10.1%, 13.6%, 8.7%, and 8.3% by mass, respectively. Each catalyst, with the exception of sMWNT-FeCuK, was thus near the targeted 9.1 wt.% loading.

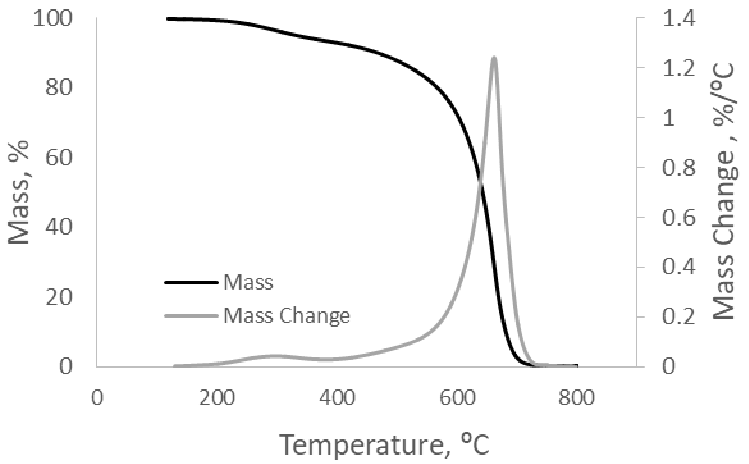

Figure 3.1 TGA curves for the uncalcined, HNO_3-treated GNP support in air

BET surface area, pore volume, and average pore radius obtained from nitrogen physisorption are summarized in Table 3.1 alongside the D/G ratios from Raman spectroscopy. No physisorption data is shown for the acid treated, uncalcined GNP sample because 4 repetitions of the analysis all yielded a BET surface area of ~5 m^2/g and negligible pore volume. As such a low surface area is unlikely to be an accurate representation of the material in the context of the results for the as-received GNP and the GNP-FeCuK catalyst, it is likely that the post-wash separation and processing led to agglomeration of the GNP flakes.

Adsorption isotherms are shown in Figure 3.2 for each support before and after acid treatment as well as for the final promoted catalysts. Almost all isotherms are Type II,[86] where the middle region persists to the lower P/P_0 limit of the instrument and a small or negligible hysteresis loop. Type II isotherms are

Table 3.1 Characterization results for carbon support material and catalysts

	CNF[1]	CNF-FeCuK	sMWNT[1]	sMWNT-FeCuK	GNP[1]	GNP-FeCuK	MWNT[1,2]	MWNT-FeCuK[2]
BET surface area (m^2/g)	21/30	25	180/340	360	880/--	260	13/17	36
Pore volume (cm^3/g)	0.06/0.08	0.07	0.73/1.3	1.4	1.4/--	0.24	0.043	0.065
Avg. pore radius (nm)	6.3/6.0	6.3	8.0/8.0	7.8	4.0/--	2.1	5.1	3.6
Temp. of Max Decomp. Rate (ºC)	682/673	583	591/598	449	625/662	457	788/765	609
Residual Ash (%)	3.5/1.3	15.1	2.3/0.7	20.3	0.9/0.2	12.9	0.66/0.9	12.3
Low T. Mass Loss (%)[3]	0/0	0.1	0.7/3.8	1.2	2.7/5.7	0.85	0/0	0.5
D (Raman shift, cm^{-1})	1357±2/1357±1		1357±1/1355±1		1347±1/1356±1		1355±1/1358±1	
G (Raman shift, cm^{-1})	1579±1/1580±1		1593±1/1594±1		1577±1/1588±2		1582±1/1582±1	
Raman D/G	0.49±0.04 0.61±0.02		1.16±0.01 1.12±0.01		0.756±0.001 0.953±0.008		0.13±0.01 0.135±0.003	

[1]Data for as-received/acid washed support material [2]Data from previous paper for comparison[80] [3]Percent dry wt. lost prior to reaching 350 ºC during TGA temperature ramping

characteristic of materials with little to no microporous or mesoporous volume. The only exception to the trend of Type II isotherms is GNP-FeCuK, which has a significant hysteresis loop at higher relative pressure, indicative of a Type IV isotherm. Type IV isotherms are closely related Type II, but indicate a non-negligible volume of micropores or mesopores.

As might be expected due to their similar dimensions, the CNF support and catalyst had physisorption results comparable to those reported for large-diameter MWNTs. Both the sMWNT and GNP supports and catalysts had far higher surface area than the large-diameter materials, however. For the CNF and sMWNT supports, the acid treatment increased surface area but only increased pore volume for the sMWNT support. As end caps and defect sites are more susceptible to reaction,[99] this could be a result of the acid treatment opening the sMWNT end caps and exposing the tube interior to N_2.

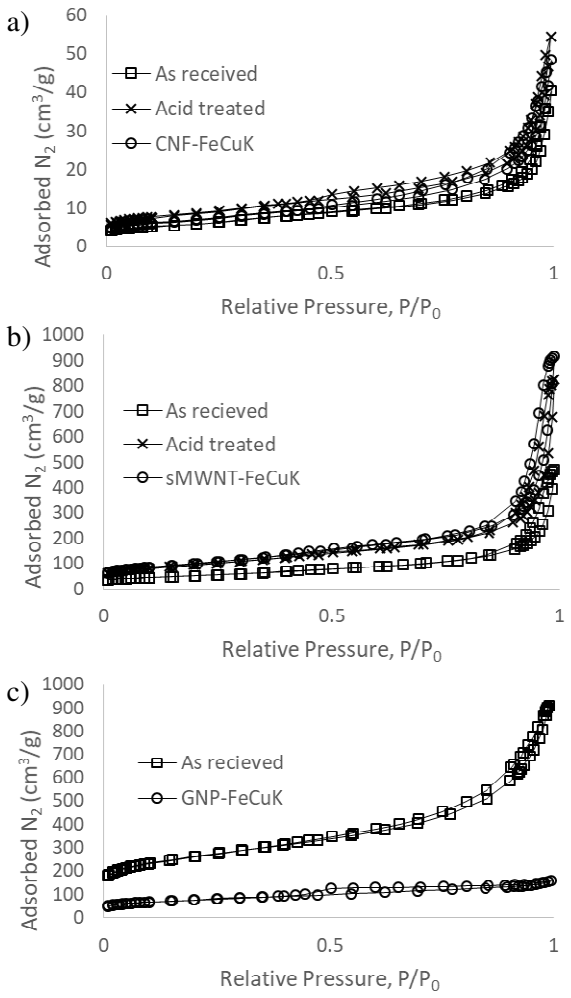

Figure 3.2 Adsorption isotherms for the a) CNF support and catalyst, b) sWMNT support and catalyst, and c) GNP support and catalyst

In Raman spectroscopy, the D band (~1350 cm^{-1}) and G band (~1580 cm^{-1}) peaks are, respectively, associated with defects (sp^2-hybridized or amorphous carbon) and graphitization (sp^3-hybridized carbon) in the surface of carbon materials. The ratio of the D and G band intensities is thus a popular way to quickly assess relative quality of carbonaceous samples.[100,101] As with the large-diameter MWNT support, the sMWNT support was only minimally affected by the acid treatment. For the CNF support, acid treatment had a slight effect on the D/G ratio, which indicates some minimal reaction of the HNO_3 with the tube sidewalls. In contrast, and GNP supports seemed more susceptible to the acid, as, in addition to the GNP

support's observed solubility in water, its Raman D/G ratio increased more significantly, indicating an increased quantity of defects in its carbon structure relative to the as-received material.

TEM images of the CNF-FeCuK, sMWNT-FeCuK, and GNP-FeCuK catalysts are shown in Figure 3.3, Figure 3.4, and Figure 3.5, respectively. These figures can be used to see the approximate structure and size of the carbon supports and catalyst particles dispersed on the carbon surfaces, but as each represents such a minute sample size, are not necessarily representative of the catalyst as a whole. From Figure 3.3, it can be seen that the CNF support is on the order of 60-120 nm in diameter, while the catalyst particles on it are polydisperse, ranging from a few nm up approximately 50 nm. Similarly, Figure 3.4 shows sMWNT

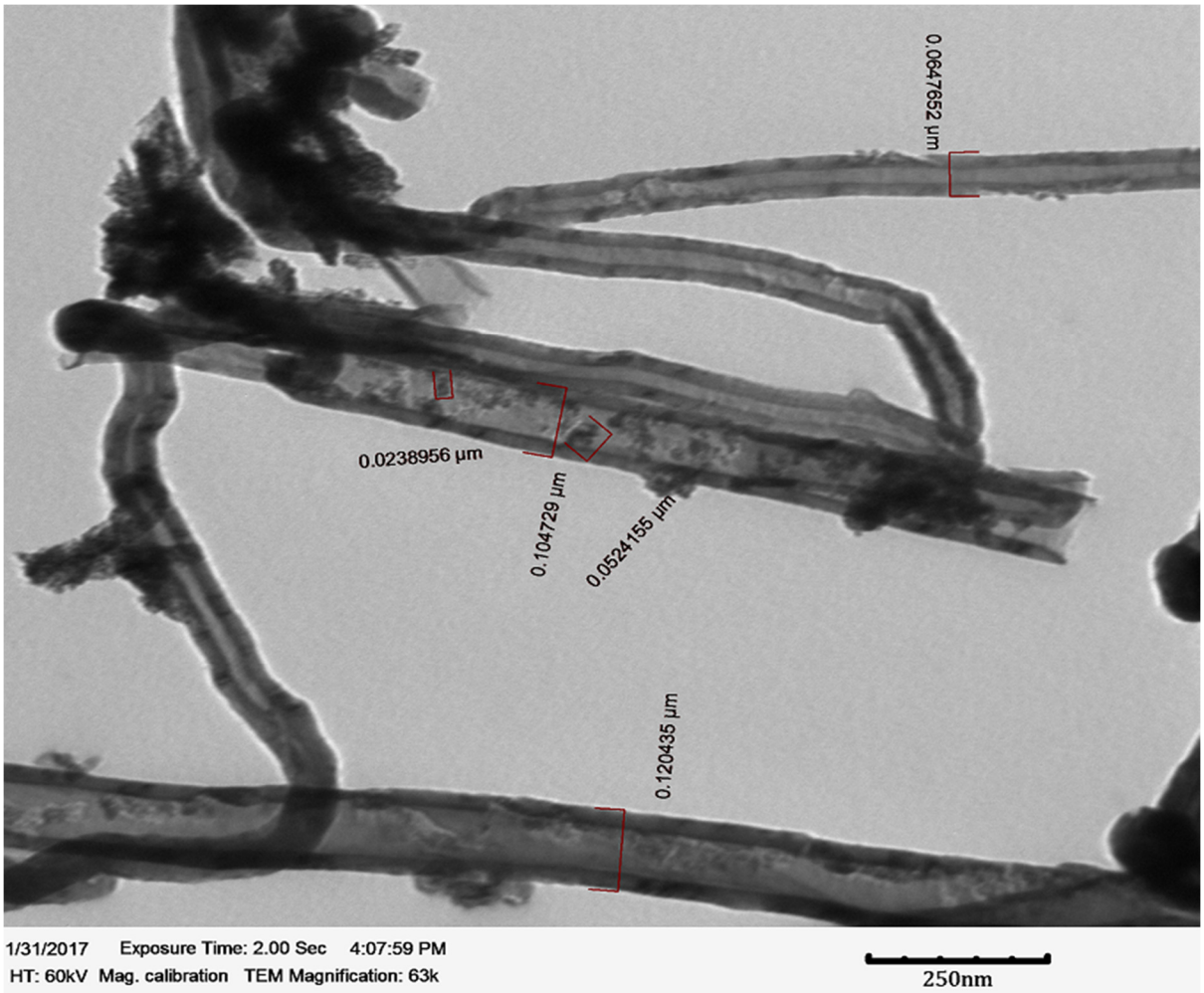

Figure 3.3 TEM image of the CNF-FeCuK catalyst. Note: the measurements displayed in the image are a product of the image processing software and the number of displayed digits does not indicate precision.

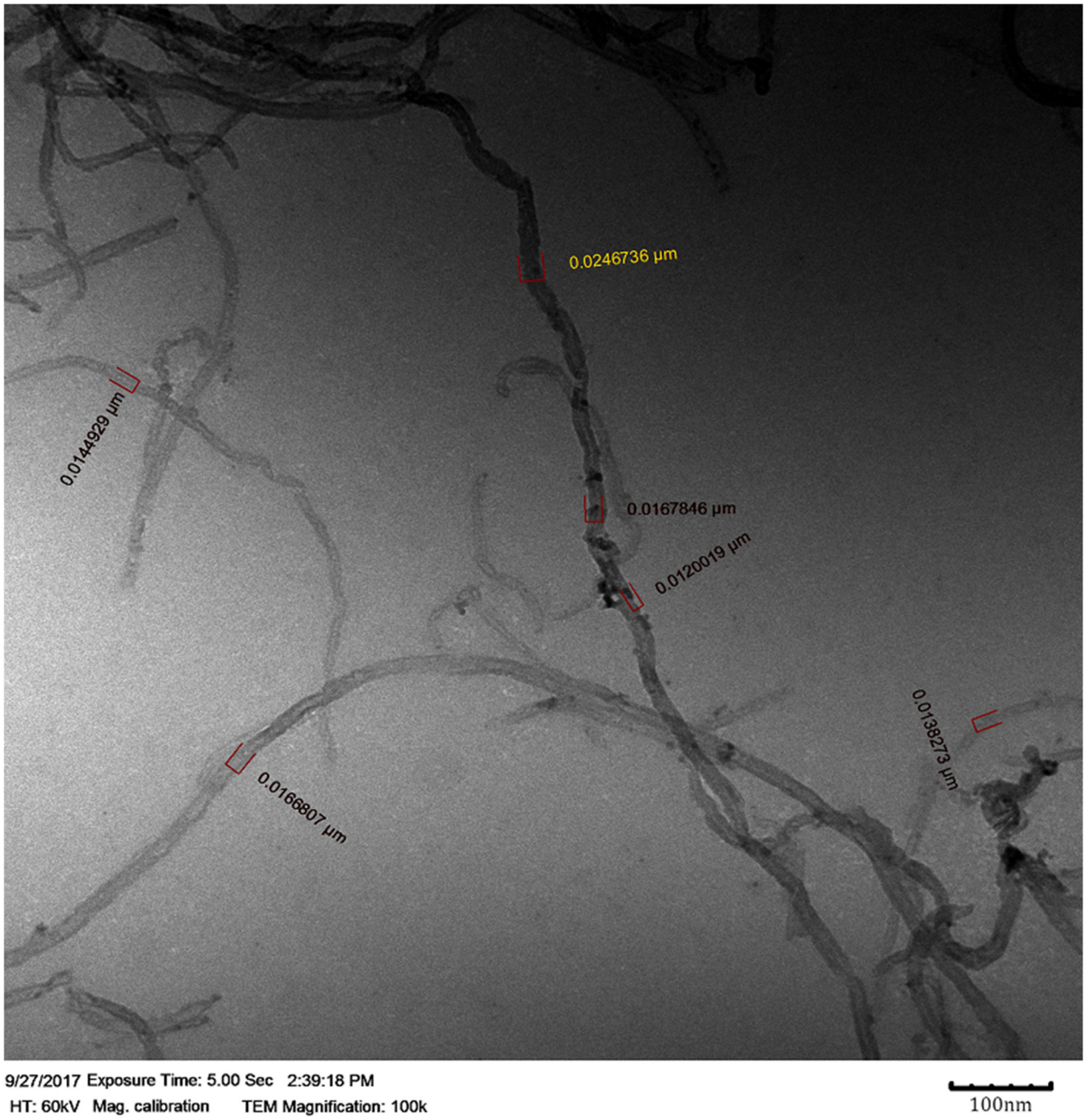

Figure 3.4 TEM image of the sMWNT-FeCuK catalyst. Note: the measurements displayed in the image are a product of the image processing software and the number of displayed digits does not indicate precision.

tubes ranging from 10-25 nm in diameter, while the catalyst particles are smaller on average, but on the order of 10-20 nm. Finally, Figure 3.5 shows that the GNP flakes can be as small as ~150 nm in diameter and, as with CNF-FeCuK, the catalyst particles are polydisperse and range up to ~30 nm.

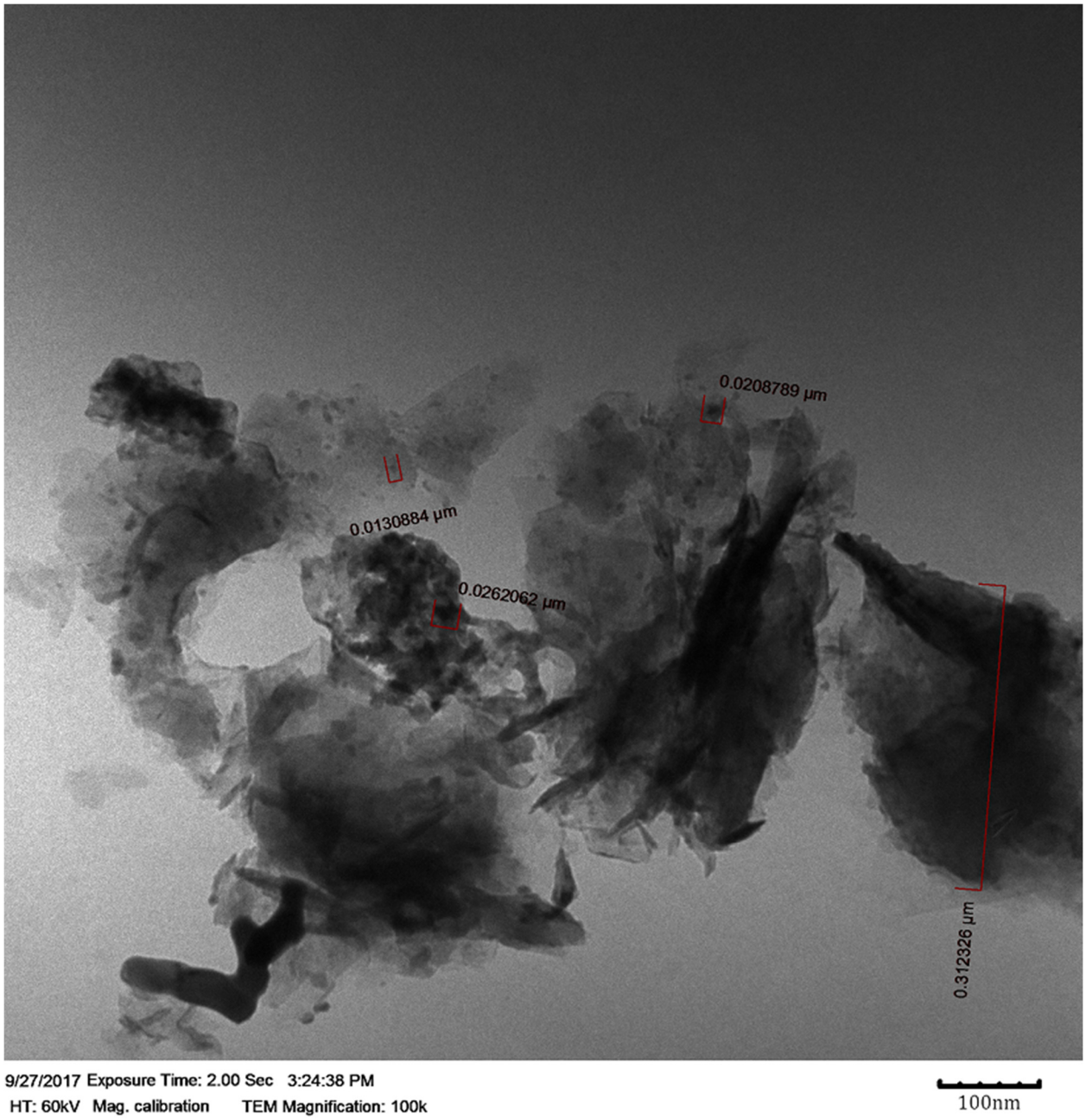

Figure 3.5 TEM image of the GNP-FeCuK catalyst. Note: the measurements displayed in the image are a product of the image processing software and the number of displayed digits does not indicate precision.

3.3.2 Reaction Performance

The FTS performance of the CNF-FeCuK, sMWNT-FeCuK, and GNP-FeCuK catalysts was tested under gas phase (GP-FTS) conditions as well as supercritical (SC-FTS) conditions with a hexane reaction medium. The results of these tests are summarized in Table 3.2 alongside the data for the previously-studied CFeCuK catalyst, which consists of a large-diameter MWNT support loaded with iron, copper, and potassium at the same levels and by the same means as the other three catalysts. The data for CO conversion, H_2 conversion, CH_4 selectivity, and CO_2 selectivity with time on stream is shown in Figure 3.6 for each of the catalysts in this study. ASF plots were fit to liquid product data and are shown in Figure 3.7.

For the CNF-FeCuK and GNP-FeCuK catalysts, conversion and selectivity were relatively stable outside of startup and the transition from SC-FTS to GP-FTS. In contrast, while the sMWNT-FeCuK catalyst was stable under supercritical operation, in gas phase operation it exhibited deactivation with time on stream as evidenced by decreasing conversion and increasing CH_4 selectivity. As expected from the literature, conversion and the ASF α were elevated in SC-FTS for each catalyst. CH_4 selectivity was low (<5% avg.) for all catalysts in both GP-FTS and SC-FTS, but CH_4 and CO_2 selectivity trends otherwise varied between the catalysts.

The CNF-FeCuK catalyst was the least active catalyst among those investigated in this study, but had CO conversion above that of the CFeCuK catalyst. Alongside its relatively low conversion, the

Table 3.2 Fischer-Tropsch synthesis performance* for all catalysts under gas phase (GP) and supercritical phase (SC) reaction conditions

	CNF-FeCuK		sMWNT-FeCuK		GNP-FeCuK		CFeCuK[80]	
	GP	SC	GP	SC	GP	SC	GP	SC
CO Conversion (%)	18	26	40	83	25	38	16	19
H_2 Conversion (%)	16	22	15	41	23	32	10	14
CH_4 Sel. (%)	0.44	0.75	2.0	3.3	3.6	4.8	1.5	1.1
CO_2 Sel. (%)	5.3	9.4	29	29	13	14	15	13
H_2:CO Usage Ratio	1.6	1.4	0.54	0.71	1.6	1.4	1.1	1.2
Activity[1]	7.6	11	14	29	13	20	4.3	5.2
C_{7+} α	0.71	0.78	0.77/0.31[2]	0.83	0.70/0.37[2]	0.75	0.76/0.52[2]	0.79

*Data shown represents average values for stable reaction behavior at the specified conditions

[1] Activity = 10^{-2} mol_{CO} consumed g_{Fe}^{-1} s^{-1}

[2]Apparent 2-α distribution with break at C_{16} for sMWNT-FeCuK, C_{18} for GNP-FeCuK, and C_{16} for CFeCuK.

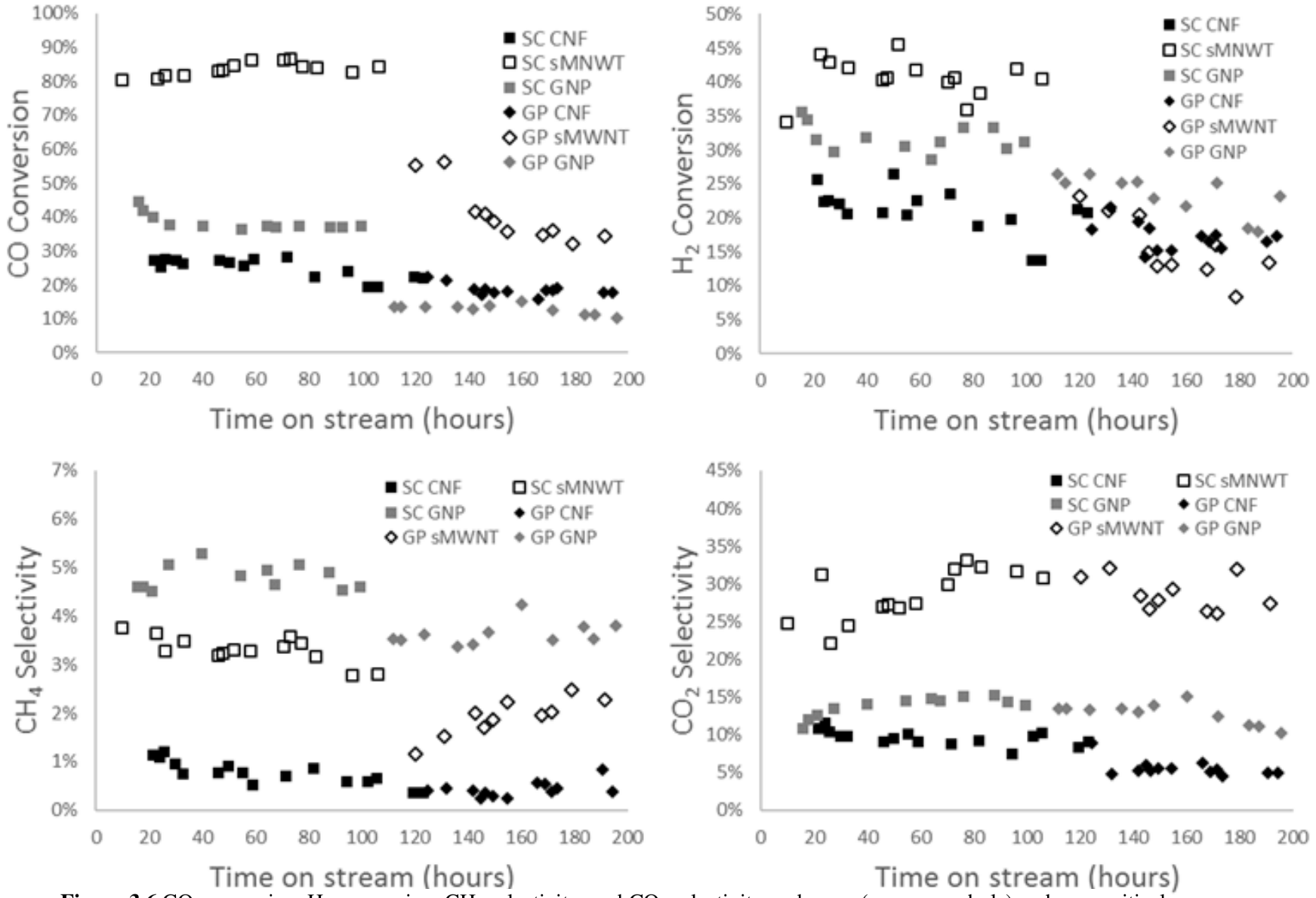

Figure 3.6 CO conversion, H_2 conversion, CH_4 selectivity, and CO_2 selectivity under gas (square symbols) and supercritical (diamond symbols) conditions

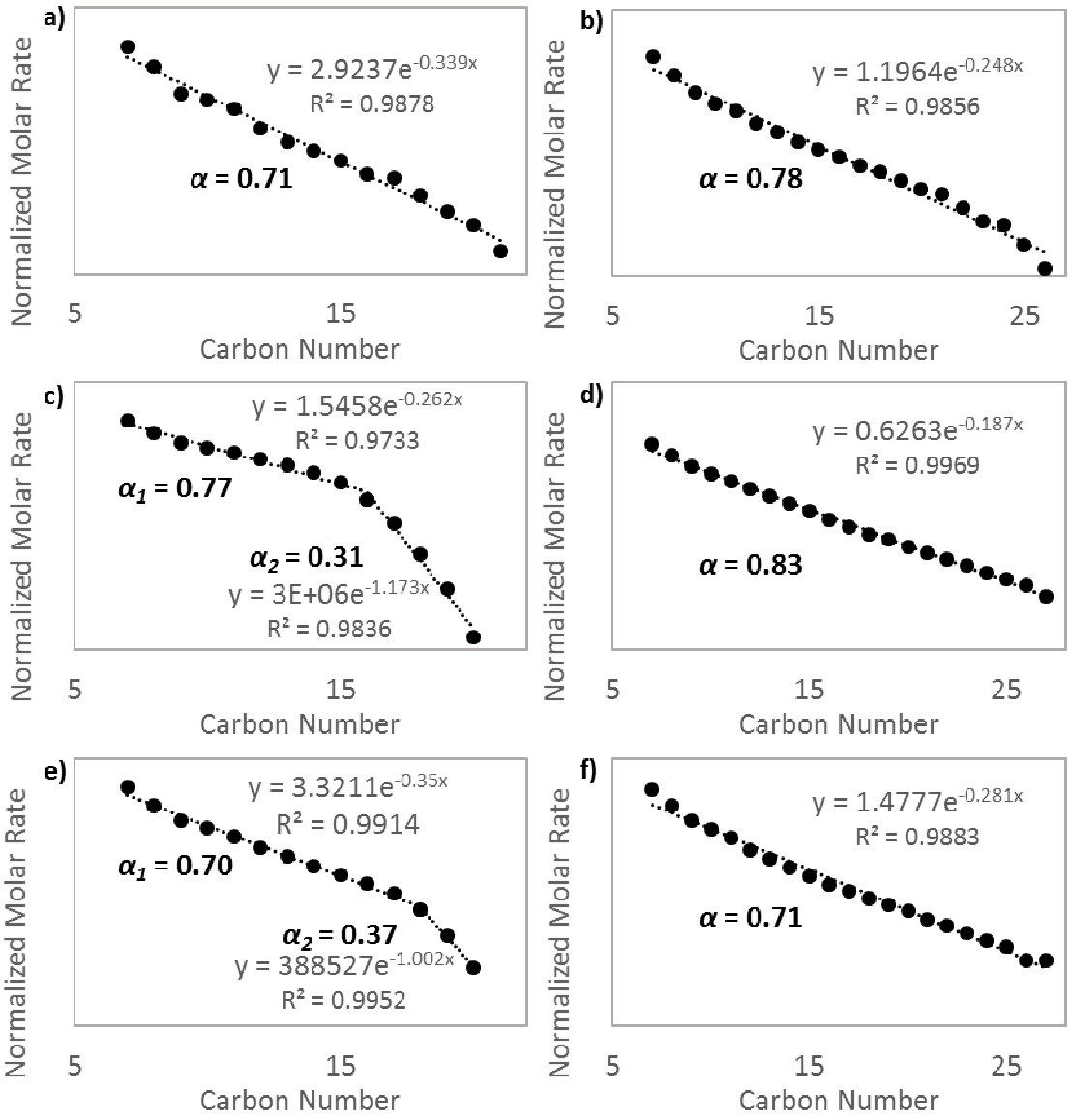

Figure 3.7 ASF plots for **a)** GP-FTS, CNF-FeCuK **b)** SC-FTS, CNF-FeCuK **c)** GP-FTS, sMWNT-FeCuK **d)** SC-FTS, sMNWT-FeCuK and **e)** GP-FTS, GNP-FeCuK and **f)** SC-FTS, GNP-FeCuK

CNF-FeCuK catalyst exhibited the lowest CH_4 and CO_2 selectivities observed among catalysts studied, though both CH_4 and CO_2 selectivity were elevated alongside increased CO and H_2 conversion in SC-FTS.

CNF-FeCuK liquid product data is shown in Figure 3.8 for GP-FTS, and in Figure 3.9 for SC-FTS. In both GP-FTS and SC-FTS, the products are dominated by alkanes and alkenes (70-80%), though there are an appreciable quantity of oxygenates as well. In GP-FTS the liquid product data can be fit to an ASF plot with $\alpha = 0.71$. Alcohols are the most prevalent oxygenate product, while methyl-ketones have a lower selectivity and aldehydes are only detectable in trace quantities and at low carbon numbers. In SC-FTS, the

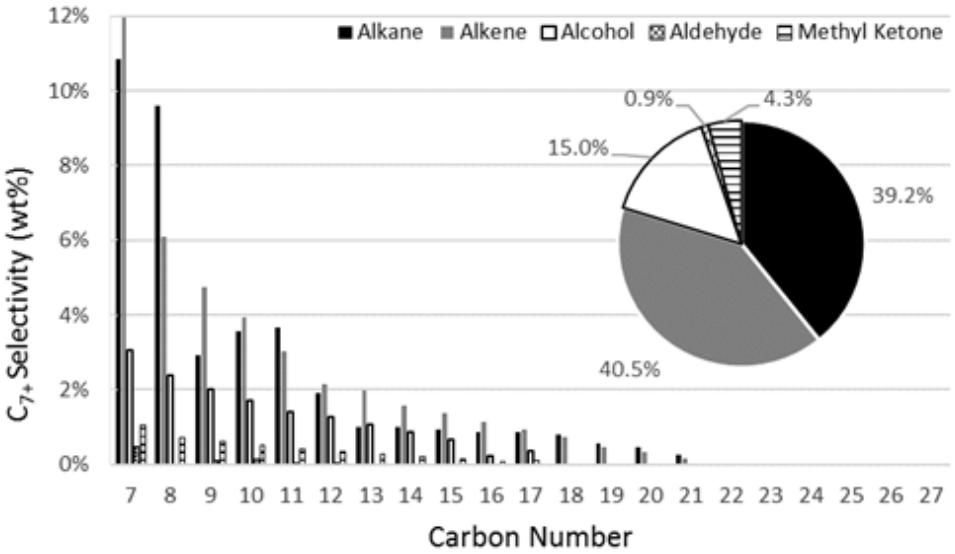

Figure 3.8 Selectivity among C_{7+} products for the CNF-FeCuK catalyst under gas phase operation (240 ºC, 250 psi)

liquid product data can be fit to an ASF plot with $\alpha = 0.78$. Selectivity in SC-FTS is more skewed toward less-hydrogenated products, with aldehydes and methyl-ketones increasing their respective shares of the product selectivity the most. The shift toward less-hydrogenated products in SC-FTS in reminiscent of a similar trend observed by Durham et al.[65] for a similarly-promoted, precipitated catalyst as well as for as the CFeCuK catalyst, where such a shifts in selectivity are attributed to enhanced product extraction by the SCF medium.

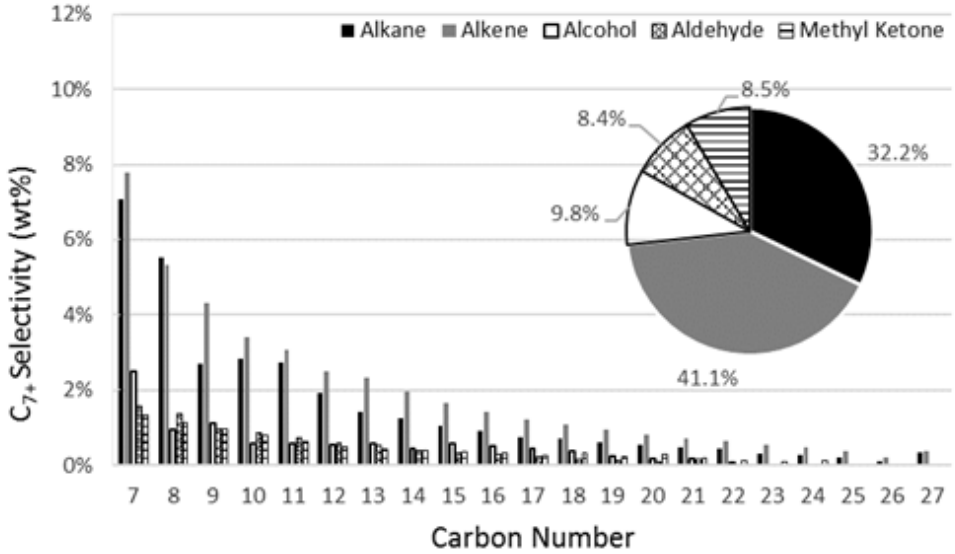

Figure 3.9 Selectivity among C_{7+} products for the CNF-FeCuK catalyst under supercritical operation (240 ºC, 1000 psi, hexanes/syngas molar ratio = 3)

On the whole, the CNF-FeCuK catalyst behaves most similarly to a precipitated catalyst: aldehydes are only extracted in SC-FTS, and products otherwise largely consist of alkenes and alkanes, with some alcohols. This product selectivity is extremely similar to that observed by Durham et al.[53] for a precipitated FeZnCuK catalyst, albeit with much higher activity and lower α. Based on this, it seems that a CNF support of this type can serve as an adequate, inert support for an active FTS catalyst with low CH_4 and CO_2 selectivities, but does not significantly affect the FTS liquid product.

Of the catalysts studied, the sMWNT-FeCuK catalyst had by far the highest CO conversion, but its low H_2/CO usage ratio and elevated CO_2 selectivity indicate that the water-gas shift reaction was responsible for a large portion of that CO consumption. Under SC-FTS operation, conversion was more than twice that of GP-FTS with only a minimal increase in CH_4 selectivity and negligible difference in CO_2 selectivity.

Liquid product data for the sMWNT-FeCuK catalyst is shown in Figure 3.10 for GP-FTS and in Figure 3.11 for SC-FTS. In GP-FTS, the product selectivity was similar to that of the CNF-FeCuK catalyst, albeit more paraffinic. Alkanes are the most abundant product, followed by alkenes, while alcohols are the only oxygenate present to a significant degree. The data for GP-FTS can be represented by a 2-α ASF plot, as the calculated propagation probability is the highest of any of the catalysts in GP-

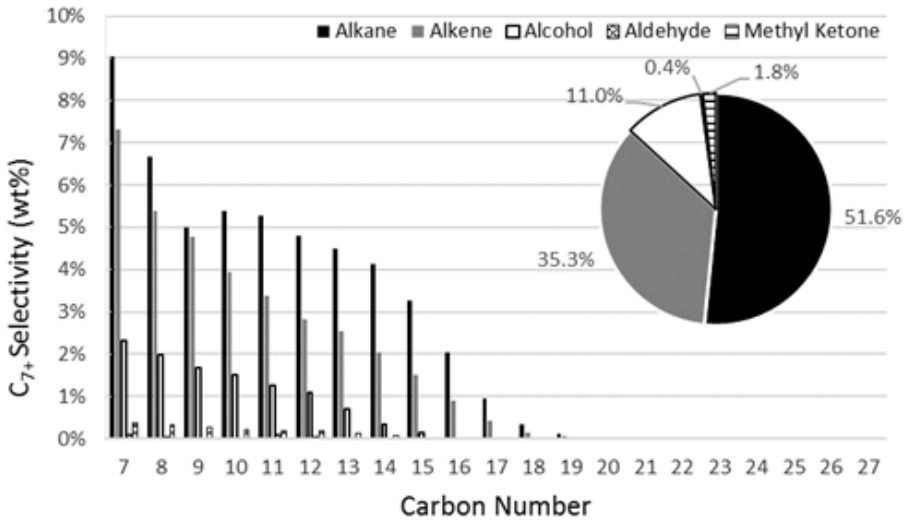

Figure 3.10 Selectivity among C_{7+} products for the sMWNT-FeCuK catalyst under gas phase operation (240 ºC, 250 psi)

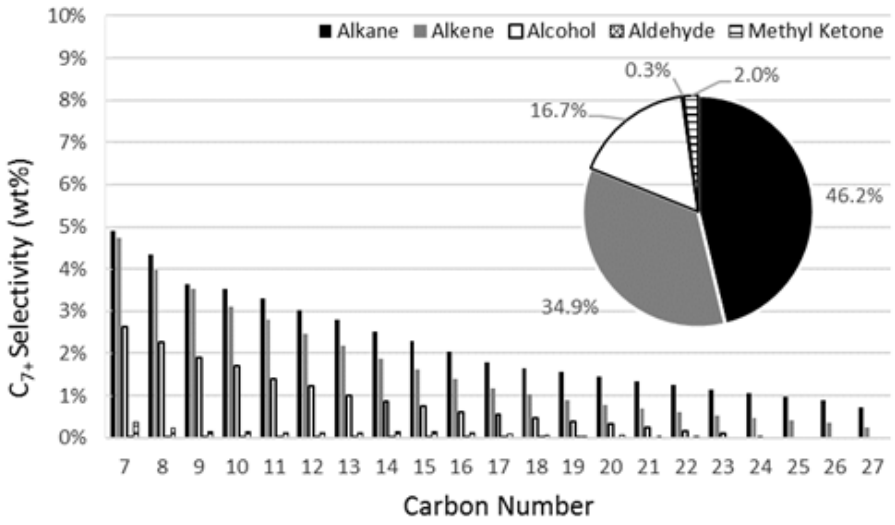

Figure 3.11 Selectivity among C_{7+} products for the sMWNT-FeCuK catalyst under supercritical phase operation (240 ºC, 1000 psi, hexane:syngas molar ratio = 3)

FTS—0.77—until approximately C_{16}, where oxygenate products are no longer detectable and α plummets to 0.31. In SC-FTS, products are slightly less hydrogenated, but still consist of alkanes, alkenes, and alcohols in order of decreasing abundance, with trace levels of other oxygenates. C_{7+} products are well-represented by a near-ideal ASF plot with $\alpha = 0.83$, the highest propagation probability of the catalysts studied

In contrast to the CNF-FeCuK catalyst, aldehydes were not extracted from the sMWNT-FeCuK catalyst under either GP-FTS or SC-FTS. Because aldehyde selectivity is inversely related to CO conversion,[53] this could be a result of the rapid conversion preventing their extraction, but that seems unlikely, as Durham et al. saw approximately 20% selectivity toward aldehydes even at high carbon numbers and 70% conversion. Because the catalyst is clearly very WGS active with high α, it also seems unlikely that the K promotion is not effective. Instead, the SC-FTS catalyst behavior is more consistent with the behavior of K-promoted catalyst in GP-FTS, where aldehydes, if they are indeed an alcohol precursor, cannot desorb and are instead always hydrogenated. If that were the case, it would indicate that—as opposed to the case of the CFeCuK catalyst, where aldehydes desorption is so uninhibited as to occur even in GP-FTS—the sMWNT-FeCuK catalyst actually binds that reaction intermediate more strongly and eliminates desorption, even under SC-FTS conditions. Functionality of liquid products aside,

its activity and selectivity toward heavy products mark sMWNT-FeCuK catalyst as promising support for FTS with further potential for optimization.

CO conversion and CO_2 selectivity for the GNP-FeCuK catalyst were intermediate between that of the CNF-FeCuK and sMWNT-FeCuK catalysts. Interestingly, the H_2/CO usage ratio is nearly identical to that of the CNF-supported catalyst, but CO_2 selectivity is higher. As CO_2 production in FTS is almost exclusively tied H_2 production via the WGS reaction,[102] there must be a corresponding H_2 'sink' to yield such equivalent usage ratio. CH_4 production could, and indeed does, contribute to elevated H_2 consumption, but it seems that the liquid product is more relevant for this catalyst.

The liquid products for the GNP-FeCuK catalyst under GP-FTS and SC-FTS are shown in Figure 3.12 and Figure 3.13, respectively. From these figures, it is apparent that the GNP-supported catalyst is the most strongly hydrogenating catalyst of those studied, with alkane selectivity in GP-FTS greatly increased relative to the CNF-supported and sMWNT-supported catalysts. This hydrogenation tendency is also reflected in the ASF α values—the lowest of the catalysts studied—where a tendency towards termination of growing chains via hydrogenation skews the product distribution towards lower carbon

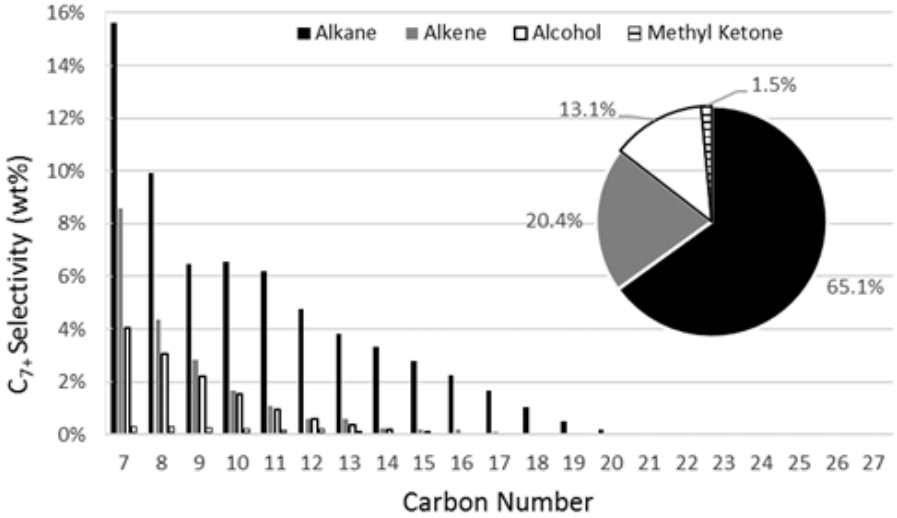

Figure 3.12 Selectivity among C_{7+} products for the GNP-FeCuK catalyst under gas phase operation (240 ºC, 250 psi)

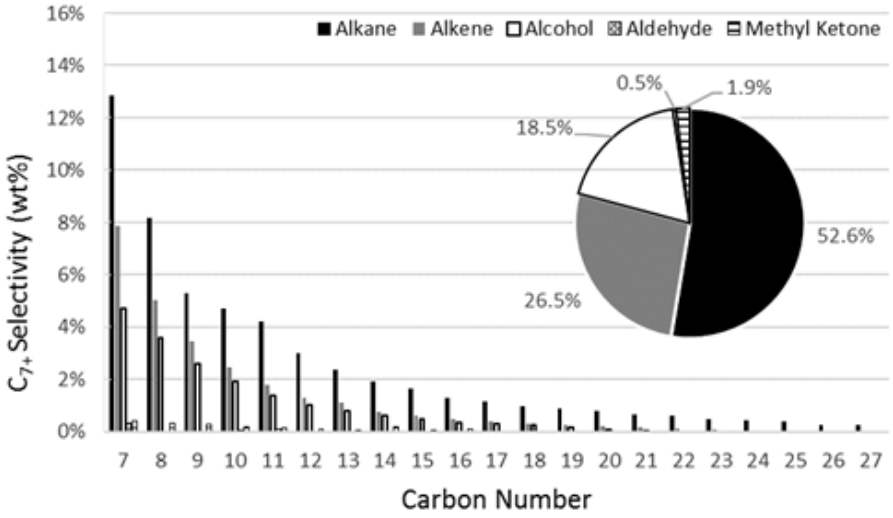

Figure 3.13 Selectivity among C_{7+} products for the GNP-FeCuK catalyst under supercritical phase operation (240 ºC, 1000 psi, hexane:syngas molar ratio = 3)

numbers. This behavior is somewhat mitigated in SC-FTS, where enhanced product extraction resulted in elevated selectivity towards alcohols and olefins.

Like with the sMWNT-FeCuK catalyst, aldehydes are not produced by the GNP-FeCuK catalyst to a significant extent in either GP-FTS or SC-FTS. Though this catalyst is more strongly hydrogenating than sMWNT-FeCuK, the same potential explanations, e.g. excessive conversion, ineffectual K promotion, and inhibited desorption of aldehydes, apply. As with the sMWNT-supported catalyst, the literature and moderate CO_2 selectivity allow us to discard the first two possibilities, leaving only inhibited aldehyde desorption as plausible among the proposed explanations.

The GNP-supported catalyst did not demonstrate low CH_4 and CO_2 selectivities like the CNF-supported catalyst or activity as high as the sMWNT-supported catalyst. Additionally, the liquid product selectivity is generally undesirable, so utility of GNPs as an FTS catalyst support seems limited unless its interactions with the catalyst particles can be significantly altered.

Collectively, the results of this study seem to corroborate our previous[80] observations regarding SCFs and carbon-supported nanoscale catalysts, namely that for these types of catalysts and FTS reaction conditions, the use of a SCF reaction medium appears to primarily impact performance as a result of

improving mass transfer. Mass transfer improvement relative to GP-FTS is evidenced by increased extraction of heavy and unhydrogenated products, increased α, reduction of ASF deviations (indicated by a 2-α distribution), and increased CO conversion. As methanation is correlated with poor heat management,[1,46,50] the low CH_4 selectivity observed in GP-FTS and lack of improvement in SC-FTS seem to indicate a well-managed heat of reaction even without the SCF reaction medium for the catalysts studied.

3.4 Conclusions

In this chapter, we have presented data from the preparation and characterization of three Fe-based nanoparticle catalysts that are supported on carbon nanofibers, small-diameter multi-walled carbon nanotubes, and graphene nanoplatelets. These catalysts each were tested in both gas phase Fischer-Tropsch synthesis as well as supercritical hexane-mediated Fischer-Tropsch synthesis. All of the catalysts were relatively active for FTS with relatively low CH_4 selectivity, though CO conversion, CO_2 selectivity, propagation probability, and liquid product functionality varied widely between the three. Under supercritical operation, CO conversion, propagation probability, and oxygenate selectivity all increased in response to the ability of the supercritical fluid to enhance mass transfer relative to the gas phase. Of particular note is the catalyst supported on small-diameter nanotubes, which had the highest FTS activity and propagation probability among the catalysts. The wide variance in behavior exhibited by the three catalysts despite near-identical pretreatment, promotion, and reaction methodologies indicates that carbon support structure can have a massive impact on the performance of iron FTS catalysts, but understanding and tailoring that influence requires additional study.

Chapter 4: Conclusions & Recommended Future Work

4.1 Overall Conclusions

Based on the data presented in this work, several conclusions can be drawn related to the effect of carbon supports on FTS catalyst performance as well as regarding the FTS reaction mechanism itself. With respect to carbon supports, the production of aldehydes in gas phase FTS by the CFeCuK catalyst demonstrates that carbon supports can significantly affect the selectivity of catalysts they support, going so far as to enable the observation of products that are previously unprecedented at the reaction conditions studied. Further, the wide spectrum of activities and selectivities exhibited by the different carbon-supported catalysts indicates that the structure of the support (e.g. its diameter, shape, and surface chemistry) can greatly influence the reaction performance of the supported catalyst metal. The selection of carbon support thus introduces a degree of tailorability to catalyst synthesis, with the ability to shift the FTS product spectrum towards lighter alkanes, oxygenates, or a higher throughput of heavier products. Additionally, each of investigated carbon-supported catalysts demonstrated activity above that of a traditional, precipitated catalyst.

Durham et al.[53] present the hypothesis that in K-promoted, Fe-catalyzed FTS, aldehydes are primary products alongside paraffins and olefins, but that hydrogenation of the aldehyde can also sequentially yield alcohols, olefins, and paraffins as secondary products. The data presented in this work, particularly the relative compositions of GP-FTS and SC-FTS liquid products for each catalyst, is consistent with and supports that hypothesis. For example, it has been demonstrated in the literature that a SCF reaction medium can help to extract products prior to secondary reactions[61] (e.g. hydrogenation) and for all catalysts in this work, the product spectrum under SC-FTS always contains fewer paraffins and more of the less-hydrogenated, oxygenate products. In other words, by preventing secondary hydrogenation, the SCF reaction media was able to extract the ‘more primary’ olefins and oxygenates before they could be converted to paraffins. Most telling however, is the observation that for the four catalysts that did not produce aldehydes, alcohol selectivity is elevated in SC-FTS. In contrast, for CFeCuK and CNF-FeCuK, alcohol selectivity is instead significantly depressed under supercritical operation. This is a result of the same trend

however, as the supercritical reaction medium instead extracts the primary aldehyde and thereby prevents formation of the alcohol.

4.2 Proposed Future Work on Aldehyde Desorption

The biggest question raised from the FTS results presented for the various carbon supports in Chapters 2 and 3 is why aldehydes either were or were not extracted from each individual catalyst. That question, if answered, has the potential to settle the near-century-long debate on what exactly takes place on the catalyst surface in FTS. If, as we have suggested in this work, aldehydes are a primary product whose extraction is dependent on a blend of catalyst surface electrochemistry and mass transport to the bulk fluid, it should be relatively straight-forward to deconvolute those two factors.

As it stands, individually testing catalysts in FTS is extremely time consuming and yields results that depend on everything from time on stream to the exact the pore volume of the support during promotion. As an alternative, any apparatus with either a very precise, temperature tolerant scale (TGA), or the ability to dynamically quantify effluent hydrocarbon flowrates (GC) could be used to quantify RCHO-metal bond strength for a catalyst sample. To do this, synthesize a sample to be tested, and, assuming the use of a TGA apparatus, place it on the scale. Heat the sample to 270-350 ºC, reduce it, then purge with He and reduce to FTS temperature (~220-240 ºC). Into an otherwise inert-filled reaction chamber, flow gaseous aldehydes of known composition. Aldehydes can function as initiators in FTS,[53] and can thus adsorb to the catalyst surface, changing the mass on the scale. Ramp temperature until aldehydes desorb, and the desorption temperature and rate should yield quantitative metrics of that bond strength.

Admittedly, there is a chance that aldehydes of length *n* can dissociate to form alkanes of length *n*-1, or react with each other in other ways (ether formation), but the idea is simple enough to be modified to accommodate challenges and, once tuned, would provide a facile way to evaluate and quantify catalyst surface chemistry which could then be correlated with actual FTS performance.

4.3 Proposed Future Work Utilizing a Statistical Approach

Another alternative would be to continue this work in a more linear way. Though there is not enough proof to bring it forward in Chapter 3, there seems to be a link between carbon support sp^2-hydridization, catalyst structure (tube vs plane/agglomerate), WGS activity, FTS activity, and product functionality. The sMWNT-supported catalyst was by far the most active catalyst for WGS, but produced no aldehydes, the GNP-supported catalyst was even more hydrogenating, and the large-diameter MWNT, which was unremarkable by every other metric, produced an entirely unique product slate. With so many interrelated variables in FTS, it seems a clear candidate for a more statistically-based approach to extracting data from tweaks to catalyst/support variables beyond diameter, geometry, and surface chemistry of pure carbon. This would present an opportunity to investigate N-doped CNTs, B-doped CNTs, as well as tubes of more varied diameter, and metallic vs. semiconducting tubes. That space between materials science, catalysis, and statistics would be tough to stake out, but could be jumping-off point to explore non-carbon supports, or even different reactions.

References

(1) Dry, M. E. *Catal. Today* **2002**, *71*, 227–241.

(2) Steynberg, A. P.; Dry, M. E. Steynberg, A. P., Dry, M. E., Eds.; Elsevier Science & Technology Books: New York, New York, 2004; pp 1–676.

(3) Durham, J. E. Supercritical Fluids for Fischer Tropsch Synthesis and Related Reactions, Auburn University, 2011.

(4) Dry, M. E. *J. Organomet. Chem.* **1989**, *372*, 117–127.

(5) U.S. Department of Energy. *Analysis of Natural Gas-to Liquid Transportation Fuels via Fischer-Tropsch*; 2013.

(6) The world's largest gas- to -liquids plant is now fully online http://www.shell.com/global/aboutshell/major-projects-2/pearl/largest-gtl-plant.html (accessed Nov 12, 2014).

(7) Arup, M.; Vishakh, M. Gas-to-liquids plants face challenges in the U.S. market http://www.eia.gov/todayinenergy/detail.cfm?id=15071# (accessed Nov 12, 2014).

(8) van der Laan, G. P.; Beenackers, A. A. C. M. *Catal. Rev.* **1999**, *41* (3–4), 255–318.

(9) Zabidi, N. A. M. In *Microemulsions - An Introduction to Properties and Applications*; Najjar, R., Ed.; 2012; Vol. 2.

(10) Subiranas, A. M. *d-nb.info* **2009**, 186.

(11) Jacobs, G.; Chaudhari, K.; Sparks, D.; Zhang, Y.; Shi, B.; Spicer, R. L.; Das, T. K.; Li, J.; Davis, B. H. *Fuel* **2003**, *82* (10), 1251–1260.

(12) Iglesia, E.; Reyes, S. C.; Madon, R. J. *J. Catal.* **1991**, *6*, 238–256.

(13) Brady, R. C.; Pettit, R. *J. Am. Chem. Soc.* **1980**, *102* (c), 6181–6182.

(14) Craxford, S. R.; Rideal, E. K. *J. Chem. Soc.* **1939**, No. Copyright (C) 2010 American Chemical Society (ACS). All Rights Reserved., 1604–1614.

(15) Maitlis, P. M.; Long, H. C.; Quyoum, R.; Turner, M. L.; Wang, Z.-Q. *Chem. Commun.* **1996**, No. 1, 1.

(16) Storch, H. H.; Golumbic, N.; Anderson, R. B. *Fischer-Tropsch and Related Syntheses*; John Wiley & Sons: New York, 1951.

(17) Davis, B. H. In *ACS Division of Fuel Chemistry, Preprints*; 2002; Vol. 47, pp 237–239.

(18) Pichler, H.; Schulz, H. *Chemie Ing. Tech.* **1970**, *42*, 1162–1174.

(19) Davis, B. H. *Catal. Today* **2009**, *141* (1–2), 25–33.

(20) Schulz, H. *Appl. Catal. A Gen.* **1999**, *186* (1–2), 3–12.

(21) Elbashir, N. O. Utilization of Supercritical Fluids in the Fischer-Tropsch Synthesis Over Cobalt-based Catalytic Systems, 2004.

(22) Jacobs, G.; Das, T. K.; Zhang, Y.; Li, J.; Racoillet, G.; Davis, B. H. *Appl. Catal. A Gen.* **2002**, *233* (1–2), 263–281.

(23) Bukur, D. B.; Mukesh, D.; Patel, S. A. *Ind. Eng. Chem. Res.* **1990**, *29*, 194–204.

(24) Li, S.; Li, A.; Krishnamoorthy, S.; Iglesia, E. *Catal. Letters* **2001**, *77* (4), 197–205.

(25) Li, S.; Krishnamoorthy, S.; Li, A.; Meitzner, G. D.; Iglesia, E. *J. Catal.* **2002**, *206* (2), 202–217.

(26) Steynberg, A. P.; Espinoza, R. L.; Jager, B.; Vosloo, A. C. *Appl. Catal. A …* **1999**, *186*, 41–54.

(27) Leckel, D. *Energy & Fuels* **2009**, *23* (5), 2342–2358.

(28) Bukur, D. B.; Lang, X.; Nowicki, L. *Ind. Eng. Chem. Res.* **2005**, *44* (16), 6038–6044.

(29) Espinoza, R. L.; Steynberg, A. P.; Jager, B.; Vosloo, A. C. *Appl. Catal. A Gen.* **1999**, *186* (1–2), 13–26.

(30) Bartholomew, C. H.; Reuel, R. C. *Ind. Eng. Chem. …* **1985**, 56–61.

(31) Khodakov, A. Y.; Chu, W.; Fongarland, P. *Chem. Rev.* **2007**, *107* (5), 1692–1744.

(32) Iglesia, E.; Soled, S. L.; Fiato, R. A. *J. Catal.* **1992**, *224* (1992), 212–224.

(33) Wang, Y.; Wu, H.; Zhang, Q.; Tang, Q. *Microporous Mesoporous Mater.* **2005**, *86* (1–3), 38–49.

(34) Bezemer, G. L.; Bitter, J. H.; Kuipers, H. P. C. E.; Oosterbeek, H.; Holewijn, J. E.; Xu, X.; Kapteijn, F.; van Dillen, A. J.; de Jong, K. P. *J. Am. Chem. Soc.* **2006**, *128* (12), 11568–11569.

(35) Abbaslou, R. M. M. Iron Catalyst Supported on Carbon Nanotubes for Fischer-Tropsch Synthesis: Experimental and Kinetic Study, 2010.

(36) Ngantsoue-Hoc, W.; Zhang, Y.; O'Brien, R. J.; Luo, M.; Davis, B. H. *Appl. Catal. A Gen.* **2002**, *236* (1–2), 77–89.

(37) Li, S.; Meitzner, G. D.; Iglesia, E. *J. Phys. Chem. B* **2001**, *105* (24), 5743–5750.

(38) Anfray, J.; Bremaud, M.; Fongarland, P.; Khodakov, A. Y.; Jallais, S.; Schweich, D. *Chem. Eng. Sci.* **2007**, *62* (18–20), 5353–5356.

(39) Dry, M. E. *Appl. Catal. A Gen.* **1996**, *138* (2), 319–344.

(40) van Steen, E.; Claeys, M.; Dry, M. E.; van de Loosdrecht, J.; Viljoen, E. L.; Visagie, J. L. *J. Phys. Chem. B* **2005**, *109* (8), 3575–3577.

(41) Fan, L.; Fujimoto, K. *Appl. Catal. A Gen.* **1999**, *186*, 343–354.

(42) O'Brien, R. J.; Xu, L.; Spicer, R. L.; Bao, S. *Catal. Today* **1997**, *36*, 325–334.

(43) Huang, X.; Roberts, C. B. *Fuel Process. Technol.* **2003**, *83* (1–3), 81–99.

(44) Linghu, W.; Li, X.; Asami, K.; Fujimoto, K. *Fuel Process. Technol.* **2004**, *85* (8–10), 1121–1138.

(45) Davis, B. H. *Catal. Today* **2003**, *84* (1–2), 83–98.

(46) Yokota, K.; Fujimoto, K. *Ind. Eng. Chem. Res.* **1991**, *30* (1), 95–100.

(47) Subramaniam, B. *Appl. Catal. A Gen.* **2001**, *212* (1–2), 199–213.

(48) Abbaslou, R. M. M.; Mohammadzadeh, J. S. S.; Dalai, A. K. *Fuel Process. Technol.* **2009**, *90* (7–8), 849–856.

(49) Baiker, A. *Chem. Rev.* **1999**, *99* (2), 453–474.

(50) Yokota, K.; Fujimoto, K. *Fuel* **1989**, *68* (2), 255.

(51) Bukur, D. B.; Lang, X.; Akgerman, A.; Feng, Z. *Ind. Eng. Chem. Res.* **1997**, *36*, 2580–2587.

(52) Lang, X.; Akgerman, A.; Bukur, D. B. *Ind. Eng. Chem. Res.* **1995**, *34* (1), 72–77.

(53) Durham, J. E.; Zhang, S.; Roberts, C. B. *Appl. Catal. A Gen.* **2010**, *386* (1–2), 65–73.

(54) Yokota, K.; Hanakata, Y.; Fujimoto, K. *Fuel* **1991**, *70* (8), 989.

(55) Bochniak, D. J.; Subramaniam, B. *AIChE J.* **1998**, *44* (8), 1889–1896.

(56) Liu, X.; Linghu, W.; Li, X.; Asami, K.; Fujimoto, K. *Appl. Catal. A Gen.* **2006**, *303* (2), 251–257.

(57) Yan, S.; Fan, L.; Zhang, Z.; Zhou, J.; Fujimoto, K. *Appl. Catal. A Gen.* **1998**, *171*, 247–254.

(58) Tsubaki, N.; Yoshii, K.; Fujimoto, K. *J. Catal.* **2002**, *207* (2), 371–375.

(59) Elbashir, N. O.; Dutta, P.; Manivannan, A.; Seehra, M. S.; Roberts, C. B. *Appl. Catal. A Gen.* **2005**, *285* (1–2), 169–180.

(60) Linghu, W.; Li, X.; Fujimoto, K. *J. Fuel Chem. Technol.* **2007**, *35* (1), 2–7.

(61) Elbashir, N. O.; Bukur, D. B.; Durham, J. E.; Roberts, C. B. *AIChE J.* **2010**, *56* (4), 997–1015.

(62) Huang, X. Supercritical fluids as alternative reaction media for Fischer-Tropsch synthesis, 2003.

(63) Irankhah, A.; Haghtalab, A. *Chem. Eng. Technol.* **2008**, *31* (4), 525–536.

(64) Elbashir, N. O.; Roberts, C. B. *Ind. Eng. Chem. …* **2005**, 505–521.

(65) Durham, J. E.; Stewart, C. E.; Roe, D.; Xu, R.; Zhang, S.; Roberts, C. B. *Ind. Eng. Chem. Res.* **2014**, *53* (23), 9695–9702.

(66) Iglesia, E. *Appl. Catal. A Gen.* **1997**, *161* (1–2), 59–78.

(67) Iglesia, E.; Reyes, S. C.; Madon, R. J.; Soled, S. L. *Adv. Catal.* **1993**, *39*, 221–302.

(68) Bahome, M. C.; Jewell, L. L.; Hildebrandt, D.; Glasser, D.; Coville, N. J. *Appl. Catal. A Gen.* **2005**, *287* (1), 60–67.

(69) Guczi, L.; Stefler, G.; Geszti, O.; Koppany, Z.; Konya, Z.; Molnar, E.; Urban, M.; Kiricsi, I. *J. Catal.* **2006**, *244* (1), 24–32.

(70) Chen, W.; Fan, Z.; Pan, X.; Bao, X. *J. Am. Chem. Soc.* **2008**, *130* (29), 9414–9419.

(71) van der Lee, M. K.; van Dillen, A. J.; Bitter, J. H.; de Jong, K. P. *J. Am. Chem. Soc.* **2005**, *127* (39), 13573–13582.

(72) van Steen, E.; Prinsloo, F. F. *Catal. Today* **2002**, *71* (3–4), 327–334.

(73) Abbaslou, R. M. M.; Tavasoli, A.; Dalai, A. K. *Appl. Catal. A Gen.* **2009**, *355* (1–2), 33–41.

(74) Park, J.-Y.; Lee, Y.-J.; Khanna, P. K.; Jun, K.-W.; Bae, J. W.; Kim, Y. H. *J. Mol. Catal. A Chem.* **2010**, *323* (1–2), 84–90.

(75) den Breejen, J. P.; Radstake, P. B.; Bezemer, G. L.; Bitter, J. H.; Froseth, V.; Holmen, A.; de Jong, K. P. *J. Am. Chem. Soc.* **2009**, No. 22, 7197–7203.

(76) Coleman, J. N.; Khan, U.; Blau, W. J.; Gun'ko, Y. K. *Carbon N. Y.* **2006**, *44* (9), 1624–1652.

(77) Dillen, A. Van; Terörde, R.; Lensveld, D. *J. Catal.* **2003**, *216* (1–2), 257–264.

(78) Malik, M. A.; Wani, M. Y.; Hashim, M. A. *Arab. J. Chem.* **2012**, *5* (4), 397–417.

(79) Eriksson, S. *Appl. Catal. A Gen.* **2004**, *265* (2), 207–219.

(80) Roe, D. P.; Xu, R.; Roberts, C. B. *Appl. Catal. A Gen.* **2017**, *543* (February), 141–149.

(81) Abbaslou, R. M. M. Iron catalyst supported on carbon nanotubes for Fischer-Tropsch synthesis: experimental and kinetic study, 2010.

(82) Guczi, L.; Stefler, G.; Geszti, O.; Koppany, Z.; Konya, Z.; Molnar, E.; Urban, M.; Kiricsi, I. *J. Catal.* **2006**, *244* (1), 24–32.

(83) van der Lee, M. K.; van Dillen, a J.; Bitter, J. H.; de Jong, K. P. *J. Am. Chem. Soc.* **2005**, *127* (39), 13573–13582.

(84) Scanlon, J. T.; Willis, D. E. *J. Chromatogr. Sci.* **1985**, *23* (8), 333–340.

(85) Gheorghiu, C. C.; Machado, B. F.; Salinas-Martínez de Lecea, C.; Gouygou, M.; Román-Martínez, M. C.; Serp, P. *Dalt. Trans.* **2014**, *43* (20), 7455.

(86) Sing, K. S. .; Everette, D. H.; Haul, R. A. W.; Moscou, L.; Pierotti, R. A.; Rouquerol, J.; Siemieniewska, T. *Pure Appl. Chem.* **1985**, *57* (4), 603–619.

(87) Motchelaho, M. A. M.; Xiong, H.; Moyo, M.; Jewell, L. L.; Coville, N. J. *J. Mol. Catal. A Chem.* **2011**, *335* (1–2), 189–198.

(88) Hou, P.-X.; Liu, C.; Cheng, H.-M. *Carbon N. Y.* **2008**, *46* (15), 2003–2025.

(89) Abbaslou, R. M. M.; Tavasoli, A.; Soltan, J.; Dalai, A. K. *Appl. Catal. A Gen.* **2009**, *367* (1–2), 47–52.

(90) Jager, B.; Espinoza, R. L. *Catal. Today* **1995**, *23*, 17–28.

(91) Dictor, R. A.; Bell, A. T. *J. Catal.* **1986**, *97* (1), 121–136.

(92) Xiang, Y.; Kruse, N. *Nat. Commun.* **2016**, *7*, 13058.

(93) Butts, S. B.; Strauss, S. H.; Holt, E. M.; Stimson, R. E.; Alcock, N. W.; Shriver, D. F. *J. Am. Chem. Soc.* **1980**, *102* (15), 5093–5100.

(94) Sgobba, V.; Guldi, D. M. *Chem. Soc. Rev.* **2009**, *38* (1), 165–184.

(95) Bukur, D. B.; Sivaraj, C. *Appl. Catal. A Gen.* **2002**, *231* (1–2), 201–214.

(96) Cheng, X.; Yang, H.; Tatarchuk, B. J. *Catal. Today* **2016**, *273*, 62–71.

(97) Qiu, Y.; Guo, F.; Hurt, R.; Külaots, I. *Carbon N. Y.* **2014**, *72*, 215–223.

(98) Krishnan, D.; Kim, F.; Luo, J.; Cruz-Silva, R.; Cote, L. J.; Jang, H. D.; Huang, J. *Nano Today* **2012**, *7* (2), 137–152.

(99) Park, K. C.; Hayashi, T.; Tomiyasu, H.; Endo, M.; Dresselhaus, M. S. *J. Mater. Chem.* **2005**, *15* (3), 407–411.

(100) DiLeo, R. A.; Landi, B. J.; Raffaelle, R. P. *J. Appl. Phys.* **2007**, *101* (6).

(101) Ureña-Benavides, E. E.; Kayatin, M. J.; Davis, V. A. *Macromolecules* **2013**, *46* (4), 1642–1650.

(102) Raje, A. P.; Davis, B. H. *Catal. today* **1997**, *36*, 335–345.